UNIVERSITAT DE BARCELONA

Boosting the infection and oncolysis of adenovirus VCN-01 with topotecan

Victor Burgueño Sandoval

University of Barcelona

Faculty of Medicine

Doctorate program: Biomedicine

Research line: Molecular and cellular biology of cancer

Boosting the infection and oncolysis of adenovirus VCN-01 with topotecan

Pediatric Cancer Program

Institut de Recerca Sant Joan de Déu

&

Department of Pediatric Oncology

SJD Pediatric Cancer Center Barcelona

PhD candidate: Víctor Burgueño

Thesis director: Dr. Ángel M. Carcaboso

Thesis tutor: Dra. Teresa Maria Ribalta Farrés

Dr Angel Montero Carcaboso, director of the thesis entitled ***Boosting the infection and oncolysis of adenovirus VCN-01 with topotecan*** completed by the PhD candidate Víctor Burgueño Sandoval, endorses the originality of the research work included in this thesis.

A mis padres e Irene

“La educación es el arma más poderosa que puedes usar para cambiar el mundo”

Nelson Mandela

Agradecimientos

Me gustaría agradecer a **Ángel Montero Carcaboso** por darme la oportunidad de formar parte de su equipo y por todos estos años de continuo aprendizaje. Ángel ha sido mi mentor durante mi trabajo final de máster y doctorado. Estoy agradecido por su apoyo, orientación y motivación. Su experiencia ha sido una fuente constante de inspiración.

Durante los últimos cinco años, he tenido el privilegio de conocer y trabajar junto a personas maravillosas. Hemos compartido bonitos momentos y he aprendido mucho de ellos. Quiero agradecer a **Rosi** su paciencia y su apoyo en los malos momentos. No sé qué voy a hacer sin ti en mi post doc. ¡¿Qué persona me va a aguantar tanto como tú?! Siempre has tenido una sonrisa para mí. Gracias de corazón. **Leire** has sido un apoyo esencial. Que habría sido de mi tesis sin los momentos graciosos que hemos compartido. Recordaré toda la vida el día en que envolviste el modem con papel de plata para ver si "funcionaba". Gracias por estar aquí estos cinco años. Por cierto, me debes un paraguas nuevo. **María**, mi mentora, a ti si te he de dar las gracias por la PACIENCIA en mayúsculas. Has sido una maestra excepcional. Me quedo con tu pasión por la ciencia y las risas que nos echamos en el estabulario. **Mercè**, mi catalana de Tona preferida, gracias por los debates tan intensos que tuvimos y, que por fortuna, siempre acabaron bien. Una vez terminemos el doctorado, espero que me invites a tu pueblo a comer fuet y al Aplec. **Claudia,** no sé si ets més amiga meva o del HPLC, però bueno, aquesta maquina del dimoni no et pot dedicar unes paraules, jo sí. Agraeixo les teves ganes d'ajudar sempre als altres amb un somriure. La teva energia i vitalitat ens ha ajudat en moltes ocasiones a passar els moments dolents una mica millor. Et desitjo lo millor en la teva pròxima etapa, però si us plau, pentinat. **Yasmine**, quien diría que dos personas tan diferentes se podrían llevar tan bien (profundamente bien). Te deseo lo mejor en esta nueva etapa en Dublín, sé que lo harás genial porque eres una científica excepcional. Nunca dejes de sonreír y de tener esa alegría que tanto te caracteriza. Eres una inspiración para la gente que te rodea. Gracias de corazón

por todos los momentos compartidos. **Pablo**, mi gallego preferido (junto con Estela). Te quiero dar las gracias por tu alegría y risas. Hemos sido compañeros de bromas, aunque muchas veces, nos las hacíamos el uno al otro. Gracias por llenarme la mochila de serrín, eres súper gracioso. Gracias también por llenarme la botella de agua de vinagre, sal, aceite entre otras muchas otras sustancias, eres mazo gracioso. Por todo esto, te quiero mucho y te deseo lo mejor en tu futuro por Alemania. **Chao Liang**, you have been my first Chinese friend, and I hope not the last. When you leave, I will miss you so much, but I am sure that I will visit you in China. Thank you for always helping me and sharing your knowledge with me. I will put here some of the most important sentences that you have taught me: “today not good”, “gpt told me”, “cheap good, free better”, “why not good?”. **Carla,** en aquest últims mesos la nostra amistat ha guanyat força i el teu cabell n’ha perdut. Trobaré a faltar les nostres xerrades a cultius i els nostres debats. Espero anar més vegades de visita a Girona i de pas, molestar-te una estona pues porque sí, porque es la moda.

No quiero olvidarme del resto de mis compañeros: **Estela, Juana, Elena, Clara, Mercè R, Alba, Helena, María S, Ana, Oscar, Joan, Jara, Alex, Nuria, Valentin, Sara, Monica, Ana D, Marta, Noelia, Isa, Laura, Silvia, Sara S y Carlos**. Nunca olvidaré nuestro tiempo juntos en el laboratorio, en el estabulario, y nuestras cerves después del trabajo.

También me gustaría agradecer a los profesionales de nuestro hospital, Sant Joan de Déu, que han participado activamente en el proyecto. Gracias a ellos, hemos podido comprender de primera mano las necesidades de nuestros pacientes. Gracias, **Margarida Simao, Guillermo L Chantada** y **Jaume Catalá**, por vuestra dedicación e implicación en el proyecto.

Estoy también muy agradecido al equipo de VCN Biosciences, y a **Luciano Di Croce** y **Cecilia Julia Ballaré** del Centro de Regulación Genómica.

Finalmente, quiero dar las gracias a mis **padres** y a mi hermana **Irene**. Sin vosotros esto no hubiese sido posible. Muchas gracias por confiar en mí y estar siempre a mi lado. Habéis sido un apoyo y una fuente de inspiración indispensable. Sois la mejora familia que alguien podría desear. Os quiero.

Mis abuelos me han criado y no sería la persona que soy sin ellos. Por eso quiero dar las gracias a mis yayos **Cipriano, Antonio, Lola** e **Isabel** por su tiempo, ayuda y amor incondicional.

Agradecer también al resto de mi familia por todo el apoyo y tiempo que han pasado conmigo. A mis **tíos**, a mis **primos** y a mi cuñado **Dani**.

Gracias a todos por creer en mí.

Table of contents

Summary

Dysregulation of the retinoblastoma (RB1) pathway is a frequent oncogenic event and results in high levels of the free (not bound to the retinoblastoma protein) transcription factor E2F-1 in cancer cells. The oncolytic adenovirus VCN-01 was engineered to use E2F-1 to activate its replication and lyse tumors. However, efficient viral delivery and infection of cancer cells remains a challenge. In this study, we show that the topoisomerase I inhibitor topotecan increases the ability of VCN-01 to infect and lyse several pediatric cancers through the upregulation of E2F-1 and the induction of S-phase arrest in the tumor cells. We observed a powerful synergistic activity of local VCN-01 injections and systemic topotecan in human cancer xenografts in mice, including intraocular and leptomeningeal retinoblastoma, and aggressive models of Ewing sarcoma and neuroblastoma. At the selected dosages, individual treatments were not active, while the combination significantly increased mouse survival. In a patient with chemo-refractory intraocular retinoblastoma receiving intravitreal VCN-01 in the frame of a phase 1 clinical trial, we observed a ten-fold increase in viral genomes in the aqueous humor after the administration of topotecan. The patient achieved complete response and remains disease free four years following therapy. These results support new clinical trials.

Chapter I: Introduction

1. The RB1-E2F pathway

The Retinoblastoma 1 – E2F transcription factor (RB1-E2F) axis (**Fig. 1.1**) is a critical regulatory pathway involved in cell cycle control and cell proliferation (*1*). The main components of the pathway are the retinoblastoma protein (pRB, encoded by the tumor suppressor gene *RB1*), the E2F family of transcription factors, the cyclins, the cyclin-dependent kinases (CDKs, such as CDK4 and CDK6), and a group of proteins working as CDK inhibitors, among which the most important are the INK4 proteins (inhibitors of CDK4, like p16), together with the CIP/KIP family (CDK interacting protein/Kinase inhibitory protein) which include p21, p27 and p57 (**Fig. 1.1**). One or more components of this axis are deregulated in the vast majority of human cancers, including pediatric cancers, such as retinoblastoma, Ewing sarcoma and neuroblastoma, which I will address in this thesis (Section 3). The interaction between pRB and the E2F family of transcription factors is essential for the accurate development and regulation of cell processes.

Targeting proteins of the RB1-E2F axis is a significant therapeutic strategy for cancer (*2*). CDKs are the most commonly targeted proteins in the pathway and there are clinically available CDK small molecule inhibitors, such as palbociclib, ribociclib and abemaciclib, for the treatment of breast cancer, melanoma and sarcomas (*3-5*). These therapies aim to restore the normal function of the pathway, thereby inhibiting the uncontrolled cell growth and division observed in cancer cells. In this thesis, I will focus on a radically new therapy, the oncolytic virus VCN-01, targeting the overexpression of the factor E2F-1 in cancer cells, and I will study small molecules, such as the topoisomerase 1 inhibitor topotecan, that might enhance the expression of E2F-1 in cancer cells (Section 2).

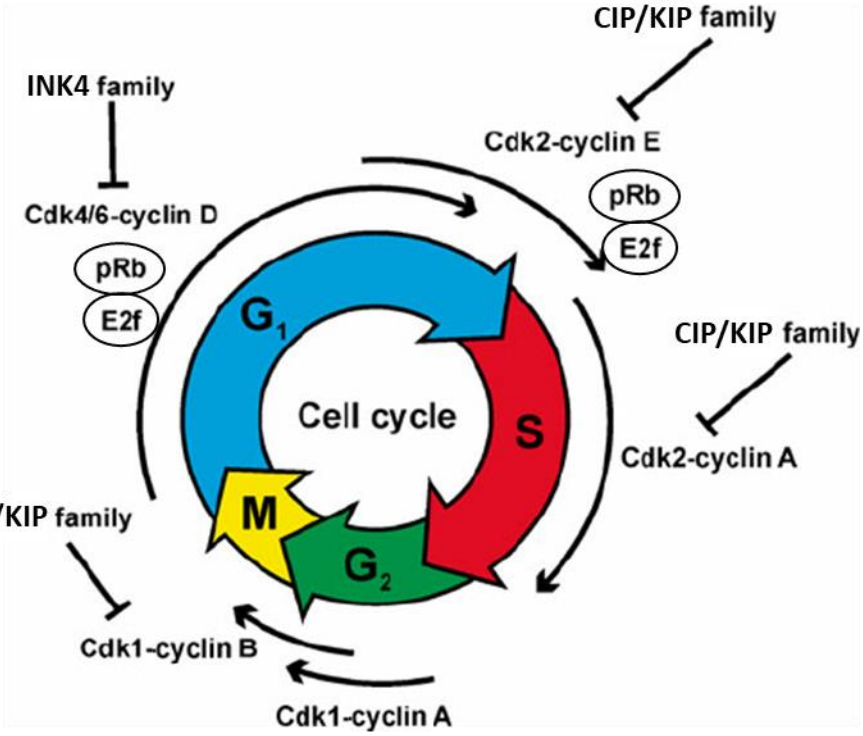

Figure 1.1. The RB1/E2F axis. Schematic representation of the RB1-E2F pathway. The pathway involves the tumor suppressor protein pRB, E2F transcription factors, cyclins, CDKs, and CDK inhibitors (INK4 and CIP/KIP family of proteins). Modified from: Cheffer A, Tárnok A, Ulrich H. Cell cycle regulation during neurogenesis in the embryonic and adult brain. Stem Cell Rev Rep. 2013 Dec;9(6):794-805

1.1. The RB1-E2F pathway members

The retinoblastoma protein, pRB, is a tumor suppressor protein that serves as a transcriptional corepressor (*6*). pRB, together with the pRB-related proteins p107 and p130, is part of the pocket protein family (*7*) **(Fig. 1.2)**. This family of tumor suppressor proteins interacts with the E2F family of transcription factors to regulate cell cycle progression and gene expression (*7*). For instance, pRB prevents cell cycle progression through its ability to bind and repress E2F-1 activity (*8*). Traditionally, the E2F family members have been classified into three distinct groups based on their ability to activate or suppress gene transcription, their patterns of expression, and their regulatory mechanisms. Group 1 includes activators E2F-1, E2F-2 and

E2F-3a, which become inactivated upon interaction with pRB. However, when they are unbound, their primary function is to increase the transcriptional activity of certain genes related to cell cycle progression and DNA synthesis. Group 2 are canonical repressors E2F-3b, E2F-4, E2F-5 and E2F-6, which typically inhibit gene expression. Group 3 comprises atypical repressors E2F-7 and E2F-8, which do not interact with the pocket protein family but contribute to the repression of the transcriptional program promoted by E2F activators (*9*).

In vitro studies indicate that the sequential binding of E2F activators and repressors to their specific promoters drives the oscillatory pattern of gene expression during the cell cycle (*9*). Nevertheless, evidence from in vivo studies to support this hypothesis is incomplete. Loss of individual E2Fs in mice has minor consequences for animal development (*10*) whereas knockout of E2F activators *E2F1*, *E2F2* and *E2F3* produce neonatal lethality in mice (*11*). Recent studies suggest the dual function of E2F-3b, which despite exhibiting expression patterns similar to conventional repressors, can function as a transcriptional activator as well (*12*).

E2F activators also have a pro-oncogenic role. The first genetic evidence for the oncogenic role of E2Fs activators was provided by Jacks and colleagues, who demonstrated that ablation of *E2F1* in $RB1^{+/-}$ mice reduced the incidence of pituitary and thyroid tumors and prolonged the lifetime of the mice (*13*).

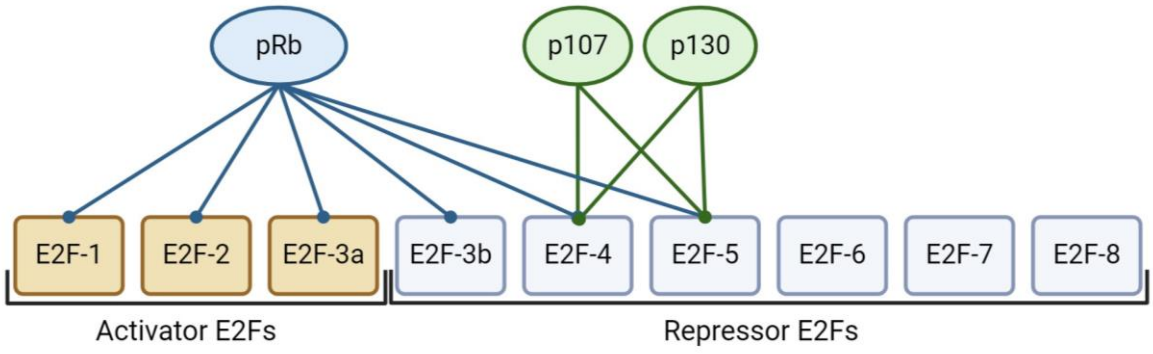

Figure 1.2. Pocket family – E2Fs transcription factors interaction. RB1 binds to E2F-1, E2F-2, E2F-3a, E2F-3b, E2F-4, and E2F-5, while p107 and p130 only bind to E2F-4 and E2F-5. E2F-6 does

not bind pocket proteins but is instead regulated by Polycomb group proteins. E2F-7 and E2F-8 lack dimerization and transactivation domains and do not bind to pocket proteins.

1.2. Regulation of the RB1-E2F axis

In quiescent cells, pRB binds to E2F transcription factors in G0 and early-G1 phase. The complex formed by pRB and E2F prevents the transcriptional program promoted by E2F, thus impeding cell proliferation (**Fig. 1.3A**) (*7, 14*). Upon mitogenic stimuli, the cyclin D-CDK4/6 complex phosphorylates pRB (*15*), leading to the release of E2F transcription factors (**Fig. 1.3B**). This is further enhanced by the cyclin E1-CDK2 and cyclin A-CDK2 complexes, which increase pRB phosphorylation (**Fig. 1.3C**). Phosphorylated pRB persists in this state until mitosis, when it is dephosphorylated through the action of phosphatases and reactivated to continue its role as a transcriptional repressor (*16*). In parallel, free E2F increases the transcription of cyclin E1 (gene *CCNE1*), establishing a feedback loop that boosts the activity of the cyclin E1-CDK2 complex and, consequently, promotes the hyperphosphorylation and complete deactivation of pRB (*17, 18*). Finally, pRB inhibition (or dysfunction) enables the expression of genes that are under the control of E2F activators (**Fig. 1.3D**) (*19*). This positive feedback creates a critical period for the cell to enter the S phase of the cell cycle (*20*).

Negative regulation of the cell cycle is important to prevent inappropriate proliferation and tumorigenesis. Upon receiving anti-proliferative signals, the cell expresses p16 (*CDKN2A*), which is the most important CDK inhibitor. Together with p21 (*CDKN1A*) and p27 (*CDKN1B*), p16 prevents cell cycle progression through the inhibition of the cyclin-CDK complexes (**Fig. 1.3E**) (*21*).

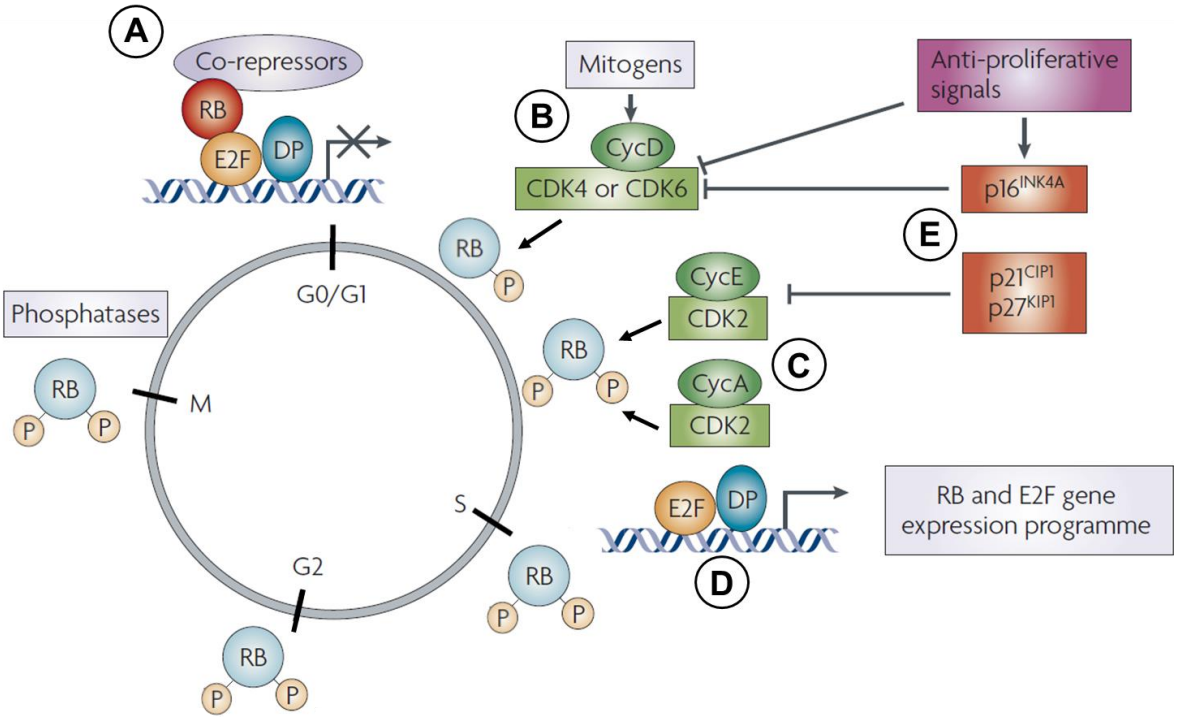

Figure 1.3. **Role of RB1-E2F pathway in cell cycle control.** Mitogenic signals stimulate the formation of complexes between cyclins and CDKs. These complexes have the ability to phosphorylate pRB (RB). The phosphorylation of pRB disrupts its association with E2F. Then, free E2F transcribes genes that are essential for the progression through the S-phase and mitosis. During the transition from mitosis to G1, pRB undergoes dephosphorylation mediated by phosphatases. Modified from: Knudsen ES, Knudsen KE. Tailoring to RB: tumour suppressor status and therapeutic response. Nat Rev Cancer. 2008 Sep;8(9):714-24.

1.3. Regulation of the transcription factor E2F-1

E2F-1 is a special member within the E2F family because of its ability to promote cell cycle progression through precise regulation of genes required for DNA synthesis at the G1/S boundary, along with its capacity to contribute to apoptosis induction by cooperating with p53 or p73 (*22*). The proper regulation of E2F-1 is crucial to ensure the adequate progression of the cell cycle and the integrity of the cell division process. In quiescent cells, pRB binds to E2F-1, thereby inhibiting its transcription activity. Upon receiving mitogenic signals, pRB is phosphorylated and E2F-1 is released. The activity of E2F-1 increases with the progression from G1 to S-phase (**Fig. 1.4**). The transcriptional activity of E2F-1 increases as cells progress from the G1 to the S phase, reaching its peak at the G1/S boundary (*23, 24*). Finally, the cyclin A-CDK2 complex binds to E2F-1 and inhibits its DNA-binding activity by phosphorylation (*25*).

Different mechanisms regulate the expression of E2F-1. DNA damage increase expression and transcriptional activity of E2F-1 (*26-29*). For instance, Huang *et al.* (*28*) observed that ionizing radiation increase E2F-1 activity and entry of cells into S phase. Lin *et al.* (*30*) showed that exposure to adriamycin, cisplatin or etoposide leads to the overexpression of E2F-1. This occurs through a post-transcriptional mechanism, likely involving protein stabilization, and as a secondary phenomenon resulting from an enrichment of the G1/S arrested population. Whether E2F-1 is predominantly overexpressed or stabilized following DNA damage is not totally clear. E2F-1 is stabilized through post-transcriptional modifications such as acetylation (*31*). Acetylation increases E2F-1 DNA binding capacity and transcriptional activity (*32*). Galbiati *et al.* (*33*) observed an increase in both the total and acetylated forms of E2F-1 in U2O2 osteosarcoma cells after only 8 hours of exposure to camptothecins (topoisomerase I inhibitors). In the same study, the levels of acetylated E2F-1 peaked when cells entered the S-phase of the cell cycle and accumulated inside cells following the induction of S-phase DNA damage promoted by camptothecin (*33*).

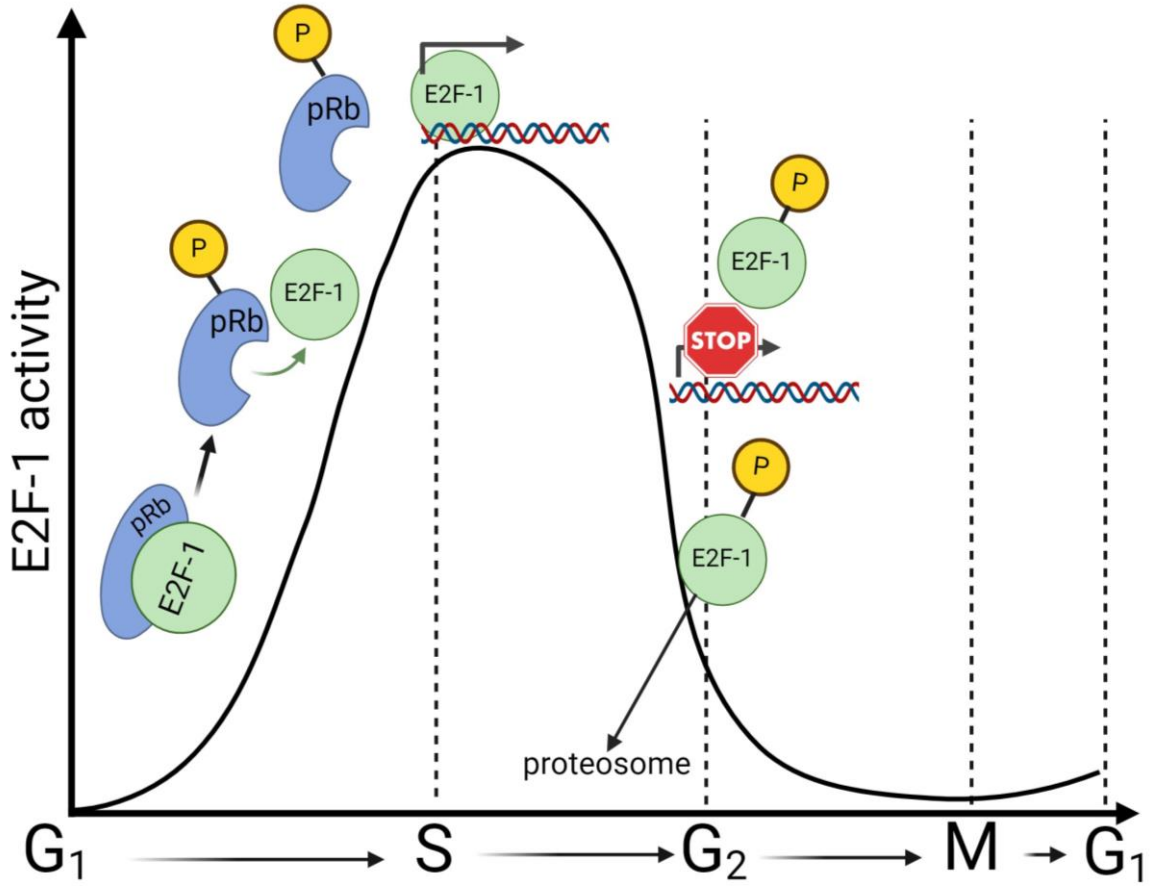

Figure 1.4. **Cell cycle regulation of E2F-1**. In G1 phase, pRB protein binds to E2F-1 and represses its transcriptional activity. Upon mitogenic stimuli, pRB is phosphorylated and free E2F-1 progressively increases in G1 and peaks in S phase to promote the expression of genes required for the S-phase transition. At the end of the S phase, E2F-1 is phosphorylated resulting in a decrease in its transcription activity. Finally, phosphorylated E2F-1 is transported to the proteasome for degradation.

1.4. The RB1-E2F pathway in cancer

The interaction between the pRB and the family of E2F transcription factors is deregulated in the majority of human cancers (*34*). Deregulation is a direct consequence of altered pRB function, which can arise from a variety of mechanisms, such as alterations of the *RB1* gene itself or in upstream pathway regulators (*34*). **Table 1.1** shows specific alterations in the RB1-E2F pathway occurring in several types of adult and childhood cancers.

Table 1.1. Frequency of the pRB pathway alterations in *RB1*, *CDKN2A* and *CCND1* in pediatric and adult cancer. Adapted from (*34*).

Cancer	*RB1*	*CDKN2A*	*CCND1*	Refs.
Pediatric high-grade gliomas	2% - Mutation	19% - Genomic loss		(*35, 36*)
Retinoblastoma	97% - Mutation 15% - Promoter methylation			(*37-39*)
Osteosarcoma	63% - Genomic Loss 6% - Mutation			(*40*)
Neuroblastoma			75% - Elevated mRNA and protein	(*41*)
Ewing sarcoma		>50% - Genomic loss		(*42*)
Head and Neck		17-27% - Promoter Methylation 25-66% - Genomic Loss		(*43*)
Breast	72% Basal-like Breast - Genomic Loss 2.7% Breast - Mutation	31% - Promoter Methylation	15-30% - Gene Amplification	(*44-47*)
Ovarian		12% - Genomic loss		(*48*)
Pancreatic		10-37% - Genomic Loss	17% - Gene Amplification	(*49-52*)

The paradigm of the alteration of the RB1-E2F pathway is found in the most frequent cancer of the retina, the retinoblastoma, in which the gene *RB1* is directly inactivated in 95% of cases (**Fig. 1.5**), most frequently due to germinal and somatic point mutations, and less frequently to gene deletions, copy-neutral loss of heterozygosity and promoter methylation (*37, 39*). Other cancers also exhibit *RB1* inactivation. Deletion of *RB1* has been found in as many as 91%–100% of small cell lung cancer (SCLC) (*53*), 72% of basal-like breast cancer (*47*), 63% of luminal B breast cancer (*47*), and 30% of prostate cancer (*54*). In childhood cancers, 63% of osteosarcomas have *RB1* deletion, and 6% of them have *RB1* mutation (*40*).

In addition to pRB aberrations, other alterations in the RB1-E2F pathway are well known mechanisms in cancer development. Negative regulators of the pathway like p16, p21 and p27 are frequently inactivated, while positive regulators such as CDKs and cyclins are often overactivated (*55*). For instance, most neuroblastomas and

25% of pancreatic adenocarcinomas show elevated protein expression of cyclin D1 due to amplification of the *CCND1* gene (*41, 52*). Loss of p16 function (gene *CDKN2A*) is another common dysregulation of the RB1-E2F pathway. *CDKN2A* deletion is present in almost 20% of pediatric high grade gliomas (*35*) and more than half of Ewing sarcomas (*42*). In adult cancer, *CDKN2A* inactivation affects 12% of ovarian cancer (*48*) and 70% of nasopharyngeal carcinoma (*56*).

Some of the main target genes overexpressed as a consequence of the action of free E2F-1 are DNA polymerase α, thymidylate synthase, proliferating cell nuclear antigen (PCNA) and ribonucleotide reductase, which are essential for G1/S-phase transition (**Fig. 1.5**) (*57*).

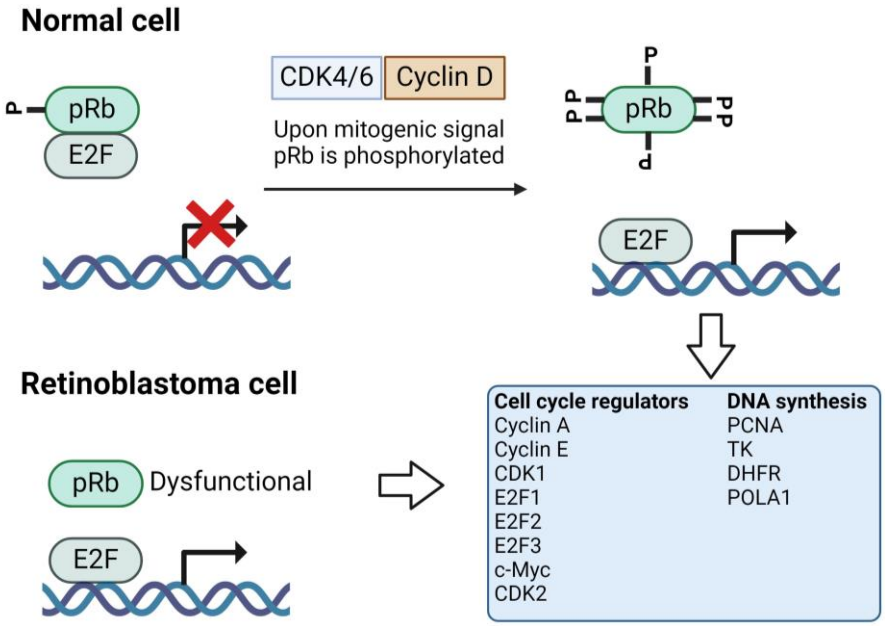

Figure 1.5. **RB1-E2F pathway**. Simplified scheme of RB1-E2F pathway in normal cells and retinoblastoma cells with dysfunctional RB1-E2F pathway. Some of the E2F target proteins that regulate different key biological pathways are shown.

1.5. Targeting the RB1-E2F pathway

As mentioned above, the main actionable targets of the RB1-E2F pathway are its upstream proteins CDK4 and CDK6 (*5*). Small molecule inhibitors of CDK4 and CDK6 (CDK4/6i) palbociclib, ribociclib and abemaciclib have been approved by the US Food and Drug Administration (FDA) for the treatment of advanced breast cancer, and several other clinical trials are ongoing (*9*). Normally, these therapies require a functional pRB to achieve antitumor response and, therefore, CDK4/6i are less effective in cells with deficient *RB1* gene (*58*).

In recent years, scientists have developed new strategies to target E2Fs with therapeutic intention (*9*). The small molecule HLM006474 has the ability to interact with the E2F4–TFDP2 complex thus decreasing the overall E2F-4 protein levels (*59*). In vivo, HLM006474 prevents tumor growth when administered in embryos in a retinoblastoma-prone mouse model (*60*). Truncated versions of the E2F-1 protein may also offer therapeutic benefit. One example is the shortened form of E2F-1 lacking the transactivation domain (*61*). This truncated protein retains its ability to bind DNA and can trigger cell death but cannot regulate genes involved in the cell cycle (*61*). By using an adenoviral delivery system, truncated E2F-1 successfully induced tumor cell death and inhibited tumor growth in tumor cells and xenograft models (*62*).

In the last years, the clinical use of oncolytic adenoviruses has become relevant in the treatment of tumors with aberrant RB1-E2F. In the next section, I will address the use of oncolytic adenoviruses with the ability to selectively replicate and induce cell lysis in cells with a dysfunctional RB1-E2F pathway.

2. Oncolytic adenoviruses

Oncolytic virotherapy consists in the use of genetically modified viruses that specifically infect and replicate in cancer cells. By introducing key genetic modifications into the viral genome, virotherapy enhances the virus ability to recognize, internalize and replicate into cancer cells, thus improving selectivity and reducing the infectivity in normal cells. The infection culminates in the lysis of the malignant cell, resulting in the release of viral particles that potentially infect surrounding cells (*63, 64*).

Among the oncolytic viruses, adenoviruses gained popularity for the treatment of cancer due to their unique biological features: i) they efficiently transfer genes to infected cells, ii) they can be easily gene-edited for better tumor targeting, and iii) they are appropriately stable during the manufacturing process (*65-67*).

Several oncolytic adenoviruses have shown promising results as monotherapy in clinical trials. DNX-2401 (Delta-24) is an exemplary case of an oncolytic adenovirus that has successfully translated from preclinical models to clinical trials, improving the outcomes for both adult and pediatric patients with high-grade gliomas (*68, 69*). In a study, a group of 25 adults with high-grade gliomas received a single intracerebral dose of DNX-2401 targeting the tumor. Five patients survived longer than 3 years from treatment and three of them had reduction of at least 95% in the enhancing tumor (*68*). The study suggested that some patients did not benefit from this therapy due to poor infection and spread of DNX-2401 after the administration, possibly because of inefficient delivery (*68*). Factors contributing to poor viral delivery and infection include i) rapid viral clearance through innate antiviral resistance mechanisms of the patient, such as antiviral cytokines (*70*) or antiviral antibodies (*71*), ii) viral sequestration and up-take in non-targeted tissues such as the liver and spleen (*72*), and iii) physical barriers, including the extracellular matrix, tumor fibrosis and tumor necrosis, which play a critical role in the penetration and propagation of the virus into the tumor (*72, 73*). Different approaches have been developed to overcome these challenges, including the modification of the viral fiber to prevent liver transduction (*74*) or the incorporation of transgenes codifying for

enzymes, such as hyaluronidase, which degrade the extracellular matrix of the tumor (*75*).

The delivery route of adenoviruses plays an important role in its oncolytic activity. Intratumoral administration directly releases the virus into the tumor site, thus circumventing many of the hurdles associated to systemic delivery. Injecting the oncolytic adenoviruses directly into the tumor ensures high local concentrations of the virus, maximizing oncolytic activity while minimizing exposure of healthy tissues and toxicity. Intratumoral injection has proven efficacy and safety for brain tumors (*68, 69, 76*). Nevertheless, despite intratumoral delivery concentrates the virus at the tumor site, activity is limited due to poor local spread of the virus through the tumor (*77*). For this reason, and to maximize virus exposure time in the tumor, repeated intratumoral injections are performed during the therapy. In some patients with difficult-to-access lesions, each intervention represents a risk. For instance, in a recent study carried out in children with high-grade pediatric gliomas located in the brainstem, 9 out of 12 patients presented adverse events related to intratumoral delivery. Most frequent side effects were vomiting, fever and trigeminal nerve disorder (*69*). Systemic (intravenous) delivery of oncolytic viruses has been evaluated for the treatment of melanoma, colorectal, lung or renal tumors (*78, 79*). This option is less invasive, but the rapid clearance by neutralizing antibodies, the sequestration of the virus in tissues and the inability of the virus to extravasate through the tumor vasculature makes intravenous delivery a still suboptimal way to target tumor cells (*72*).

Thus, the design of new therapies based on oncolytic adenoviruses must focus on enhancing virus infection and spread, thereby reducing the total number of administrations and the associated risks of such interventions. Novel therapies must overcome these barriers by incorporating new transgenes or by therapeutic combination of oncolytic adenoviruses and other agents that potentiate oncolytic activity and spread. In my thesis, I have developed a straightforward pharmacological strategy to enhance infection and spread of the oncolytic

adenovirus VCN-01 in tumors, through the concomitant administration of one anticancer drug.

2.1. Wild-type adenovirus structure

The adenovirus virions consist of a single linear segment of double-stranded DNA encased within an icosahedral protein shell known as the capsid (**Fig. 1.6**). The capsid is comprised of 240 hexon proteins, while each of the twelve corners of the icosahedral structure is capped by penton bases (*80*). The penton bases are associated to the fiber of the virus, which facilitates the attachment to the host cell via the receptor in its surface (*81*).

Each adenovirus genome has a length between 26,000 and 45,000 base pairs and has the capacity to encode more than 30 genes (*82, 83*). The genome of the adenovirus encodes for 5 units of early transcription (proteins E1A, E1B, E2, E3, and E4), two delayed early units (IX and IVa2), and a major late unit that undergoes processing to generate 5 families of late mRNAs (L1-15) (*84*). The last proteins encoded in the adenovirus genome are the components of the capsid, including the hexon (protein II), penton base (protein III), and fiber (protein IV). These proteins play essential roles in forming the capsid, which is the protective protein shell of the virus (*85*).

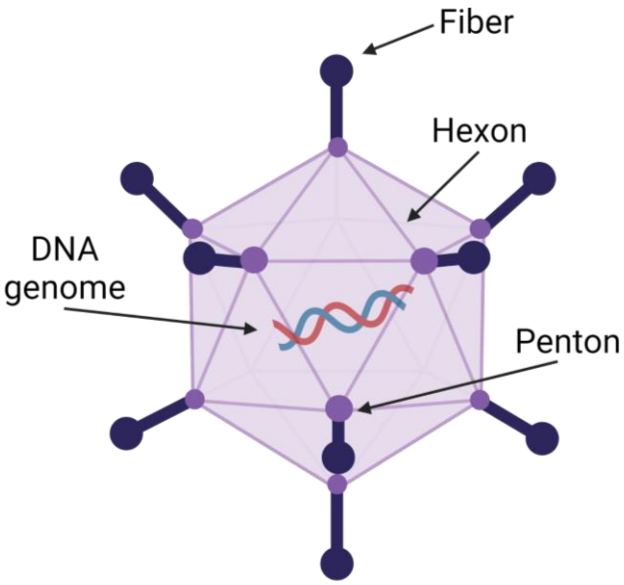

Figure 1.6. **Oncolytic adenovirus structure**. Adenoviruses have an icosahedral structure formed by the hexon proteins. Fiber proteins and penton bases mediates the virus-cell attachment. The genome of the adenovirus is a double-stranded DNA.

2.2. Transcription and replication of a wild-type adenovirus

In this PhD work, I have analyzed and quantified two specific genes codified in the adenovirus genome: the adenovirus early region 1A (*E1A*) and early region 1B (*E1B*). Both proteins are expressed during the early phase of the viral life span (*86*). E1A is the first viral transcription unit to be expressed after the adenoviral genome reaches the nucleus of the host cell. The protein encoded by *E1A* activates viral transcription and reprograms gene expression in the host cell (*86*). One of the main functions of E1A is to promote the transition from the G0 or G1 into the S-phase of the cell cycle (**Fig. 1.7**). E1A induces the expression of genes required for DNA synthesis, thus providing an optimal environment for the correct viral replication (*87*). To alter the cell cycle of the host cell, E1A interacts with endogenous proteins expressed in the infected cell, such as pRB (*88*) (**Fig. 1.7**). E1A binds to hypophosphorylated pRB (*89*). As a consequence of the interaction between E1A and pRB, E2F is released and results in the stimulation of E2F-dependent

transcription (*90*). E1A also has a pro-apoptotic behavior, through the stabilization of the tumor suppressor protein p53 (*91*) (**Fig. 1.7**).

E1Bs are antiapoptotic proteins that prevent the premature death of the host cell. The gene *E1B* codifies for two different proteins: E1B 55K and E1B 19K. E1B 55K forms an ubiquitin-ligase complex with E4Orf6 that induces the degradation of p53 (*92*). In consequence, E1B inhibits the apoptosis promoted by E1A (*93*) (**Fig. 1.7**). E1B-19K is a Bcl-2 homolog protein that directly binds the proapoptotic proteins Bax and Bak, thus inhibiting E1A-induced apoptosis through the p53-dependent and p53-independent mechanisms and allowing an efficient viral lytic cycle (**Fig. 1.7**) (*87*).

In conclusion, E1A and E1B synergistically create an optimal environment for an efficient viral replication.

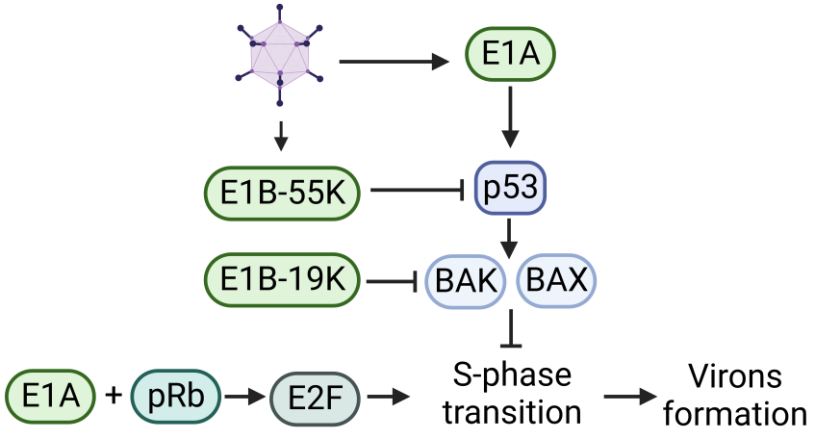

Figure 1.7. **Viral-host cell interaction**. Upon infection, E1A and E1B are the first two proteins expressed by the virus. E1A promotes cell proliferation through its binding to pRB while E1B prevents the apoptosis induced by E1A.

2.3. Oncolytic adenoviruses with E2F promoters

Recently, therapies with oncolytic viruses targeting tumor cells with high levels of E2F have emerged. By inserting E2F-responsive elements into their genome, these viruses are able to express genes and proteins in response to high levels of free E2F in the host cell, leading to enhanced viral replication and selective cell lysis (*94, 95*).

The first two oncolytic adenoviruses designed to selectively replicate in cancer cells with high free levels of E2F-1 were Ar6pAE2fE3F and Ar6pAE2fF (*96*). The selectivity of Ar6pAE2fF against tumors relied on the insertion of an E2F-1 promoter region in its genome, leading to its replication in pRB-deficient cancer cells (*96*). Ar6pAE2fF and Ar6pAE2fE3F demonstrated potent antitumor activity in a xenograft model of hepatocellular carcinoma following intratumoral administration (*96*).

The next generation of adenoviruses incorporated new modifications to improve anticancer activity. Our collaborators Ramon Alemany and Manel Cascalló at the Institut Català d'Oncologia (Barcelona) pioneered the engineering of a family of adenoviruses known as ICOVIR. These innovative adenoviruses have potent antitumor activity and achieved clinical translation. The first was ICOVIR-2, which has a deletion of eight amino acids in the pRB-binding CR2 domain that disables its capacity to release E2F from preexisting pRB/E2F complexes, thereby conferring selective replication in cells with already dysfunctional pRB control. ICOVIR-2 also contains an integrin-targeting Arg-Gly-Asp (RGD) sequence into the HI loop of the fiber, to increase the selectivity of the virus for cancer cells (*97*).

Later, ICOVIR-5 incorporated a Kozak sequence, a specific nucleotide sequence that facilitates the initiation of translation, to increase E1A levels in tumor cells by stabilizing the mRNA molecules and enhancing protein translation (*94, 98*). Further improvements led to the incorporation of eight new E2F-binding sites organized as four palindromes in addition to the endogenous ones present in the wild-type E2F1 promoter (*99*). This modification increased E1A transcription in cancer cells, leading to an improvement in viral replication and anticancer activity of ICOVIR-7 (*99*). In 2010, Guedan *et al.* incorporated a human sperm hyaluronidase (PH20) expression cassete under the control of the major late promoter (MLP) in order to degrade the extracellular matrix and enhance viral distribution into the tumor (*75*). The resulting virus was called ICOVIR-17, the predecessor of ICOVIR-17k (also known as VCN-01), which arrived to clinical phase.

In clinical trials, these oncolytic viruses have proven efficacy and safety in the treatment of patients with chemorefractory solid tumors (*100*) and pediatric gliomas (*69*). At our institution, we have recently completed a phase 1 trial of VCN-01 for

chemo-refractory intraocular retinoblastoma (*101*). **Figure 1.8** represents the genetic modifications included in the ICOVIR-family of adenoviruses.

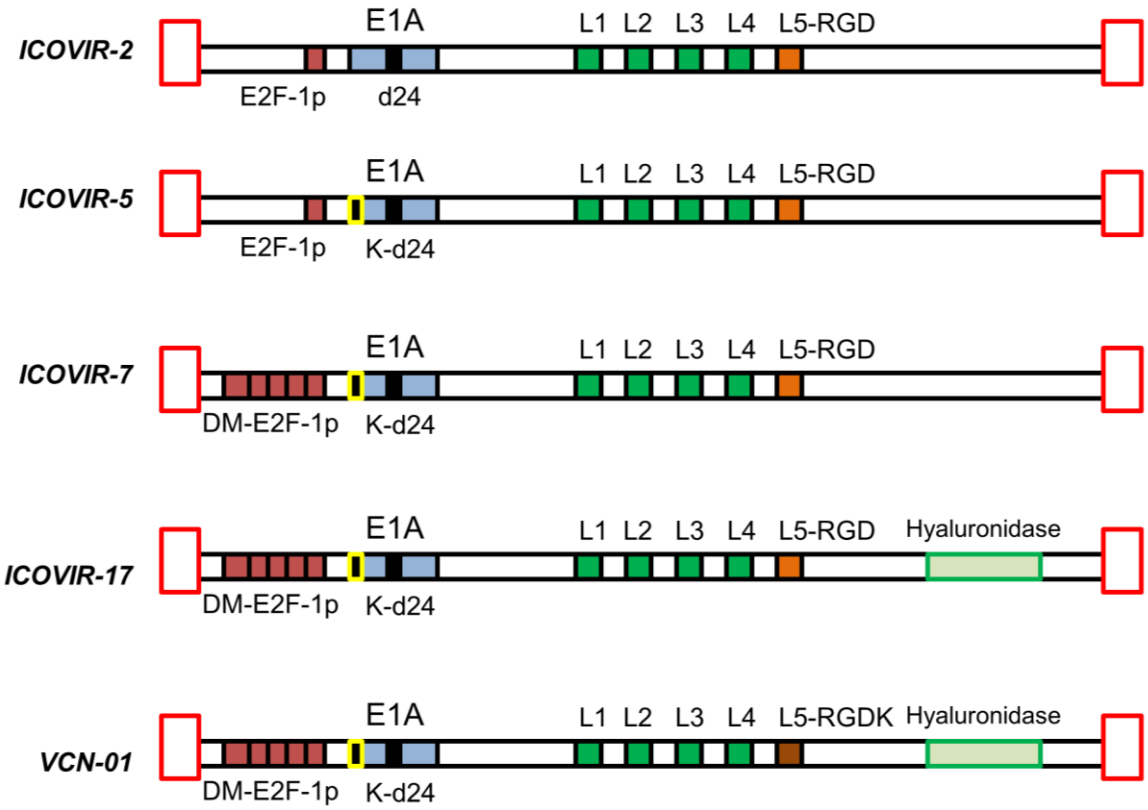

Figure 1.8. **ICOVIR-family of oncolytic adenoviruses**. Schematic representation of the genetic modifications included in ICOVIR viruses.

2.4. The oncolytic adenovirus VCN-01

VCN-01 gathers the modifications previously reported for ICOVIR-5, ICOVIR-7 and ICOVIR-17 (*95*). VCN-01 contains an additional modification in the KKTK domain of the fiber shaft, which is responsible for liver transduction in mice, rats, and nonhuman primates by interacting with heparan sulfate glycosaminoglycan receptors (*95*). The deletion of this domain prevents liver transduction of adenoviral vectors (*74*). VCN-01 also harbors a modification in the capside to incorporate the tetrapeptide RGDK (Arg-Gly-Asp-Lys) potentiating its biodistribution to tumor cells via the coxsackievirus adenovirus receptor (CAR) and α5β1 integrin receptors (**Fig. 1.9A**) (*102*). The overall goal was to increase viral internalization and selectivity, and

to promote viral transcription in cells with high levels of free E2F-1 (*94, 95*). Once internalized by endocytosis, VCN-01 replicates using components of the host cell nuclear machinery (**Fig. 1.9B, C**). Finally, cancer cells experience lysis and release new virions to infect surrounding cells (**Fig. 1.9E**) (*94*). One of the main limitations of the virotherapy is the limited penetration and distribution into the tumor (*103*). This was the reason to include a recombinant human hyaluronidase PH20 (HAse) gene in VCN-01. Following transduction, the enzyme degrades the hyaluronic acid of the tumor matrix and improves the distribution of chemotherapy in desmoplastic tumors (**Fig. 1.9D**) (*104*). As a single agent, VCN-01 is promisingly active and safe in patients with advanced solid tumors enrolled in Phase 1 clinical trials, including patients with intraocular retinoblastoma (*101, 104, 105*).

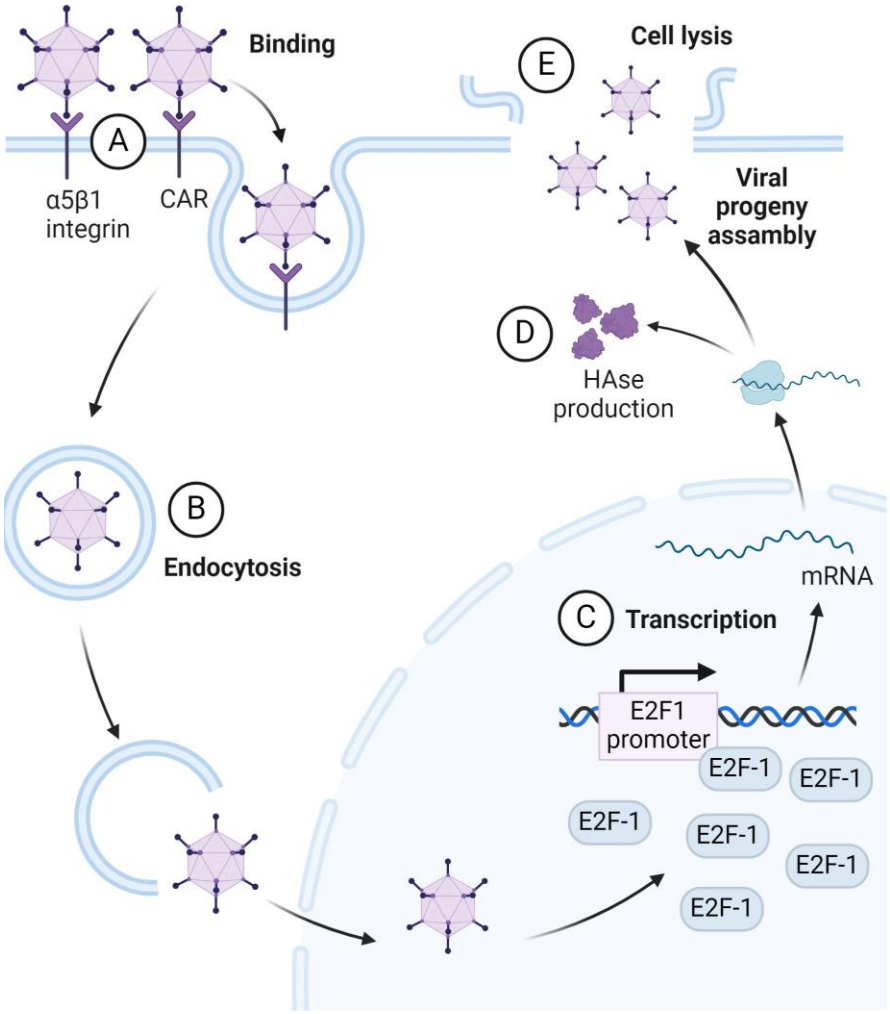

Figure 1.9. Viral cycle of VCN-01. Endocytosis of VCN-01 is mediated by CAR and α5β1 integrin receptors. In the nucleus, VCN-01 replicates using the DNA replication machinery of the host cell. VCN-01 produces hyaluronidase before cell lysis.

2.5. Combining oncolytic virus with chemotherapy

As already mentioned in this section, virotherapy has limited activity due to suboptimal tumor penetration and infection. Thus, the clinical use of oncolytic viruses will be most likely in combination with other antitumor agents that potentiate the oncolytic activity of the virus.

Viruses and chemotherapeutics interact through different mechanisms. For instance, Gomez-Manzano *et al*. (*106*) demonstrated that concomitant treatment with the oncolytic adenovirus Delta-24 and irinotecan produced a synergistic antitumor effect in gliomas, which they attributed to the virus increasing the expression of topoisomerase I, the target of irinotecan. Other study showed that pretreatment with gemcitabine or 5-FU in pancreatic cancer cells promoted the overexpression of adenoviral receptors CAR or α5β1, facilitating virus entrance into the cell (*107*). Bazan *et al*. (*104*) demonstrated that disruption of the extracellular matrix by the hyaluronidase encoded in VCN-01 enhanced tumor-uptake of gemcitabine. Gros *et al.* (*108*) demonstrated that alterations in the intracellular calcium concentration induced by verapamil enhanced antitumoral activity of ICOVIR-5, as several viruses induce cell death and progeny release by disrupting intracellular calcium homeostasis.

Chemical compounds modifying cell cycle and synchronizing tumor cells in S-phase potentiate adenoviral vector transgene expression in colon and hepatocellular carcinoma cells (*109*) and increase the oncolysis of mouse melanoma cells by reoviruses (*110*).

Recently, Koch *et al.* (*111*) demonstrated that combining the CDK4/6 inhibitor ribociclib with the oncolytic adenovirus XVir-N-31, which harbors an E2F-1 promoter, significantly enhanced viral genome production, particle formation and virus oncolytic effect. Ribociclib downregulates the expression of RB1 and E2F-1. Nevertheless, the authors reported that E2F-1 levels recovered after 12 h post

infection, indicating that adenovirus-related molecular factors regulate E2F-1 protein levels even in the presence of CDK4/6 inhibitors. This leads to an accumulation of free E2F-1, as it cannot interact with inhibited pRB. Moreover, the expression of E1A by the adenovirus directly targets the E2F/DP1 complex, resulting in the release and stabilization of E2F-1, which in turn promotes viral gene expression and replication. Ribociclib also potentiated the anti-tumor effect of XVir-N-31 in bladder cancer and Ewing sarcoma xenograft models. Two intratumoral administrations of XVir-N-31 followed by 5 daily doses of ribociclib significantly reduced tumor volume compared to the control group and the individual treatments (*111*).

Several clinical trials emerged from such preclinical studies combining virotherapy and chemotherapy. Phase 1/2 clinical trials have evaluated combinations of viruses with chemotherapeutic agents for the treatment of breast cancer (*112, 113*), advanced solid tumors (*105*), soft-tissue sarcomas (*114*), glioblastoma (NCT01956734), pancreatic cancer (*115*) and ovarian cancer (*116*).

In my thesis, I have explored the preclinical effect of the combination of VCN-01 with drugs used in the treatment of retinoblastoma.

3. Targeting the RB1 pathway in pediatric cancers

Cancer is the leading cause of death in humans under the adult age. Each year, approximately 300,000 children, teenagers and young adults are diagnosed with cancer worldwide (*117, 118*). The main pediatric and young adult cancers are grouped as (i) leukemias and lymphomas, (ii) soft-tissue and bone tumors (such as osteosarcomas or Ewing sarcomas), (iii) other solid tumors (such as neuroblastic tumors, germ cell tumors, eye tumors, genital tumors, digestive system tumors, endocrine tumors, head and neck tumors, thoracic tumors and skin tumors) and (iv) central nervous system (CNS) tumors (such as diffuse intrinsic pontine gliomas, ependymomas or meduloblastomas) (*119*). Pediatric cancers are heterogeneous, making diagnosis and treatment especially challenging (*120*). Recent improvements in their molecular and genetic characterization have led to more accurate diagnosis and novel therapies, such as molecularly targeted therapies, or immunotherapy (*121*). Despite 80% of pediatric cancers are curable, over 40% of survivors will experience significant long-term side effects resulting from their disease of from the therapies they received (*122, 123*). Malignancies such as retinoblastoma or sarcomas might require radical and aggressive measures including eye enucleation or limb amputation, respectively (*122*). Thus, there is an urgent need to seek for alternative therapies or to enhance the existing ones, in order to reduce the side effects of cancer therapies and to prevent second pathologies.

The main goal of this doctoral thesis was to develop a new and selective treatment for retinoblastoma, the most frequent cancer of the retina in children. I expanded the results of the thesis to neuroblastoma and Ewing sarcoma. These tumors represent a particular challenge for pediatric oncologists due to their high morbidity and mortality rates after they develop resistance to conventional therapies. My thesis, and previous work by my laboratory mate Guillem Pascual Pastó, leveraged on the abnormality of the RB1-E2F pathway in these cancers (*101*). As already mentioned, more than 95% of retinoblastoma cases show mutations in the gene *RB1* as the key driver of tumorigenesis. Most patients with Ewing sarcoma and neuroblastoma also have a dysfunctional RB1-E2F pathway in their tumors, although usually not through

RB1 mutations (*41, 42*). In all cases, the final result of this genomic malfunction is the accumulation of a transcription factor E2F-1 in malignant cells, which is the common ground of these cancers and the targeting strategy addressed by this thesis. In this section, I will describe the diseases for which we intend to develop new treatments, with a focus on the RB1/E2F aberrations identified in these conditions. I will introduce different types of chemotherapeutics used in retinoblastoma and I will also mention the preclinical models of disease used in this work.

3.1. General genomic landscape of pediatric cancers

Childhood cancers present unique sets of genomic alterations, both somatic (i.e., those located only in the cancer cells) and germline (i.e., those carried by all cells of the patient, including cancer cells) (*124*). Recent genomic discoveries have improved our comprehension of the mechanisms driving pediatric cancer and have facilitated the identification of novel clinically relevant subtypes (*120*). Genetic alterations found in childhood cancer are very different, in general, than those of adult cancers. One notable distinction is the significantly lower number of somatic mutations found in most pediatric cancers in comparison to adult cancers (**Fig. 1.10**) (*125, 126*), which are due to aging-related events accumulating during the lifetime of one individual (*127*). Most cancers in adults develop after prolonged exposure to carcinogenic substances such as tobacco or UV radiation (*127*). Understanding these genetic differences is crucial for developing tailored treatments that improve outcomes for pediatric cancer patients.

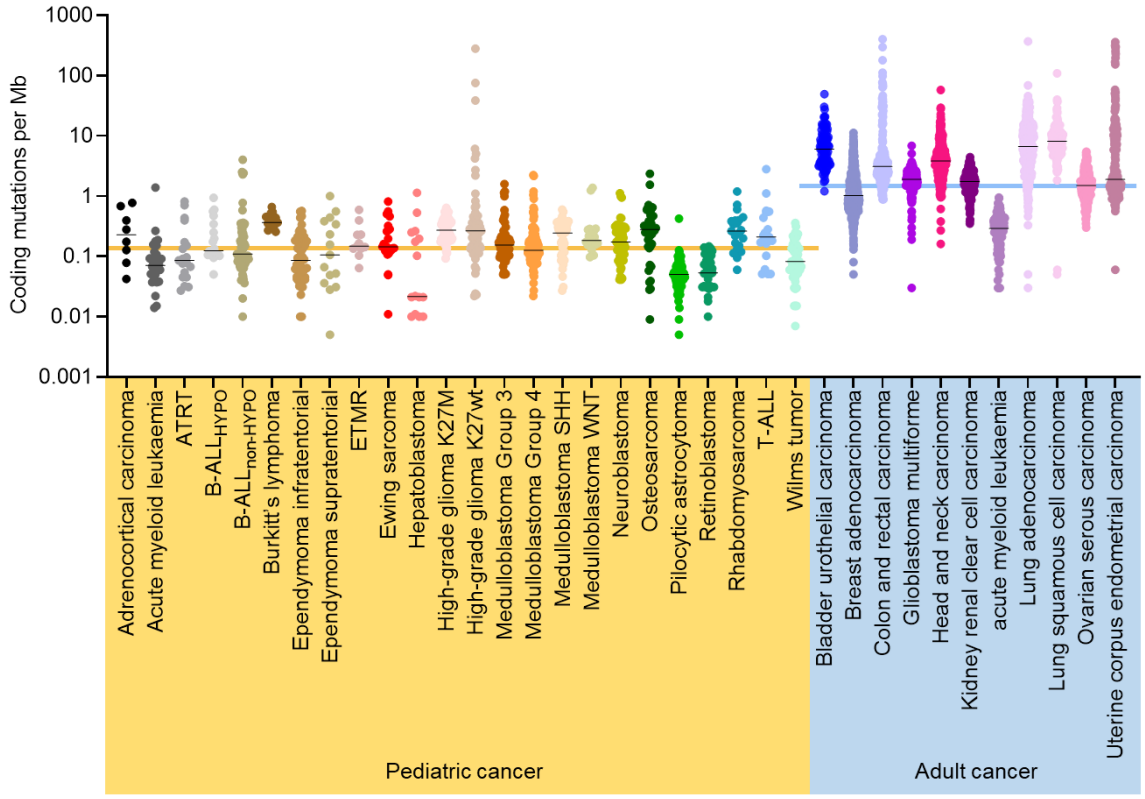

Figure 1.10. Somatic mutations in a pediatric and adult cancer cohort. Somatic coding mutation frequencies in 24 pediatric (n = 879 primary tumors) and 11 adult (n = 3,281) cancer types. Median mutation loads are shown as lines (orange, all pediatric; blue, all adult). Adapted from: Gröbner, S., Worst, B., Weischenfeldt, J. *et al*. The landscape of genomic alterations across childhood cancers. Nature 555, 321–327 (2018).

Germline mutations are less frequent than somatic ones, but they are relatively common in both adult and pediatric cancers (*128, 129*). A recent study in 1,120 patients estimated that about 8% of children with cancer harbor a hereditary predisposition in their genome (*130*). Another study identified the most usual germline mutations in pediatric cancer, being *TP53* the most frequently mutated gene (4% of childhood tumors), followed by *NF1, BRCA2* and *RB1* (1–2% of tumors; **Fig. 1.11**) (*129*). These mutations predominantly occur in tumor suppressor genes (*129*).

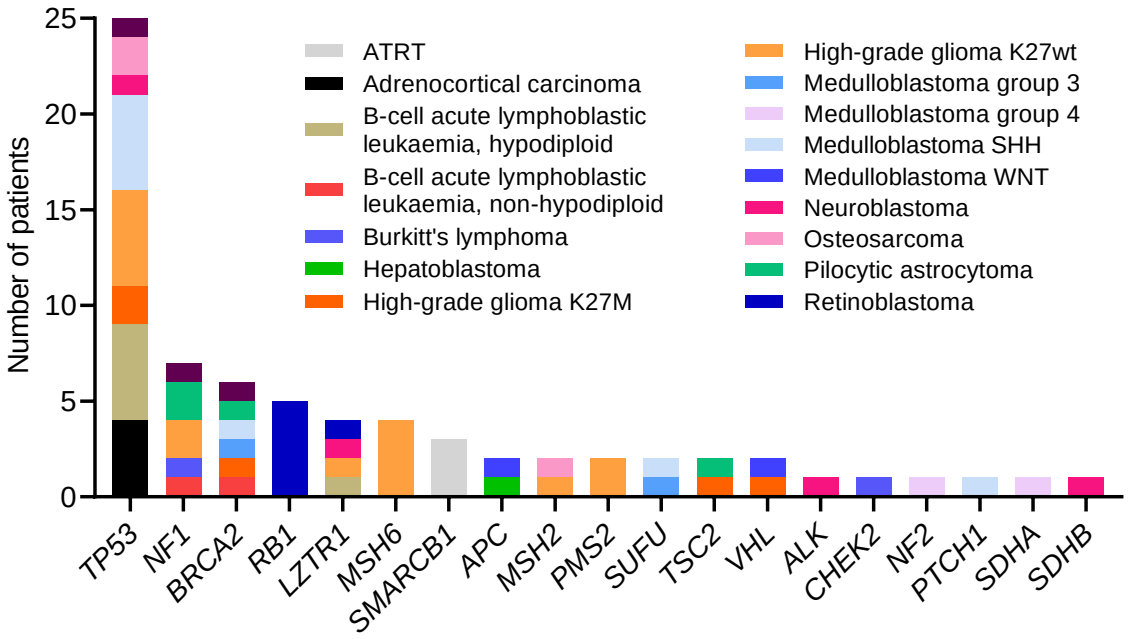

Figure 1.11. Germline mutations in cancer predisposition genes. Top mutated genes sorted by number of affected samples in 16 different pediatric tumors (n = 914 tumors). Adapted from: Gröbner, S., Worst, B., Weischenfeldt, J. *et al*. The landscape of genomic alterations across childhood cancers. Nature 555, 321–327 (2018).

Tumorigenesis of pediatric cancers can be attributed to several genomic alterations, most of them uniquely found in the pediatric setting (*120, 131*). *PAX3-FOXO1* and *EWSR-FLI1* gene fusions are drivers of alveolar rhabdomyosarcomas and Ewing sarcomas, respectively (*120*). Specific genome regions containing oncogenes are recurrently amplified. *MYCN* amplification is present in 16% of neuroblastomas (*132*) and approximately 2% of retinoblastomas, being these subtypes the most aggressive (*39*). Furthermore, some types of childhood cancer tumorigenesis are driven by epigenetic events (*120*). For instance, mutations in histone 3 in diffuse midline gliomas lead to epigenomic reprogramming events that trigger tumorigenesis (*133*).

In summary, understanding the genetic backgrounds of pediatric cancers is crucial for delivering optimal treatments. Our research has specifically targeted the disruption of the RB1-E2F pathway, particularly relevant in retinoblastoma and other

pediatric tumors. These alterations underscore the importance of precisely identifying genetic abnormalities to tailor therapy and enhance clinical outcomes in pediatric patients.

3.2. Retinoblastoma: the prototype of cancer with mutant *RB1*

Retinoblastoma is the most frequent intraocular cancer in children, with approximately 8,000 newly diagnosed cases per year worldwide (*134-136*). This disease occurs during the development of the retina, due to the inactivation of both alleles of the retinoblastoma gene (*RB1*) within the adequate precursor retinal cell (*136, 137*). The intraocular tumors can develop unilaterally (in one eye, 60% cases) or bilaterally (in both eyes, 40% cases, related to germinal mutations in *RB1*) (*136, 138*). One of the most characteristic signs of retinoblastoma at diagnosis is the leukocoria (white pupillary reflex) (*134*). Although it is the first event, loss of function of pRB is usually not sufficient for tumorigenesis. Most $RB1^{-/-}$ retinoblastomas have chromosome copy-number alterations in the 1q+, 2p+ and 6p+ regions that trigger overexpression of *MDM4, KIF14, CRB1, NEK7*, *MYCN, DEK, E2F3* and *SOX4* genes, driving retinoblastoma malignant transformation (*135, 136*). Whereas both *RB1* alleles are mutated in nearly all retinoblastomas, a subset of unilateral tumors (less than 2%) show no evidence of *RB1* mutation but instead present high-level of amplification of the oncogene *MYCN* (*135*). In this thesis, I handled samples from retinoblastoma patients having biallelic *RB1* mutation with or without *MYCN* amplification alterations. Recently, a new study of retinoblastoma identified two distinct subtypes characterized by different molecular, pathological, and clinical features. Subtype 1 tumors are those diagnosed at early ages and exhibit a more differentiated phenotype. In contrast, subtype 2, diagnosed later, have higher heterogeneity and significantly increased activation of *E2F* and *MYC/MYCN* (*39*). This subtype also has a higher propensity for metastasis and displays high stemness features. The study validated these transcriptomic signatures in two independent retinoblastoma cohorts, underscoring the relevance of this classification (*39*). The identification of these subtypes holds significant implications for retinoblastoma,

particularly in developing targeted therapies. For instance, therapies like VCN-01, which specifically targets high levels of E2F-1, could be more effective for treating subtype 2 tumors.

Patient survival is higher than 95% in high-income countries but lower than 30% globally (*135*) (**Fig. 1.12**). Early detection is crucial for successful treatment of these tumors, as it enables rapid intervention that can potentially cure the cancer and preserve the affected eye(s) and vision (*134, 135*).

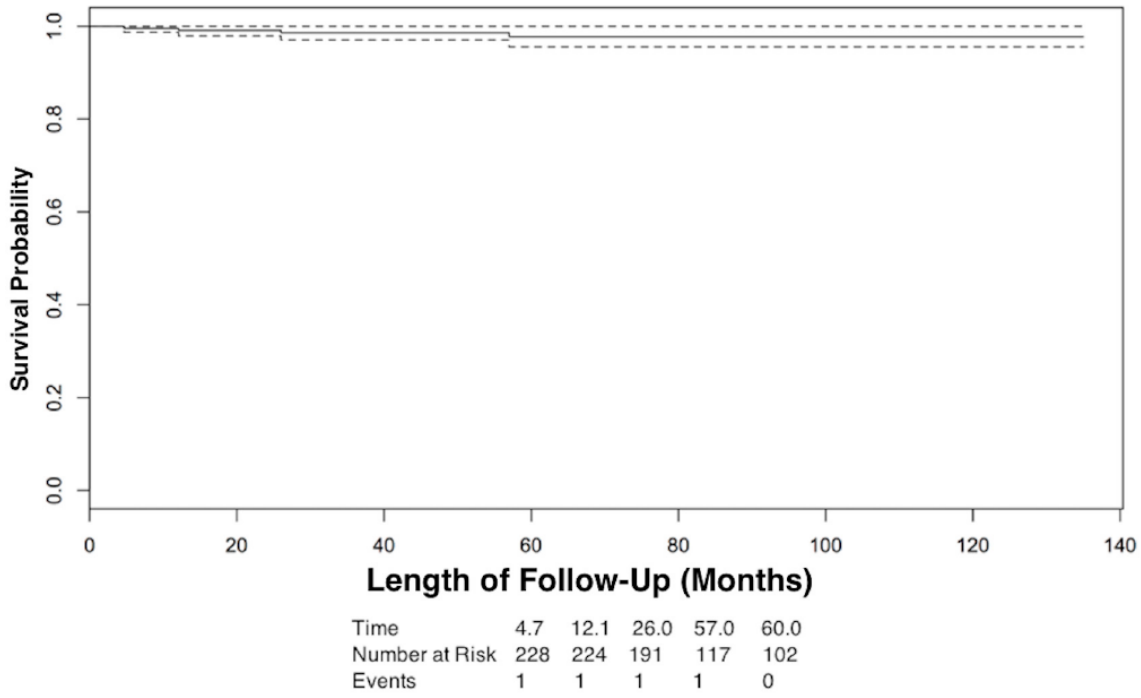

Figure 1.12. Retinoblastoma overall survival at 5 years. Kaplan-Meier survival curve of overall survival over time of follow-up of 228 patients. The dotted line is the 95% CI. Extracted from: Lu JE, *et al*. Metastases and death rates after primary enucleation of unilateral retinoblastoma in the USA 2007–2017. British Journal of Ophthalmology, 103:1272-1277;2019.

Metastatic retinoblastoma is very rare in high-income countries (*139*). However, in low-income countries the delayed diagnosis contributes to tumor extension, which may be fatal (*134*). Retinoblastoma may metastasize to the CNS, bone, bone marrow or lymph nodes (**Fig. 1.13**). In most cases, when metastatic disease is

present at the time of diagnosis, the cancer has extensively spread beyond the eye to the surrounding orbital area and distant locations (*140*). Analysis through quantitative polymerase chain reaction (RT-qPCR) of the tumor marker called cone-rod homeobox (*CRX*) transcription factor messenger RNA now allows for the detection of minimal residual disease in the bone marrow and cerebrospinal fluid (CSF), at the time of diagnosis and during follow-up (*141*). In this thesis, I have used the CRX technique, which we used previously (*101, 142*) to quantify tumor burden in a murine model of CNS metastatic retinoblastoma.

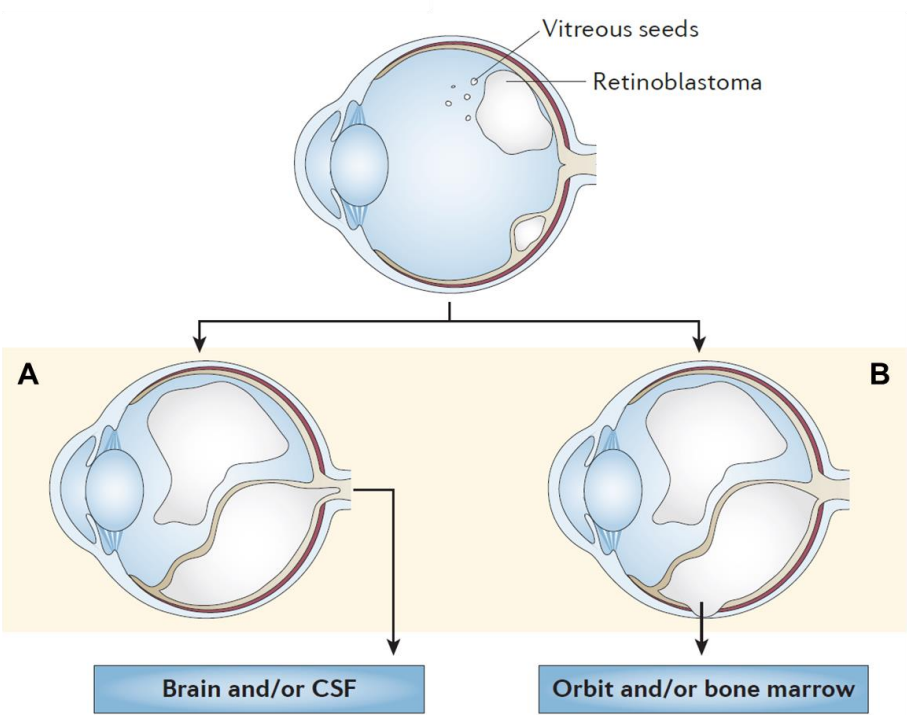

Figure 1.13. Retinoblastoma dissemination pattern. Retinoblastoma invades the brain and cerebrospinal fluid (CSF) through direct optic nerve dissemination (A) whereas tumors with choroid and scleral infiltration metastasize to systemic tissues through the blood (B). Modified from: Dimaras H, *et al*. Retinoblastoma. Nat Rev Dis Primers. 2015 Aug; 27;1:15021.

Patients with CNS metastases have the poorest prognosis (*134, 140*). Recently, a study conducted on 228 retinoblastoma patients diagnosed between 2007 and 2017 revealed that among the nine observed cases of metastasis (3.9% of patients), five of them (2.2%) had CNS dissemination (*143*). The overall survival for the group was

98% at five years, but the four patients who died from the disease were among those having CNS metastatic retinoblastoma (*143*). CNS dissemination primarily occurs through direct extension of the tumor via the optic nerve (*144*). Then, cells settle in the CSF and occupy the leptomeningeal space of the brain and the spinal cord (**Fig. 1.14**) producing intracranial pressure which may cause headache, irritability, vomiting, vision loss, and less commonly, focal neurological signs in the patient (*134*). Cytological analysis can identify retinoblastoma dissemination into the CSF or the bone marrow, but molecular techniques such as quantifying *CRX* mRNA or detecting patient-specific *RB1* mutations or genomic alterations are more sensitive to monitor CSF disease progression (*145*). In this PhD thesis, I will present data of a CNS metastatic model of retinoblastoma which occupies the leptomeningeal space of immunodeficient mice.

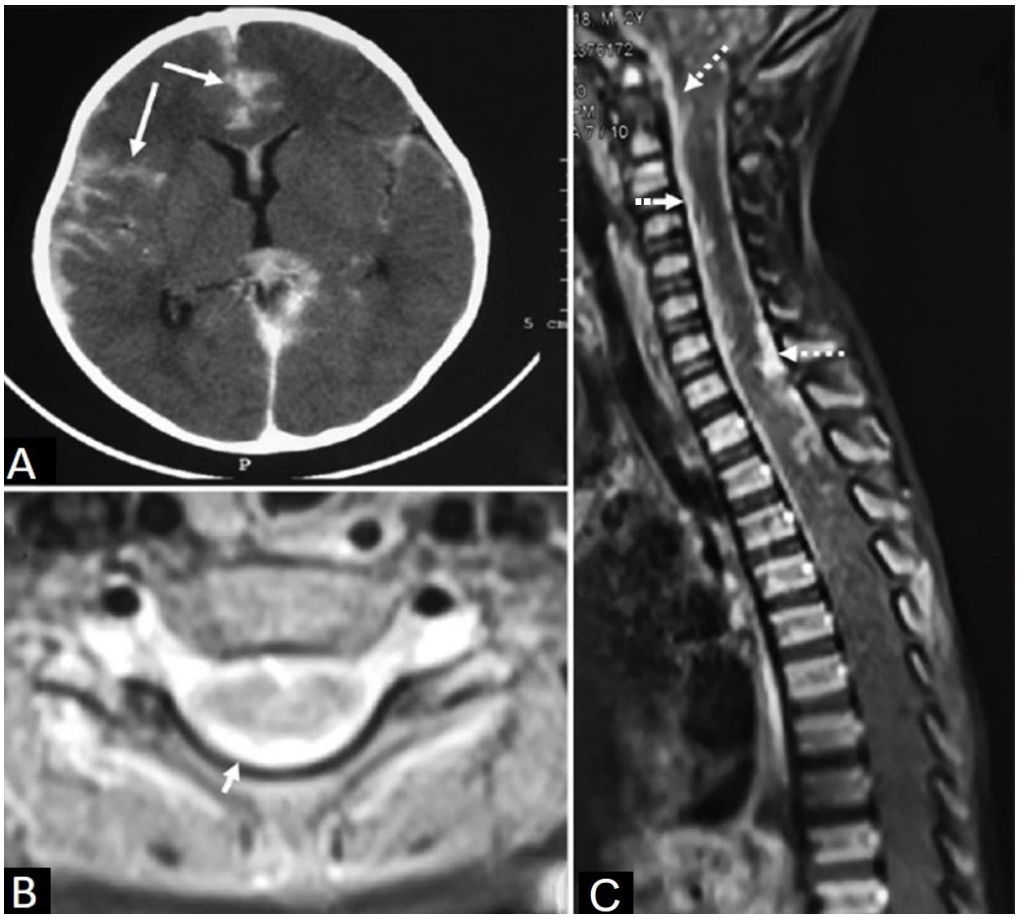

Figure 1.14. **Magnetic resonance of a patient with CNS metastatic retinoblastoma**. A, Diffuse leptomeningeal infiltration (solid arrows). B, Sagittal image of the cervical spine with leptomeningeal

extension (solid arrow). C, Axial image of the spinal cord with multifocal metastasis (dotted arrows). Extracted from: Roy P, Singh U, Tadepalli S, Ahuja C, Bansal D. Retinoblastoma with spinal cord metastasis: When an eye tumor bites the cord! Indian Journal of Ophthalmology - Case Reports. 1(4):842-3; 2021.

When it remains confined into the ocular globe, retinoblastoma does not represent a life-threatening risk to the patient and is generally recognized as a tumor with a favorable prognosis. Clinical management is focused on the eradication of the ocular tumor and the conservation of the vision. In the case the ocular tumor cannot be eradicated, enucleation (surgical removal) of the eye is prioritized, to prevent metastasis. Among the current therapies, the most important is the intra-arterial delivery of chemotherapy in the ophthalmic artery. This approach is effective to cure retinoblastoma because it increases drug concentration in the retinal tumor, by saturating the blood-retinal barrier after achieving high local drug concentration (*146, 147*). Nevertheless, the presence of vitreous seeds (free floating tumor in the vitreous humor of the eye) makes difficult the preservation of the eye, because even the selective intra-arterial chemotherapy is not sufficiently penetrant and persistent in the vitreous humor. In such cases, intravitreal chemotherapy enhances drug bioavailability in the vitreous and leads to improving ocular salvage (*148*).

Elevated drug exposure in the ocular globe is associated with long-term retinal toxicity in a significant number of patients, which may lead to vision problems (*149, 150*). In addition, even after receiving local chemotherapies, some tumors progress to a chemorefractory phenotype (*151*). In such cases, enucleation is performed to prevent extraocular metastases, at the cost of complete vision loss in bilaterally affected patients. My thesis aims to develop alternative therapies for those patients who do not respond to current treatments. Combinatorial regimens with chemotherapy and virotherapy may represent the next step in the treatment of refractory patients.

For the treatment of metastatic retinoblastoma, a more aggressive approach is often required, which may involve administering high doses of chemotherapy, radiotherapy and autologous stem cell rescue (*152*). In these difficult cases, systemic exposure to genotoxic agents increases the risk of secondary malignant

neoplasms in individuals harboring germline *RB1* mutation. For instance, among patients who have undergone radiotherapy, there is a 50% probability of developing secondary induced neoplasms within a 50-year follow-up period (*153*). Another study performed in 602 retinoblastoma survivors revealed that the most prevalent induced tumors were sarcomas (68%), carcinomas (14%), melanomas (8%), leukemia and lymphoma (4%) (*154*). Thus, for refractory and especially for CNS metastatic retinoblastomas, there is an urgent need to seek for more selective and less toxic therapies. One of such potentially fewer toxic therapies developed for patients with CNS metastases is the intrathecal chemotherapy with topotecan (*155*). Nevertheless, results of these studies are still insufficient and CNS metastatic retinoblastoma is still considered an incurable disease (*134*). In this PhD thesis, I will present a new and effective treatment for CNS metastatic retinoblastoma in murine models, based on the combination of topotecan and the oncolytic virus VCN-01.

3.3. Neuroblastoma and Ewing sarcoma are additional pediatric tumors with dysfunctional RB1/E2F-1

Neuroblastoma, a neuroendocrine tumor, is the most common extra cranial solid tumor of the childhood (*156*). Neuroblastoma originates during the early stages of development of the sympathetic nervous system, specifically from neural crest elements (*157*). Primary tumors arise in the adrenal glands and/or the sympathetic ganglia (*156*).

Neuroblastoma tumorigenesis is associated to genomic alterations including gene amplifications, polymorphisms and chromosomal alterations. High-risk neuroblastoma is often associated with the amplification of the gene *MYCN*, which is detected in roughly 20% of tumors. The protein codified in *MYCN*, N-MYC is a key regulator of the transcription, activating genes involved in cell cycle progression and growth and simultaneously repressing genes associated with cellular differentiation (*158*). Dysfunctional N-MYC drives abnormal cell proliferation and impaired differentiation (*158*). The relationship between N-MYC and the RB1/E2F axis is well established. N-MYC induces the expression of positive cell cycle regulators,

including CDKs, cyclins and E2F transcription factors. N-MYC induces the hyperactivation of cyclin/CDK complexes and it also antagonizes cell cycle inhibitors such as p21 and p27 by blocking p21 transcription and inducing Skp2, which leads to p27 degradation (*159, 160*).

Among other genomic alterations in neuroblastoma, the amplification of *CDK4* and deletion of the *CDKN2A* gene have a significant impact on the RB1/E2F axis, leading to enhanced cell cycle progression (*161*).

The Staging System of the International Neuroblastoma Risk Group (INRGSS) classifies metastatic disease (stage M) as any primary tumor spreading to distant lymph nodes, bone marrow, bone, liver, skin or other organs, except in children younger than 18 months with metastases restricted to liver, skin, and/or limited marrow involvement, which are categorized as metastatic special (stage MS)(*162*). All patients with stage M neuroblastoma are classified as high-risk, with the exception of those with age < 12 months without MYCN amplification and those aged between 12 and 18 months without MYCN amplification, with favorable histology following the International Neuroblastoma Pathology Classification (INPC) (*163*), as well as a ploidy greater than 1, who are classified as intermediate-risk (*162*). In summary, all patients with stage M neuroblastoma are classified as high-risk if their tumors have MYCN amplification or if they are diagnosed after 18 months of age, regardless of their MYCN status (*162*).

Standard of care treatment for high-risk neuroblastoma has changed significantly along the last 20 years, increasing the 5-year survival from less than 20% to more than 50% (*164*). Treatment outcomes improved considerably upon the addition of anti–disialoganglioside 2 (GD2) immunotherapy to the standard of care (intensive chemotherapy, surgery and radiation)(*165*). With the approved clinical use of anti-GD2 immunotherapy, the natural history of the disease is changing and patients who were considered incurable before, now achieve long-term survival (*166*). The best series report over 70% long term survival rates for high-risk neuroblastoma patients with the integration of anti-GD2 immunotherapy into the standard of care management (*165, 167, 168*). Nevertheless, a significant number of patients still experience relapsed and refractory disease, carrying very poor prognosis (*169, 170*).

Treatments for relapsed neuroblastoma are high doses of topotecan with cyclophosphamide (*171*), irinotecan with temozolomide (*172*) or topotecan with temozolomide (*173*), but they are not sufficiently efficacious and the overall-survival rates remain low (*174*).

Ewing sarcoma is an aggressive bone tumor of children and young adults, with an incidence of one case per 1.5 million population, accounting for approximately 2% of childhood cancers (*175*). It is the second most prevalent bone cancer in children and can develop in any area of the body, with the pelvis and proximal long bones being the most frequently affected regions (*176*).

Genetically, Ewing sarcoma is characterized by the *EWSR1–FLI1* translocation occurring in 85% of the cases (*176*). This translocation involves the fusion of the *EWSR1* gene on chromosome 22 with the *FLI1* gene on chromosome 11. The resulting EWSR1–FLI1 fusion protein plays a crucial role in the development of the disease. Ewing sarcoma can also exhibit other genomic aberrations such as *STAG2*, *TP53* and *CDKN2A* deletions (*42*). Some of the aberrations found in Ewing sarcoma are involved in the RB1/E2F1 pathway. For instance, more than half of the tumors carry a *CDKN2A* (p16) deletion (*42*). Dysfunctional p16 fails to inhibit cyclin D-CDK4/6 complex, leading to a lack of pRB phosphorylation and further promoting uncontrolled cell proliferation (*21*).

Survival rate of Ewing sarcoma is around 65-70% for patients with localized disease (*177*). Patients with early diagnosed disease may benefit from a treatment plan that involves a combination of chemotherapeutics and local control measures, such as surgery and/or radiotherapy. Current protocols include the intense use of chemotherapy with vinca alkaloids, alkylating agents, anthracyclines and topoisomerase ll inhibitors (*178*). Alternative options such as the combination of systemic vincristine, irinotecan, and temozolomide (*179*) or vincristine, topotecan and cyclophosphamide (*180*) have also been tested for the management of Ewing sarcoma.

At our institution, Hospital SJD, we classify Ewing sarcoma patients into two groups: standard risk or high risk. High risk Ewing sarcoma is defined by the presence of

metastasis, a primary tumor located in the pelvis or axial skeleton, or bone marrow metastasis. Patients who do not meet any of these criteria are classified as standard risk (*181*).

Ewing sarcoma predominantly spreads via the bloodstream and the most common metastatic sites are the lungs, bones or bone marrow, whereas other sites are rare (*176*). Survival rate for metastatic disease drops to approximately 30% (*176*).

Management of metastatic disease represents one of most challenging aspect of Ewing sarcoma treatment. Therapeutic options for this stage are few but some patients with lung metastases may benefit from irradiation (*182*). Some centers have used high-dose busulfan and melphalan chemotherapy and autologous stem cell transplantation, but we do not use such therapeutic strategies at our center (*183*). After treatments, survivors experience treatment-related complications as limb amputations or secondary malignancies that can significantly impact in their quality of life (*184*).

Patients with relapsed Ewing sarcoma carry very poor prognosis; patients who relapse within 24 months after diagnosis have a 5-year survival of less than 10% (*185*). Relapse in patients with Ewing sarcoma can occur due to the presence of highly resistant clone of tumor cells, which may have either pre-existed in the primary tumor or developed during anticancer treatment (*186*). Even though treatment for relapsed Ewing sarcoma is relatively limited, some patients may benefit from the combination of specific agents. One combination includes the use of vincristine, irinotecan, and temozolomide agents (*179*) while another combination involves temsirolimus in combination with irinotecan and temozolomide (*187*).

In conclusion, despite current advances in treatments, high-risk neuroblastoma and metastatic or relapsed Ewing sarcoma remain life-threatening diseases. The development of targeted and effective therapies is critical for addressing these challenges and improving patient outcomes. In this thesis, I have tested the combination of VCN-01 with irinotecan/topotecan for Ewing sarcoma and neuroblastoma tumors, both characterized by a dysfunctional RB1/E2F1 pathway.

3.4. Chemotherapy for retinoblastoma

Chemotherapy involves the administration of one or more anticancer drugs as part of a structured regimen. These chemotherapeutic agents are categorized based on their chemical structure and specific mechanisms of action, targeting key molecules or proteins involved in cell cycle regulation and mitosis (*188, 189*). For instance, alkylating agents directly bind to DNA, producing double-strand breaks and ultimately inducing apoptosis (*190*). Other chemotherapeutic agents, such as vinca alkaloids, interfere in the mitotic process by disrupting microtubules (*191*).

The selection of chemotherapy depends, among other factors, on the molecular characteristics of the tumor. Ideally, for each type of tumor there should be corresponding chemotherapeutic agents developed to specifically target and inhibit tumor-specific features. However, due to the uniqueness of pediatric cancer alterations, there are less drugs available, compared to those used for adult cancers. In fact, the majority of chemotherapy drugs are initially approved only for adult cancers, creating a gap between pediatric and adult diseases. Also, the selection of the chemotherapy used for pediatric cancers requires special attention, because patients are still developing and growing organs are more susceptible to long-term toxicities (*192*). Recently, the FDA approved drugs such as trametinib and nivolumab for specific types of pediatric cancers, highlighting the feasibility to develop more specific treatments for our set of patients.

The introduction of chemotherapy in the treatment of retinoblastoma reshaped the landscape in ocular oncology. In the late 1990s, the approach to conservative treatment evolved, moving away from external beam radiotherapy towards systemic chemotherapy in combination with focal therapies. The introduction of intra-arterial and intravitreal drug delivery methods resulted in remarkable success where systemic chemotherapy had previously shown poorer results (*193, 194*). These innovative therapies have now become the standard treatment in many centers in high and middle income countries. At our institution, we advocate for the selective release of chemotherapy within the ocular globe through either intravitreal or intra-arterial administration of the drugs. We employ three different chemotherapeutic

agents delivered via these different routes: carboplatin, melphalan, and topotecan (*135*). Localized delivery of chemotherapy allows us to achieve high cure rates of up to 95% (*135*). However, these therapies are associated with adverse effects, such as chorioretinal atrophy (*134, 193*). In fact, other institutions avoid intra-arterial chemotherapy due to its associated toxicity. They opt for a standard combination of systemic chemotherapy, including carboplatin, vincristine, and etoposide (*135*). Systemic chemotherapy typically causes mild acute toxicity, mostly involving alopecia, nausea/vomiting, and moderate myelotoxicity (*135*), but they are clearly less effective than localized chemotherapies to preserve the eyes (*195*) .

Carboplatin and melphalan work as alkylating agents, etoposide inhibits topoisomerase II, and topotecan is a topoisomerase I inhibitor. Chemotherapeutic agents used in the treatment of retinoblastoma can also be used in other pediatric cancers. For instance, drugs like topotecan and irinotecan, from the camptothecin family, are used in the treatment of Ewing sarcoma and neuroblastoma (*171-173, 179, 187*).

In the following subsections I will describe the main chemotherapeutic agents used in this PhD work.

3.4.1. Camptothecins: inhibitors of topoisomerase I

Camptothecins are a group of cytotoxic drug derivatives from the alkaloid camptothecin, extracted from the Chinese tree *Camptotheca acuminata* (*196*). They bind to the complex formed between topoisomerase I and DNA, leading to the formation of a ternary complex which induces DNA damage (*197*). Camptothecins specifically cause DNA damage during the S-phase of the cell cycle, but have no effect during the G1 (*198*). Upon camptothecin treatment, cells experience an S-phase arrest (*199, 200*). Thus, cell cycle arrest promoted by camptothecins may create an opportunity for synergy with viruses that exploit cell cycle dysregulation for replication.

In this work, we have used three drugs derived from camptothecins, topotecan, irinotecan and SN-38 (the active metabolite of irinotecan). Its structures are represented in the **Figure 1.15**.

Retinoblastoma sensitivity to topotecan has been reported in preclinical models (*201*) and in pediatric patients (*202, 203*). In 2005, Laurie *et al.* (*204*) first reported the 50% inhibitory concentration (IC_{50}) of topotecan in two retinoblastoma cell lines, 30 nM for Y79 and 20 nM for Weri1. They demonstrated strong antitumor activity in mice treated with topotecan in combination with systemic carboplatin (*204*). In 1994, it was reported that the optimal clinical schedule of systemic topotecan for pediatric patients involved a short 30-minute daily infusion over 5 consecutive days, starting with a fixed dose of 3 mg/m² and repeating the same schedule after a one-week break (*205*). For *in vivo* efficacy studies, we and others have adapted this schedule (*201, 206*). We used a dose of 0.6 kg/mg daily for 5 consecutive weeks and repeated the same schedule after 2 days off. In 2013, Schaiquevich *et al.* (*207*) demonstrated the superior efficacy of intra-arterial compared to sequential periocular-intravenous topotecan-based regimens in 18 patients with intraocular retinoblastoma. Intrathecal administration of topotecan is also used for patients with CNS dissemination of retinoblastoma (*208*). Topotecan offers several advantages over other chemotherapeutics. For instance, it has a longer intraocular half-life, minimal ocular toxicity, and is cheaper compared to melphalan (*195*).

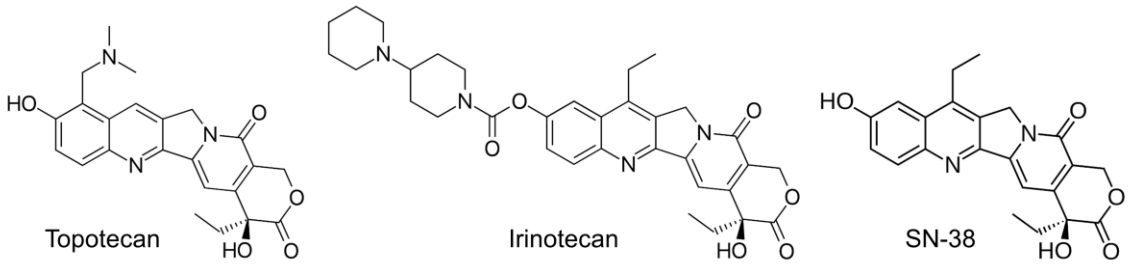

Figure 1.15. Chemical structure of topotecan, irinotecan and SN-38. The derivatives of camptothecin maintain the principal structure of the original compound with minimal modifications.

3.4.2. Alkylating drugs

Alkylating agents react with the DNA, causing DNA damage and subsequent cell death (*190, 209*).

In this work we have used two different alkylating agents: carboplatin and melphalan. Carboplatin is a platinum compound with a structure related to cisplatin that reacts with nucleophilic sites on DNA, causing intrastrand and interstrand crosslinks in the DNA (*210*). Melphalan is a nitrogen mustard-derived compound that binds and reacts with the DNA forming interstrand or intrastrand DNA cross-links (*211*). At our institution, carboplatin is administered through the intra-ophthalmic artery route and melphalan is administered via intra-arterial or intravitreal route, with melphalan being a safer option due to its shorter half-life (1.5 hours) (*202*).

3.4.3. Etoposide, a topoisomerase II inhibitor

Etoposide is a semi-synthetic derivative of podophyllotoxin, a non-alkaloid lignin toxin extracted from the roots and rhizomes of *Podophyllum* (*212*). Etoposide inhibits enzyme-mediated DNA ligation by binding to topoisomerase II, which leads to a DNA strand breakage, interruption of cell cycle transcription and replication, and, ultimately, cell death (*213*). In retinoblastoma, the use of etoposide is limited to systemic administration in combination with carboplatin and vincristine. Nevertheless, intravitreal etoposide is under investigation in preclinical models for the treatment of retinoblastoma as a potential alternative to melphalan (*214*). Compared to topotecan, etoposide exhibits higher IC_{50} values (1.8 μM for Y79 and 0.2 μM for Weri1 cells) (*204*). Moreover, topotecan shows substantial penetration into the vitreous and retina compared to etoposide (*204, 215*).

3.5. Preclinical models for retinoblastoma

Clinical trials in the field of pediatric cancer are limited and take years to complete, due to the low number of cases compared to adult cancer (*216*). To expedite clinical translation, it is crucial to establish preclinical models in experimental animals that accurately replicate pediatric malignancies (*217, 218*).

Different cellular and animal models including rats, mouse and zebrafish have been used to study pediatric cancer (*142, 219, 220*). Xenografts established from conventional cell lines are useful to predict drug response in clinical trials, but do not represent sufficiently well the variability of the patients (*221*). At our institution, SJD, direct access to retinoblastoma samples enabled us to establish primary cell cultures and their corresponding xenografts. Following eye enucleation, we culture and establish tumor models that enable the generation of retinoblastoma xenografts. We implant primary cultures subcutaneously or orthotopically (i.e., in the same organ in which patient tumors arise) in immunodeficient mice using simple surgical procedures (*142*) (**Fig. 1.16**). We have successfully established subcutaneous patient-derived xenografts of Ewing sarcoma (*186, 222*), osteosarcoma (*223*), neuroblastoma (*224*), rhabdomyosarcoma (*225*) and orthotopic xenografts of retinoblastoma (*101, 142*) and diffuse intrinsic pontine glioma (*226*).

In retinoblastoma, the injection of tumor cells into the eyes of immunodeficient animals has been useful for preclinical research (*101, 142, 227*). Recently, joint work of our laboratory and Dr Paula Schaiquevich developed xenograft models of metastatic retinoblastoma (*228*). By directly injecting retinoblastoma cells in the 4th ventricle of the mouse, cells occupied the leptomeningeal space, the ventricles and the CSF, resembling the clinical course of patients who rapidly died of leptomeningeal disease (*228*). New efficacy studies using metastatic retinoblastoma models may highlight the potential of intrathecal and systemic topotecan treatments, given its favorable accumulation profile in the CSF (*229*).

In this thesis, we established a new leptomeningeal model derived from one patient with intraocular disease and we used this model for efficacy studies using VCN-01 in combination with systemic topotecan.

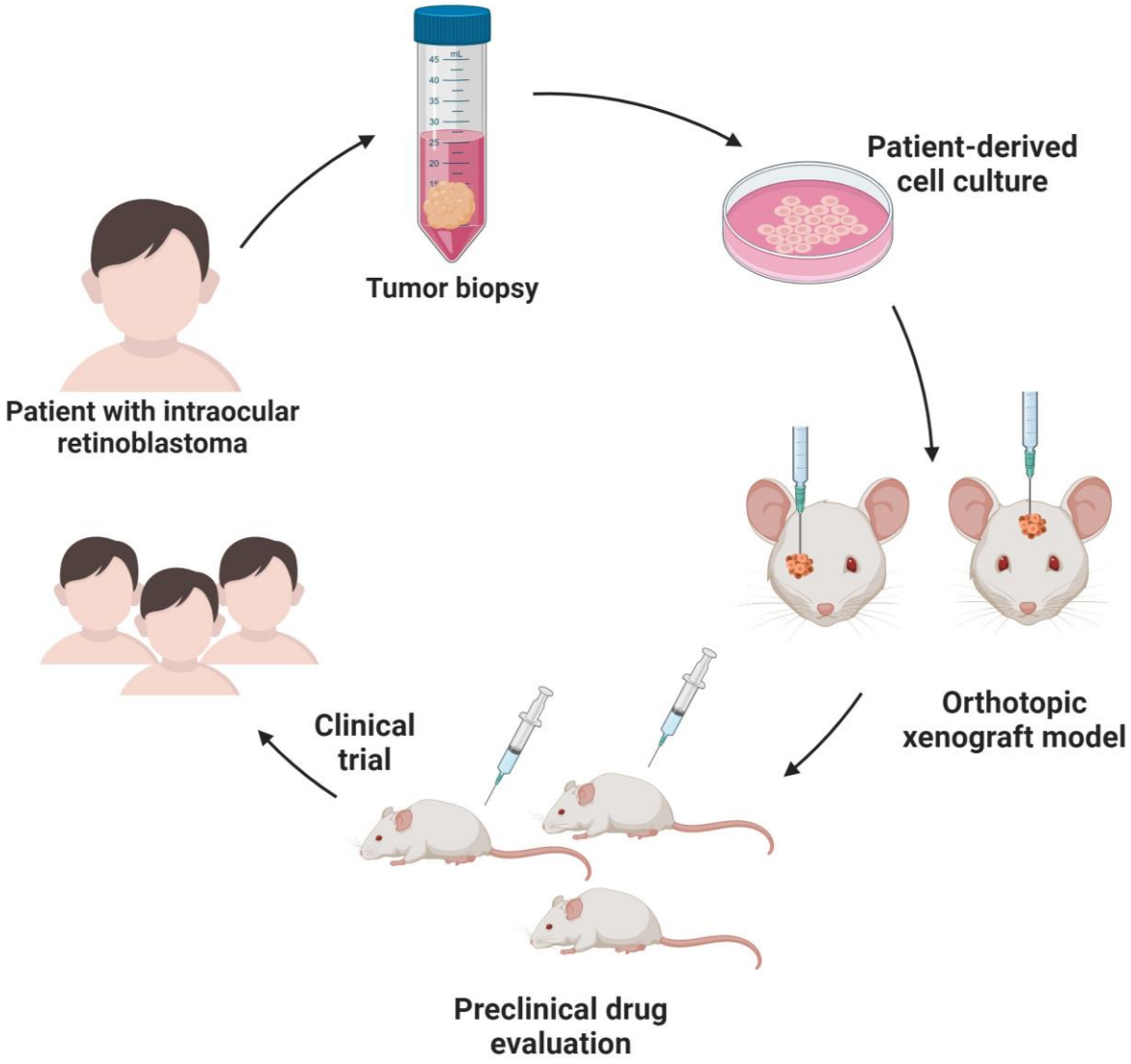

Figure 1.16. Establishment of an orthotopic model of retinoblastoma. The tumor biopsy is dissociated and cultured in a redefined medium (i.e. improved medium composition, growth factors and vitamins) until the patient-derived primary culture is successfully established. From this culture, we can derive the intraocular or metastatic orthotopic models, allowing us to conduct preclinical drug evaluation studies. Ultimately, clinical trials will be designed to evaluate new treatments.

Chapter II: Hypothesis and aims

Metastases and chemoresistance are the two main causes of therapeutic failure in patients with retinoblastoma and other solid cancers of the childhood. We recently completed the preclinical program of a “chemo-independent” oncolytic virus therapy, VCN-01, targeting the main aberrant genetic event occurring in retinoblastoma patients, i.e., the mutation of gene *RB1* leading to the overexpression of free E2F-1 in cancer cells. We showed that VCN-01 was efficacious and sufficiently safe in several models of chemorefractory retinoblastoma, which allowed us to bring this treatment to a phase 1 clinical trial. However, we foresee that the clinical use of oncolytic adenoviruses could be hindered by their likely suboptimal distribution in solid tumors, which would result in insufficient infection and activity of the viruses. We thus reasoned that there might exist interactions between oncolytic adenoviruses and the standard of care chemotherapy received by our patients, which could represent an opportunity to improve the oncolytic activity and distribute the virus evenly within the tumor. Such interactions could be related to anticancer therapies modifying target molecules of the virus in the cancer cells, physical barriers of the solid cancers, or other unknown events leading to the synergy (or antagonism) of both treatments.

The general hypothesis of this work is that the combination of VCN-01 and chemotherapy in primary cultures and xenografts models of pediatric cancers will result in complex molecular interactions leading to different-than-additive activity of both treatments in these models. We expect that such interaction will be highly dependent on the sequence in which both treatments are administered and on the mechanisms of clearance of the treatments in the different preclinical scenarios (in vitro and in vivo). Eventually, we anticipate that this work will optimize the combination of VCN-01 and chemotherapy to find the best sequence of administration in vivo and the best chemotherapy agent leading to the synergy of both treatments. To address these hypotheses, I will use preclinical models of intraocular and CNS-disseminated retinoblastoma, neuroblastoma and Ewing sarcoma.

The main objectives of my PhD thesis are:

i) To study the interaction of VCN-01 and chemotherapies in vitro, in cell lines and primary cultures of retinoblastoma, neuroblastoma and Ewing sarcoma. Chemotherapies will be selected among those used as standard of care of retinoblastoma. I will address whether the selected chemical treatments modify molecular properties of cancer cells, with focus on E2F-1 expression and cell cycle, potentially affecting the ability of VCN-01 to infect cells and replicate. I will also evaluate the impact of the sequence of administration of VCN-01 and the selected chemotherapies on cancer cell proliferation, viral infection and oncolysis.

ii) To assess the efficacy of the combination therapy of VCN-01 and chemotherapy in vivo, addressing how the type of chemotherapy and the sequence of administration affects viral infection and activity. I will test the therapies in subcutaneous xenografts of retinoblastoma, neuroblastoma and Ewing sarcoma and in orthotopic xenografts of intraocular and CNS-disseminated retinoblastoma.

iii) To study the effect of the administration of intravitreal topotecan in patients included in the phase 1 trial of VCN-01 for chemo-refractory intraocular retinoblastoma. I will quantify tumor response to VCN-01 treatment and levels of viral genomes in the aqueous humor of the patients before, during and after the administration of topotecan.

Chapter III: Materials and methods

1. In vitro assays

1.1. Cell cultures, tumor models, viral constructs and chemotherapy agents

We used primary retinoblastoma cell cultures established from enucleated eyes of four patients at hospital Sant Joan de Deu (SJD), Barcelona, Spain (*142*). We acquired the Y79 cell line from the ATCC (Manassas, VA). Clinical details of the cell lines are in **Table 1**. We cultured primary tumor cells in a stem cell medium composed of Dulbecco's Modified Eagle Medium: Nutrient Mixture F12, Neurobasal-A Medium, 1 M HEPES buffer solution, 100 nM MEM sodium pyruvate solution, 10 mM MEM non-essential amino acids solution, Glutamax-I supplement, and an antibiotic-antimycotic mixture, all sourced from Life Technologies. This medium was enriched with B-27 supplement from Life Technologies, and 20 ng/mL each of recombinant human EGF, FGF, PDGF-AA, and PDGF-BB from Peprotech, along with 2 µg/mL heparin from Sigma Aldrich. We cultured Y79 cells in Roswell Park Memorial Institute (RPMI) medium supplemented with 10% FBS, as described (*142*). We maintained the cultures at 37°C in an environment with 5% CO_2 and 95% humidity. Short tandem repeat (STR) profiles of the primary cells are reported elsewhere (*230*). Ewing sarcoma and neuroblastoma PDX were from the SJD repository and have clinically annotated data available (*222, 231*). Cell cultures and PDX are identified with the institutional prefix HSJD (**Table 3.1**), which is omitted in the text and figures for clarity purposes. The oncolytic adenovirus VCN-01 and the non-replicative adenovirus AdTLRGDK were from Theriva Biologics, Inc. (Barcelona, Spain) (*95*). We purchased topotecan and irinotecan from Accord Healthcare (Barcelona, Spain), carboplatin and etoposide from Teva Pharma (Madrid, Spain), melphalan from GlaxoSmithKline (Brentford, UK), hydroxyurea from Sigma-Aldrich (Sant Louis, MO) and SN-38 from Carbosynth (Compton, UK).

Table 3.1. Clinical details of the retinoblastoma cell models.

Cell model ID	Genomic alterations[1]	Tissue of origin	Age at diagnosis (months)	Age at enucleation (months)	Laterality	Chemotherapy
HSJD-RBT-2	*RB1*^{mut}	Tumor	8	13	Bilateral	Yes[2]
HSJD-RBT-5	*RB1*^{mut}	Tumor	7	24	Unilateral	Yes[3]
HSJD-RBT-7	*MYCN*^{A}	Tumor	6	6	Unilateral	No
HSJD-RBVS-10	*RB1*^{mut}	Vitreous	5	28	Bilateral	Yes[4]
Y79	*RB1*^{mut} *MYCN*^{A}	Tumor	30	30	Unilateral	No

[1]*RB1*^{mut}: mutation in the gene *RB1*; *MYCN*^{A}: amplification of the gene MYCN.

[2]Five tandem doses of topotecan and melphalan in the ophthalmic artery.

[3]Six cycles of systemic carboplatin, etoposide and vincristine, three tandem doses of topotecan and melphalan in the ophthalmic artery and ruthenium brachytherapy.

[4]Eight cycles of systemic carboplatin, etoposide and vincristine, ten cycles of systemic cyclophosphamide and etoposide, one dose of intravitreous melphalan and three tandem doses of topotecan and melphalan in the ophthalmic artery.

1.2. Cell proliferation experiments

First, we addressed the antiproliferative activity of topotecan (ranging 10-0.0000256 µM), carboplatin (200-0.78 µM) or melphalan (10-0.00015 µM) in retinoblastoma cells (2×10^4 cells per well, in 96-well plates) infected with VCN-01 for the three previous days, at a concentration of 10 multiplicity of infection (MOI; i.e., transducing units of virus per cell). This concentration of virus is sub-toxic for incubations of six days in these cells (*101*). We incubated the plate at 37 ºC and 5% of CO_2. Three days after the addition of drugs, we measured cell viability with the compound [3-(4,5-dimethylthiazol-2-yl)-5-(3-carboxymethoxyphenyl)-2-(4-sulfophenyl)-2H] tetrazolium (MTS assay; Promega, Fitchburg, WI). The half-inhibitory concentration (IC_{50}), defined as the concentration of the drug required to cause a reduction of 50% in cell viability, was calculated using Graphpad Prism.

To assess chemoresistance, we quantified the anti-proliferative activity of Y79 cells treated with VCN-01 alone or VCN-01 in combination 2.5 nM of topotecan. We administered VCN-01 on day 1, followed by topotecan treatment starting on day 4. We measured cell viability on day 10.

To address the sequence of the treatments on cell viability and apoptosis markers, we used topotecan (2 µM) and VCN-01 at 50 MOI (concentration sufficient to achieve viral protein transduction at early time points) and incubated them with the sequence “topotecan first” (three days before VCN-01) or “VCN-01 first” (three days before topotecan). We controlled the experiments by adding culture medium instead of the second treatment.

To address the antiproliferative activity of VCN-01 in synchronized cells, we treated RBT-7 with hydroxyurea (4 mM) for 4 h to induce S-phase cell cycle arrest. After 24 h, we added VCN-01 (200-0.8 MOI). We measured cell viability at 8 or 10 days. We controlled the experiments by using non-synchronized cells.

We performed similar experiments to address the antiproliferative activity of VCN-01 (100-0.4 MOI) in primary cultures of Ewing sarcoma and neuroblastoma PDX.

1.3. Genomic analyses

We studied the expression of viral genes *E1A* and *E1B* in 6-well culture plates containing 2 × 10^6 retinoblastoma cells. We exposed the cells to topotecan (2 µM) and VCN-01 (50 MOI) and incubated them in the sequence "topotecan first" (24 h before VCN-01) or "VCN-01 first" (24 h before topotecan). We controlled the experiments by adding culture medium instead of topotecan or VCN-01. After 24 h of the second treatment, we collected the cell pellets and isolated the mRNA with the TRIzol method (Thermo Fisher Scientific, Waltham, MA, USA). RNA was reverse-transcribed using Superscript ll reverse transcriptase (Thermo Fisher Scientific), followed by RT-qPCR (quantitative reverse transcription polymerase chain reaction) using SYBR technology (Thermo Fisher Scientific) on an Applied Biosystems QuantStudio 5. The primers were viral *E1A* (Forward 5'-ATC GAA GAG GTA CTG GCT GA-3', Reverse 5'-CCT CCG GTG ATA ATG ACA AG -3') and *E1B* (Forward 5'-GAG GGT AAC TCC AGG GTG CG-3', Reverse 5'-TTT CAC TAG CAT GAA GCA ACC ACA-3'). Differential expression was determined using the delta Ct method.

To assess the expression of genes involved in the cell cycle, we used 6-well culture plates containing 2 × 10^6 retinoblastoma cells. We added VCN-01 at 50 MOI for 48 h, followed by the addition of topotecan (2 µM), carboplatin (12.5 µM) or culture medium. We collected the cell pellets 24 h later. We plated the samples in the TaqMan® Array of Human Cyclins & Cell Cycle Regulation (Thermo Fisher Scientific). This array contains 92 assays of cell cycle-associated genes and assays of *GAPDH, 18S, HPRT1* and *GUSB* as endogenous control genes. We established the threshold cycle (Ct) value ≥ 35 as absence of expression. We used the mean expression value of the controls to normalize gene expression values. The selected thresholds for upregulation and downregulation were $2^{-\Delta\Delta Ct} \geq 2.0$ and $2^{-\Delta\Delta Ct} \leq 0.5$, respectively (*232*).

We performed RT-qPCR to validate results of the top genes overexpressed or downregulated in the array. SYBR primers were *CDKN1A* (Forward 5'-GGA CAG GAG AGG AAG ACC ATG T-3', Reverse 5'-TGG AGT GGT AGA ATT CTG TCA

TGC-3') and *CDK6* (Forward 5'-CCA GGC AGG CTT TTC ATT CA-3', Reverse 5'-AGG TCC TGG AAG TAT GGG TG-3').

Genes involved in DNA synthesis and activated by E2F-1 were *PCNA*, *TK* and *THFR* (*6, 233*). Primers were *PCNA* (Forward 5'-CAA GTA ATG TCG ATA AAG AGG AGG-3', Reverse 5'-GTG TCA CCG TTG AAG AGA GTG G-3'), *TK* (Forward 5'-AGC AGC TTC TGC ACA CAT GAC C-3', Reverse 5'-CTC GCA GAA CTC CAC GAT GTC A-3') and *DHFR* (Forward 5'-ATG CCT TAA AAC TTA CTG AAC AAC CA-3', Reverse 5'-TGG GTG ATT CAT GGC TTC CT-3').

To quantify the recombinant PH20 hyaluronidase gene (*SPAM1*) in cultures and mouse tissues, we used the SYBR primer: Forward 5′-TAC ACA CTC CTT GCT CCT GG-3′, Reverse: 5′-CTT AGT CTC ACA GAG GCC AC-3 (*104*).

To quantify the load of retinoblastoma cells in mouse tissues (i.e., to assess tumor burden), we used SYBR primers for the gene *CRX* (Forward: 5′- AGG TGG CTC TGA AGA TCA ATC TG-3′, Reverse: 5′-TTA GCC CTC CGG TTC TTG AA-3′)(*142*).

To assess the expression of *E2F1*, *CXADR* and *ITGA5* in pediatric cancers, we used available data sets of fetal retina (GSE12621; n = 12), pediatric brain (GSE44971 and GSE13564; n = 28), muscle tissue (GSE17679; n = 18), retinoblastoma (GSE29683; n = 55), neuroblastoma (GSE16237; n = 51) and Ewing sarcoma (GSE34620; n = 44). We normalized and processed data from CEL files by the robust multichip averaged (RMA) algorithm using R statistical software and the Affymetrix library available through Bioconductor (*234*).

1.4. Cell cycle assays

We treated 10^6 retinoblastoma cells with topotecan (2 µM), carboplatin (12.5 µM), melphalan (10 µM) or hydroxyurea (100 µM) for 24 h. Then, we collected and fixed the cells in 70% ethanol for 2 h at 4 ºC. We used the propidium iodide (PI)-based assay FxCycle™ PI/RNase (Thermo Fisher Scientific) as staining solution prior to quantification by flow cytometry (NovoCyte flow cytometry system, ACEA Biosciences, San Diego, CA).

To synchronize cells in the S phase of the cycle, we exposed 10^6 cells to high concentration of hydroxyurea (4 mM). After 4 h, we washed the cells with phosphate buffered saline (PBS), and we quantified the percentage of cells in the S phase at 0, 4, 6, 18, 24, and 48 h after HU exposure.

1.5. Protein expression assays

In all experiments, we used 6-well culture plates containing 2×10^6 cells. First, we infected cells with VCN-01 (50 MOI, 24 h), exposed them to topotecan (2 µM), carboplatin (12.5 µM) or melphalan (10 µM), and collected the pellets 24 h later for the analysis of apoptosis, cell cycle and infection markers. We controlled the experiments by adding culture medium instead of the second treatment. To address whether the sequence of treatments affected their interaction, we applied the sequence "topotecan first" (24 h before VCN-01) or "VCN-01 first" (24 h before topotecan). We expanded the analyses to other chemotherapeutic agents including hydroxyurea (100 µM), etoposide (2 µM), irinotecan (10 µM) or SN-38 (1 µM).

In a time course experiment, we analyzed cell cycle proteins upon cell exposure to chemotherapeutic agents. We treated retinoblastoma cells with topotecan (2 µM), carboplatin (12.5 µM), melphalan (10 µM), hydroxyurea (100 µM) or SN-38 (1 µM) and collected cell pellets at 1, 2, 4, 8, 16, 24 and 48 h.

We lysed the cells with RIPA buffer (50 mM HEPES, 150 mM NaCl, 1 mM EDTA, 10% glycerol, 1% Triton-X 100, 0.1% SDS, 1% Na deoxycholate) to obtain whole protein extracts. We quantified the proteins with the BCA assay (Thermo Fisher Scientific) and equal amounts of cell extracts were loaded into Bis-Tris gels, transferred to nitrocellulose membranes, incubated with primary antibodies overnight at 4ºC and incubated with fluorescently-labeled secondary antibodies 1 h at room temperature. Primary antibodies were p53 (2527S, 1:1000, Cell Signaling, Danvers, MA), E1A (adenovirus type 5 infection marker; ab33183, 1 µg/mL, Abcam, Cambridge, MA), cPARP (apoptosis marker; 9541S, 1:1000, Cell Signaling), p21 (2947, 1:1000, Cell Signaling), E2F-1 (VCN-01 promoter; 3742, 1:1000, Cell Signaling), Cyclin E1 (sc-377100, 1:200, Santa Cruz Biotechnology, Santa Cruz,

CA), topoisomerase 1 (ab85038, 1:1000, Abcam), adenovirus type 5 (Hexon; ab6982, 1:1000, Abcam), β-tubulin (MAB374, 1:10,000, Millipore, Darmstadt, Germany) and GAPDH (1:10,000, Millipore). We used the LI-COR Odyssey CLx Infrared Imaging System (LI-COR Inc. Bad Homburg, Germany) for detection.

To study proteins induced by the adenovirus, we used AdTLRGDK, which expresses GFP under a genetic background similar to VCN-01 (*95*). In a first experiment, we synchronized Y79 cells in the S phase with hydroxyurea (4 mM). After 24 h, we washed cells with PBS and exposed them to 50 MOI of AdTLRGDK. We acquired fluorescence images of the cells at 24, 48 and 72 h post infection, and collected the pellets for GFP analysis by flow cytometry (NovoCyte), using the auto-fluorescence of untreated cells to gate infected cells signal. We analyzed data using the NovoExpress software (ACEA Biosciences). In a second cytometry experiment, we infected Y79, RBT-5 and RBT-7 cells with 50 MOI of AdTLRGDK. After 24 h, we added topotecan (2 µM), carboplatin (12.5 µM), melphalan (10 µM), hydroxyurea (100 µM) or fresh culture medium. After 24 h, we quantified the expression of GFP. To address the sequence of treatments on GFP expression, we exposed cells to topotecan (2 µM) or hydroxyurea (100 µM) 6 h before AdTLRGDK infection at 50 MOI and collected the cells 48 h later.

1.6. Viral production assay

We infected Y79 cells with a concentration of 500 MOI, which was sufficient to achieve 80% to 100% infectivity. After 4 h, we washed the cells three times with PBS, added fresh medium and incubated them with or without topotecan (2 µM). At time points 30, 48 and 72 h post-infection, we collected the cell pellets and exposed them to three rounds of freeze-thaw lysis. We extracted total DNA according to the QIAamp DNA Mini Kit (QIAGEN, Valencia, CA). We quantified genome copy levels by real-time PCR–based method using VCN-01–specific oligonucleotides (forward primer: 5′-ACATTGCCCAAGAATAAAGAATCG-3′, reverse primer: 5′-TGGAATCAGAAGGAAGGTGAA-3′).

1.7. Apoptosis

We plated 10^6 retinoblastoma cells per well in 6-well plates. After 24 h, we added 50 MOI of VCN-01. The next day, we added topotecan (2 µM). We collected the cells after 24 h, washed them twice with 1% of bovine serum albumin (BSA) in PBS and fixed them with 70% ethanol for 2 h at 4 ºC. We labeled the cells with primary antibody cPARP (5625S, 1:1000, Cell Signaling) and with secondary antibody (ab150077, 1:2000, Abcam) before flow cytometry (NovoCyte).

1.8. Confocal microscopy

We incubated 10^6 Y79 cells in a 24-well plate coated with poly- L-Lysine (A3890401, Thermo Scientific) overnight. We infected the cells with 50 MOI of VCN-01. After 24 h, we treated the cells with topotecan (2 µM), carboplatin (12. 5 µM) and SN-38 (1 µM). We used untreated cells as controls.

After 24 h of drug exposure, we fixed the cells with 4% paraformaldehyde in washing solution (20 mM glycine in PBS) for 30 min. We incubated the cells with permeabilization solution consisting in 20 mM glycine and 0.1% Triton in PBS for 45 min. We incubate the cells with blocking solution in (20 mM glycine, 1% BSA and 0.01% of Triton in PBS) for 1 h. We incubated with the E2F-1 primary antibody (sc-251; 1:100; Santa Cruz Biotechnology) for 1 h. We washed the cells three times with washing solution and added the secondary antibody goat Anti-mouse IgG Alexa Fluor 488 (ab150113, 1:500, Abcam) for 1 h. After secondary antibody incubation, we washed the cells three times with a solution containing Hoechst in a dilution of 20 nM (Hoechst Solution; 33342; Thermo Fisher Scientific). We mounted slides with vectashield antifade mounting medium (Vector laboratories, Newark, CA). We kept the samples at -20 degrees until the day of analysis. Immunofluorescence images were acquired using inverted TCS SP8 spectral confocal laser scanning microscope with HyVolution (Leica Microsystems, Barcelona, Spain) with 0.4 and 1.4 numerical aperture objective lens.

1.9. DNA-protein binding assay

We quantified functional E2F-1 protein by evaluating its binding to the E2F-1 promoter of VCN-01. We used a colorimetric assay in which E2F-1 was captured by synthetic biotin-labeled oligonucleotides containing the sequence of the E2F-1 promoter. For these experiments, we plated 2×10^6 cells per well in 6-well plates. To quantify E2F-1 following the action of chemotherapeutics, we incubated cells with topotecan (2 µM), carboplatin (12.5 µM), melphalan (10 µM), hydroxyurea (100 µM), irinotecan (10 µM), SN-38 (1 µM) or culture medium for 24 h. To obtain nuclear protein extracts, we used a nuclear extraction kit (ab113474, Abcam). We obtained biotin-labeled (5′) E2F-1 promoter oligonucleotide (5′- CGT GGC TCT TTC GCG GCA AAA AGG ATT TGG CGC GTA AAA GTG GTT CGA GT -3′) by oligo synthesis from IDT (Integrated DNA Technologies, Coralville, IA). The oligos were annealed and used for in vitro DNA-protein binding assay by the DNA-Protein Binding Assay Kit (Colorimetric; ab117139). The assay was performed according to manufacturer's protocol. We plated 2-20 µg of nuclear protein extract for each reaction. We performed triplicates for each condition. We used blank that contained biotinylated oligonucleotides without nuclear extract. We included two negative controls that contained nuclear extract without oligonucleotides or nuclear extract without primary antibodies. We used scrambled oligo (5’-CGT GGC TCG CGA TTA ATG CGA AGG ACG CTT AAT TGC GCG GTG GTT CGA GT-3’) and non-biotylinlated oligo as controls.

2. In vivo techniques

2.1. Accumulation of topotecan in VCN-01-infected intraocular tumors of retinoblastoma

We carried out animal experiments following institutional and European guidelines (EU Directive 2010/63/EU) and the ARRIVE guidelines (*235*). For orthotopic intraocular engraftments, we anesthetized the animals with 100 mg/kg ketamine and 10 mg/kg xylazine and immobilized in a stereotaxic apparatus (Stoelting, Wood Dale, IL). With the assistance of a stereomicroscope (M80, Leica Microsystems), we performed a small incision in the corneal limbus with a 27 G needle. Subsequently, we introduced 2×10^5 cells suspended in 2 µL matrigel (BD Biosciences, Erembodegem, Belgium) through the incision, at a depth of 2 mm into the posterior segment of the eye using a dull 33 G needle attached to a 5 µL syringe (Hamilton, Bonaduz, Switzerland), utilizing a stereotaxic arm. Animals recovered, and intraocular tumors developed until invading the posterior and anterior chambers of the ocular globes, causing proptosis. After 14 days, we inoculated a single dose of VCN-01 (3×10^9 vp/eye). After another 14 days, we implanted an Alzet osmotic pump (2001D, Durect, Palo Alto, CA), loaded with 1 mg/mL of topotecan. These pumps released topotecan at a dose of 25 µg/h and reached constant levels in plasma of approximately 100 ng/mL. At the steady state (6 h), we collected tumors. We measured the levels of topotecan in tumors samples using high-performance liquid chromatography (HPLC). We placed a 100 µL aliquot of each sample in a 1.5 mL polypropylene tube, followed by the addition of 200 µL of methanol to precipitate proteins. The mixture was then vortexed for 10 seconds and centrifuged at 14,000 rpm for 5 minutes at 4 °C. Subsequently, we transferred 100 µL of the clear supernatant to autosampler vials, and 50 µL were injected into the HPLC system. The detection wavelength was set at 267 nm, with the column temperature maintained at 25 °C. The mobile phase was composed of 0.01 M potassium dihydrogen phosphate (pH 3.0) and acetonitrile in an 85:15 ratio, with a flow rate of 1.5 mL/min. We performed the analysis using a 150 mm x 4.6 mm, 5 µm Inertsil ODS

column. The area under the plasma concentration-time curve (AUC) was determined using the trapezoidal method.

2.2. Intratumoral infection of VCN-01

To establish subcutaneous tumors, we injected 10^6 retinoblastoma cells suspended in 25 µL matrigel (Corning, Glendale, AZ) in athymic nude mice (Envigo, Barcelona, Spain). Upon xenograft engraftment (tumor volumes ranging 100–200 mm^3), we started treatments. Mice received VCN-01 (3×10^9 vp in 20 µL vehicle, single intratumoral injection at day 1), alone or combined with one cycle of topotecan (0.6 mg/kg, intraperitoneal -i.p.-, daily at days 1-5), carboplatin (40 mg/kg, i.p, one single dose at day 1), or hydroxyurea (200 mg/kg, i.p., daily at days 1-5). A group of mice received one intratumoral injection of the vehicle of VCN-01 (PBS). We sacrificed mice at 5 and 15 days after VCN-01 inoculation, dissected the tumors and prepared tumor homogenates by adding 10 µL of water per mg of tissue and homogenizing with a Bullet Blender turbine Storm 24 (Quasar instruments, Colorado Springs, CO). In tumor homogenates, we quantified genome copies of VCN-01 as previously described for in vitro experiments. We processed part of the tumor in 4% paraformaldehyde and embedded it in paraffin for immunohistochemistry analysis. We used sodium citrate (pH 6) heat-mediated antigen retrieval before incubation with antibodies. In 4 µm paraffin sections, we performed hematoxylin and eosin (H&E) staining and immunostained human nuclei (MAB4383, 1:200, Merck Millipore, Burlington, MA) viral protein E1A (ab33183, 1:200, Abcam) and E2F-1 (sc-251, 1:50, Santa Cruz Biotechnology). All staining were performed using an autostainer. Slides were then mounted and imaged using a fight field microscope.

2.3. Antitumor activity in retinoblastoma

For orthotopic intraocular engraftment, we follow the same procedure as previously described for the experiment of “Accumulation of topotecan in VCN-01-infected intraocular tumors of retinoblastoma”. We followed tumor development by visual observation until eye proptosis. At that time, eyes were considered to reach the experimental endpoint and they were enucleated under general anesthesia (100 mg/kg ketamine and 10 mg/kg xylazine). To obtain subcutaneous xenografts follow the same procedure as previously described for the experiment of “Intratumoral infection of VCN-01”.

For ocular tumors, we started treatments at day 8 after inoculation (when tumors were appreciable by fundus examination). For subcutaneous tumors, we started treatments when volumes achieved 100-300 mm^3 (day 1). We measured tumor volume three times per week with an electronic caliper. We measured tumor growth rate as the time needed to achieve the experimental endpoint, i.e. tumor volume of 1,500 mm^3. Tumor volume was calculated as (length × $width^2$)/2, length being the longitudinal diameter and width the transverse diameter of the subcutaneous tumor.

In a first study, we administered one dose of VCN-01 (3×10^8 vp in 2 µL vehicle, intravitreal, day 15), therapeutic schedules of topotecan or standard of care (SoC) retinoblastoma chemotherapy, or the combinations, in the Y79 intraocular xenograft. For topotecan, mice received 0.6 mg/kg i.p. injections on days 8-12 and 29-33. For SoC, mice received i.p carboplatin 40 mg/kg, on days 8 and 29, and etoposide 6 mg/kg, on days 8-10 and 29-31.

In a second experiment, we addressed the sequence of administration of one injection of VCN-01 and one 5-day cycle of topotecan. Mice with intraocular tumors (Y79 or RBT-7) received either topotecan 0.6 mg/kg, i.p. on days 8-12, one intravitreal injection of VCN-01 (3×10^8 vp) on day 8, or the combination of topotecan and VCN-01. Y79-bearing mice also received a switched treatment sequence, with VCN-01 on day 12, after the last dose of topotecan.

In a third study, we maximized the number of cycles of topotecan (injections on days 8-12, 15-19, 29-33, 36-40, 50-54 and 57-61) and administered two intraocular

injections of VCN-01 (3×10^7 vp/eye) on days 8 and 15 to mice bearing RBT-2 xenografts (*101*).

In a fourth study, to circumvent the action of the blood-retinal barrier restraining drug delivery (*201*), we inoculated mice subcutaneous in both flanks with Y79 or RBT-7 cells. These animals were treated with either topotecan 0.6 mg/kg, i.p. on days 1-5, VCN-01 (3×10^9 vp in 20 µL vehicle, intratumoral, day 1), or the combination in the same sequence.

2.4. Antitumor activity in CNS-disseminated retinoblastoma

We established a model of retinoblastoma dissemination in the leptomeninges of the central nervous system (CNS). We anesthetized the animals with an intra-peritoneal injection of 100 mg/kg of ketamine and 10 mg/kg of xylazine and immobilized in a stereotaxic frame. Using a mouse brain atlas (*236*), a burr hole was drilled in the mouse skull at coordinates x + 0.5 mm and y - 5.4 mm, from bregma. Cells were injected at 3.5 mm depth, targeting the 4th ventricle with an inclination angle of 10 degrees. Then, we injected 10^6 million cells (RBT-7) in 10 µL matrigel with a dull 22G needle attached to a 50 µL syringe (Hamilton). One week later, we started treatments. In a first study, we assessed the efficacy of systemic topotecan (0.6 mg/kg, i.p. on days 8-12) and systemic standard of care chemotherapy (carboplatin 40 mg/kg, on day 8, and etoposide 6 mg/kg, on days 8-10). In a second experiment, we assessed the therapeutic activity of intrathecal VCN-01 alone or in combination with systemic topotecan. In this study, we included three different dosage levels of VCN-01 (3×10^9, 3×10^8 and 3×10^7 vp) delivered in 20 µL PBS at day 8. The same day, we started topotecan treatment (0.6 mg/kg, i.p., days 8-12, 15-19). The control group received PBS (intraventricular). Animals achieved experimental endpoints upon deterioration of condition or 20% weight loss. Brains collected at endpoint were embedded in paraffin and stained with hematoxylin and eosin (H&E), human nuclei (MAB4383, 1:200, Millipore), viral protein E1A (ab33183, 1:200, Abcam).

In a third experiment, we injected 10^6 cells following the same procedure in 12 mice. After one week, we treated the mice with local injections of vehicle, VCN-01 (3×10^9 vp), systemic topotecan or the combination. We sacrificed the mice 2 h after the last

dose of topotecan. We prepared brain homogenates by adding 10 µL of water per mg of tissue. We extracted DNA, protein and mRNA as previously described for subcutaneous tumors. We processed part of the tumor for immunohistochemistry analysis. In a fourth experiment, we aimed to see tumor load after treatment. We injected 10^6 cells following the same procedure. After one week, we treated the mice with local injections of vehicle, VCN-01 (3×10^9 vp), systemic topotecan (0.6 mg/kg, days 8-12), SoC (carboplatin 40 mg/kg, on day 8, and etoposide 6 mg/kg, on days 8-10) or the combination between VCN-01 and topotecan. Brains collected at selected time point (26 day after tumor implantation) were embedded in paraffin and stained with human nuclei (MAB4383, 1:200, Millipore).

2.5. Antitumor activity in extra cranial pediatric solid tumors

We implanted 5-10 mm^3 fresh fragments of Ewing sarcoma or neuroblastoma PDX (**Table 3.2**) in both flanks of mice. Upon subcutaneous engraftment (tumor volume 150-200 mm^3), mice received topotecan (0.6 mg/kg, i.p., days 1-5), VCN-01 (3×10^9 vp in 20 µL vehicle, intratumoral, day 1), or the combination. In two additional groups, we used an alternative topoisomerase 1 inhibitor, irinotecan (10 mg/kg, i.p., on days 1-5) substituting topotecan. Upon completion of treatments, we followed tumor volumes until endpoint (1500 mm^3), or until day 80.

Table 3.2. Clinical details of NB-005 and ES-033

Description	NB-005	ES-033
Patient clinical information		
Gender	Female	Male
Age at diagnosis (y)	2	9
Diagnosis	Neuroblastoma	Ewing Sarcoma
Previous treatment	N8 MSKCC[1]	GEIS 21[2]
Outcome	Deceased	Deceased
Tumor information		
Biopsy date	04/04/2011	11/05/2021
Primary tumor tissue origin	Bone marrow	Lung
Molecular tissue analysis	*MYCN*^{A} / *TP53*^{mut}	*EWSR-FLI1* fusion

[1]Clinical protocol at Memorial Sloan-Kettering Cancer Center, including five cycles of cyclophosphamide plus doxorubicin/vincristine (CAV) and cisplatin/etoposide (P/E) with anti-GD2 immunotherapy after each of the last three cycles.

[2]Clinical protocol including five cycles of mP6 chemotherapy (cycles 1, 2 and 4 with cyclophosphamide, doxorubicin and vincristine; and cycles 3 and 5 with ifosfamide and etoposide); surgery; radiation therapy.

3. Human translation

We report the first patient with intraocular relapsed retinoblastoma receiving topotecan after intravitreal VCN-01. For clinical details, see **Table 3.3.** VCN-01 and topotecan intravitreous injections were performed under general anesthesia. Blood samples and aqueous humor were obtained to quantify viral particles before and after the injection of VCN-01. Anti-adenovirus 5 neutralizing antibodies were measured in serum. For ophthalmological examinations, we used RetCam imaging (Natus, Pleasanton, CA).

Table 3.3. Clinical details of the patient of the clinical trial.

Gender, age in years	Laterality	Tumors	Sequence of previous treatments	VCN-01 dose
Male, 3	Bilateral	Left eye enucleated	Systemic chemotherapy (6 cycles of carboplatin, etoposide and vincristine), three doses of intra-arterial chemotherapy with carboplatin, melphalan and topotecan and two intravitreal doses of melphalan	2×10^{10} vp per eye and injection

4. Statistics

We performed at least three replicates for each condition in vitro. To compare means of two different groups, we used the *t* test or the Mann-Whitney test. For more than two groups, we used the ANOVA test or the Kruskal-Wallis test with Dunn's correction. We calculated median survivals using the Kaplan-Meier method and compared them using the log-rank test with the Bonferroni correction for multiple comparisons. In most studies, we compared all groups with the control (vehicle) group. In the study of the CNS-disseminated retinoblastoma, we compared all groups with the one receiving the combination of VCN-01 and topotecan. For all the analyses, we defined $P < 0.05$ as statistical significance.

Chapter IV: Results

1. Interaction of VCN-01 and chemotherapeutics in retinoblastoma cells

VCN-01 has been evaluated as a single agent in a phase 1 clinical trial in nine patients with chemorefractory intraocular retinoblastoma (NCT03284268; Principal investigator: Dr Jaume Català). The treatment demonstrated systemic safety in all patients and anticancer efficacy (objective response) in some of them. All patients experienced local inflammation that had to be treated with high doses of corticosteroids (Dr Jaume Català, personal communication). In my thesis, I tried to anticipate and design what a phase 2 trial would look like, in which we would combine VCN-01 and chemotherapy agents currently used in the treatment of retinoblastoma. In the first section of the Results chapter, I assessed the interaction of VCN-01 and several chemotherapeutics used in the standard of care of retinoblastoma, including the drugs topotecan, carboplatin, melphalan and etoposide. I used primary cultures and a cell line, all retinoblastoma, to perform assays such as the antiproliferative activity of the treatments, the infectivity of VCN-01 in the presence of chemotherapy, or the cell cycle profile in cells treated with the chemotherapeutics. I found that topotecan was the only chemotherapeutic that exhibited synergy with VCN-01, and such positive interaction could be due to the action of topotecan increasing E2F-1 and promoting S-phase cell cycle arrest in cancer cells. In the second section of this chapter, I present experiments in immunodeficient mice evaluating the anti-retinoblastoma activity of VCN-01 and topotecan, addressing the antitumor activity in orthotopic and subcutaneous (s.c.) xenografts. Additionally, I measured viral genome production and the expression of viral proteins such as E1A in s.c. tumors. I also assessed this treatment in other pediatric tumors, including metastatic retinoblastoma in the CNS, Ewing sarcoma or neuroblastoma. Finally, I describe the clinical case of a patient with chemo-refractory intraocular retinoblastoma who received VCN-01 and topotecan. We found a surprising outcome (the patient is disease-free after five years) and clinical evidence of the enhanced distribution of the virus following topotecan treatment.

1.1. Antiproliferative activity and apoptosis of VCN-01 in combination with chemotherapy

First, I evaluated the antiproliferative activity of the chemotherapeutics topotecan, carboplatin and melphalan, combined with VCN-01, in three different retinoblastoma models (all established at our hospital, SJD) and in the Y79 cell line. At exposure times long enough to measure the activity of drugs (3 days), pretreatment with VCN-01 (10 MOI) decreased cell sensitivity to topotecan, carboplatin, and melphalan (**Fig. 4.1A**) and increased the concentration of drugs required for a 50% decrease in cell proliferation (**Table 4.1**). To address the in vitro anticancer efficacy of VCN-01 with and without chemotherapy, we incubated for times long enough to detect the oncolytic activity of VCN-01 (10 days), at the same time that we had to lower down the concentration of the drugs (topotecan) below 5 nM, to avoid the excessive antiproliferative activity of the drug for such a long incubation time, which would have impeded the evaluation of the viral activity. At a non-cytotoxic concentration of topotecan, 2.5 nM, we observed synergy with VCN-01, reducing the IC_{50} of the virus from 3.7 MOI (VCN-01 alone) to 1.7 MOI (VCN-01 and topotecan) (**Fig. 4.1B**). These results suggest that (i) viral infection prevents cells from apoptosis induced by chemotherapeutics, especially at high drug concentrations, and (ii) at sub-cytotoxic concentrations, topotecan was synergistic with VCN-01 in vitro.

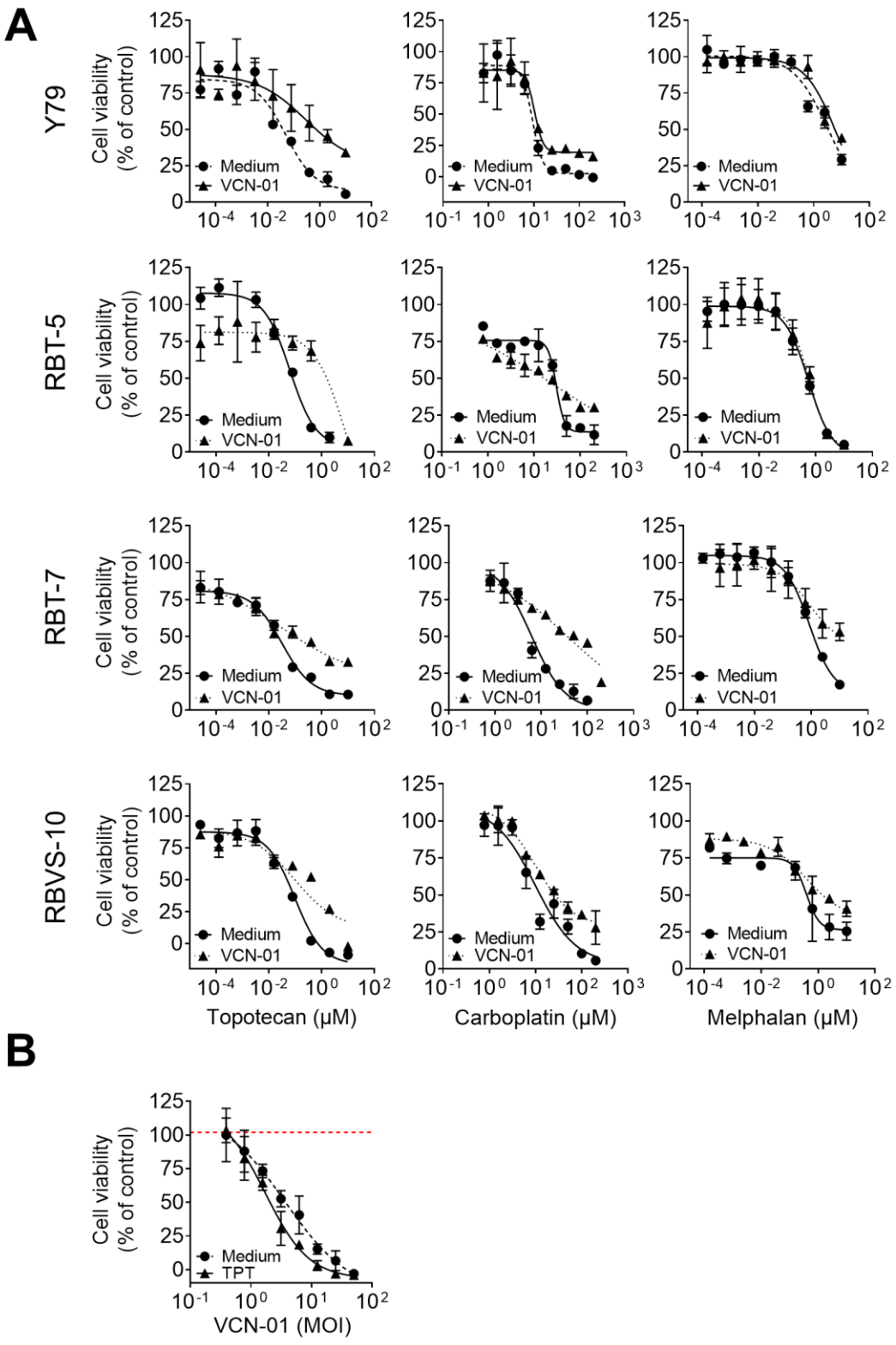
A
Y79
RBT-5
RBT-7
RBVS-10
Cell viability (% of control)
Medium
VCN-01
Topotecan (μM)
Carboplatin (μM)
Melphalan (μM)
B
TPT
VCN-01 (MOI)

Figure 4.1. Antiretinoblastoma activity of topotecan, carboplatin and melphalan in VCN-01-infected cells. A, Anti-proliferative activity of topotecan (TPT), carboplatin (CBP), and melphalan (MEL), with VCN-01 at 10 MOI (VCN-01), or without VCN-01 (Medium) in Y79, RBT-5, RBT-7 and RBVS-10 retinoblastoma cells. VCN-01 (or medium) was administered at day 1, drug treatments at day 4, and cell viability was measured at day 7. B, Anti-proliferative activity of Y79 cells treated with VCN-01 (Medium) or VCN-01 in combination with topotecan 2.5 nM (TPT). VCN-01 was administered at day 1, topotecan treatment started at day 4, and cell viability was measured at day 10. Red line represents the cell viability of cells treated with topotecan alone. Values are means and SD of three replicates. Lines are the best fitting curves built using the least square regression method of GraphPad. Cell viability is expressed as the relative percentage of the assay signal of treated cells, compared to control untreated cells, which was set as 100%.

Table 4.1. Susceptibility of retinoblastoma cells to VCN-01, chemotherapy or their combinations *in vitro*

Cell model ID	VCN-01 IC_{50} (MOI)*	Topotecan IC_{50} (µM)		Carboplatin IC_{50} (µM)		Melphalan IC_{50} (µM)	
		Single agent	**VCN-01**	**Single agent**	**VCN-01**	**Single agent**	**VCN-01**
HSJD-RBT-2	8.26 (5.72 – 11.9)	0.00738 (0.00449 – 0.0122)	0.0507 (0.0228 - 0.118)	n.p.	n.p.	n.p.	n.p.
HSJD-RBT-5	0.0865 (0.0572 –0.131)	0.0879 (0.0669 – 0.116)	0.586 (0.166 – 3.47)	19.0 (13.4 – 26.6)	15.5 (12.6 – 19.1)	0.478 (0.307 – 0.843)	0.636 (0.375 – 1.33)
HSJD-RBT-7	6.77 (4.13 – 11.1)	0.0151 (0.00996 – 0.0228)	0.118 (0.0713 – 0.200)	6.21 (5.22 – 7.41)	36.8 (29.7 – 46.2)	1.42 (1.14 – 1.83)	8.48 (4.11 – 27.1)
HSJD-RBVS-10	4.95 (3.29 – 7.45)	0.0296 (0.0191 – 0.0449)	0.126 (0.0605 – 0.265)	13.6 (10.3 – 18.1)	38.5 (30.1 – 49.9)	0.241 (0.0812 – 0.683)	2.02 (1.26 – 3.51)
Y79	0.0814 (0.0648 – 0.102)	0.0303 (0.0165 – 0.0557)	0.893 (0.243 – 3.28)	9.27 (8.09 – 10.6)	10.3 (7.74 – 13.8)	3.25 (2.23 – 4.74)	5.83 (4.21 – 8.07)

* Previously published in Pascual-Pastó *et al*, 2019

n.p., not performed

We analyzed the expression of two proteins related to apoptosis and DNA-damage, cleaved-poly(ADP-ribose) polymerase (cPARP) and p53, in cells pretreated with VCN-01. Viral infection made cells less susceptible to apoptosis induced by chemotherapeutics, as indicated by the downregulation of both proteins (**Fig. 4.2A**). In the absence of infection, cells exposed to topotecan exhibited a 2- to 3-fold increase in cPARP expression, compared to infected cells in the same condition (**Fig. 4.2B, C**). The infected cells conserved their shape and integrity during the early infection times (48 h), even in the presence of topotecan, indicating the inhibition of the apoptosis (**Fig. 4.2D**).

Then, we addressed the sequence of VCN-01 and topotecan treatments. We found that cells pre-exposed to topotecan before VCN-01 infection were sensitive to the anti-proliferative activity of the drug, regardless of the presence of the virus at a later stage (**Fig. 4.2E**). In contrast, previous infection partially abolished the activity of the drug (**Fig. 4.2E**). These results confirm that VCN-01 preinfection prevents the full cytotoxic effect of chemotherapy.

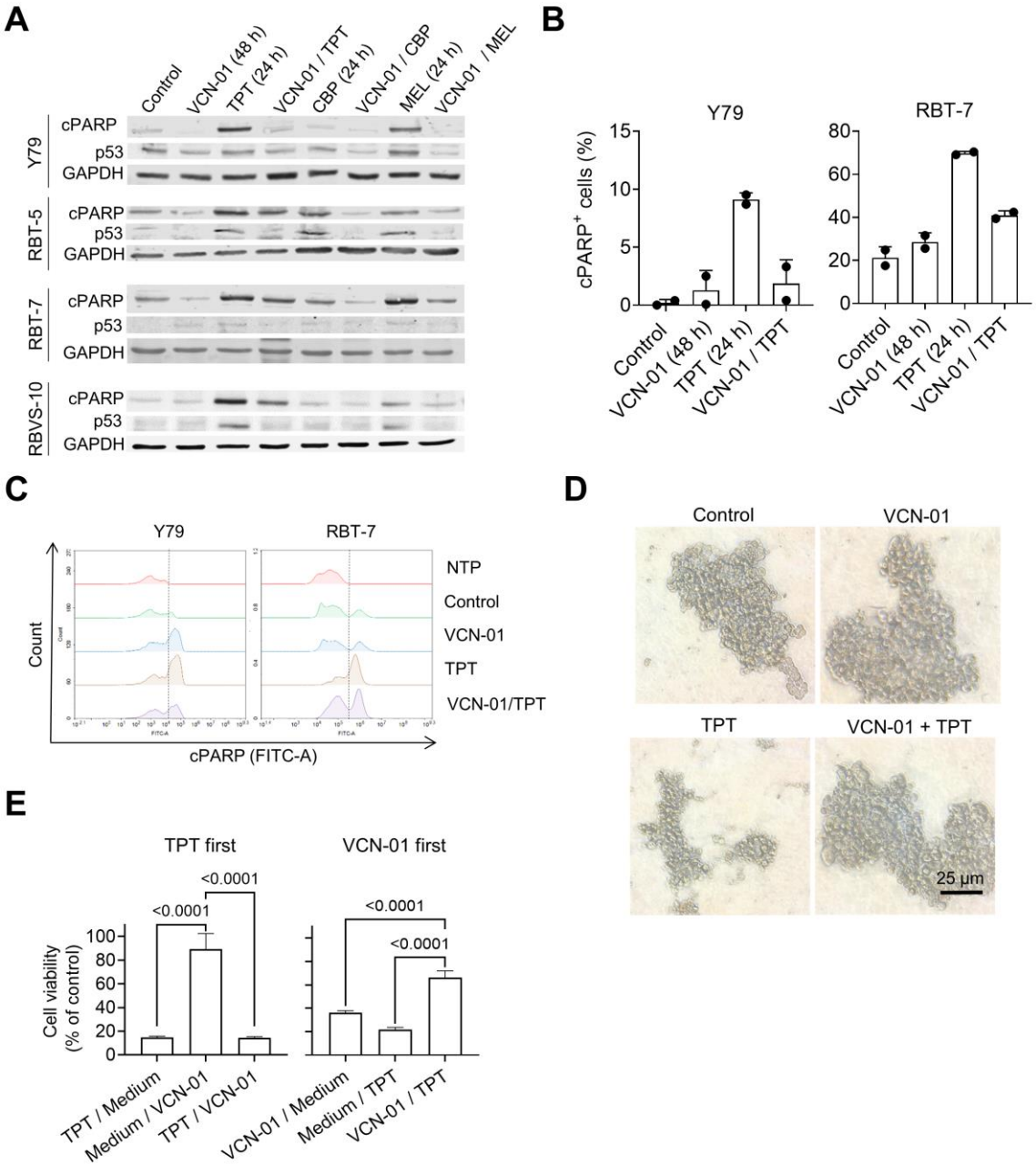

Figure 4.2. Interaction of VCN-01 and chemotherapeutics in vitro. A, Immunoblotting of cPARP and p53 following treatment of Y79 cells with VCN-01 (48 h; 50 MOI), TPT (24 h; 2 µM), VCN-01 and TPT combination (VCN-01 / TPT; 48 h; TPT added at 24 h), CBP (24 h; 12.5 µM), VCN-01 and CBP combination (VCN-01 / CBP; 48 h; CBP added at 24 h), MEL (24 h; 10 µM), and VCN-01 and MEL combination (VCN-01 / MEL; 48 h; MEL added at 24 h). Control cells were not treated. GAPDH was the loading control. B, Proportion (%) of cPARP^{+} Y79 and RBT-7 cells treated with VCN-01 (48 h; 50 MOI), topotecan (24 h; 2 µM) or the combination (VCN-01 / TPT; 48 h; TPT added at 24 h). Dots are experimental replicates and bars are mean and SD. C, Representative flow cytometry histograms of

cPARP expression in Y79 and RBT-7 cells. D, Representative bright-field images of Y79 cells (floating aggregates) treated with VCN-01 (48 h; 50 MOI), TPT (48 h; 2 μM) or the combination (48 h; TPT added at 24 h). E, Viability of Y79 cells treated for 6 days with the sequences “TPT first” or “VCN-01 first”. Treatments (TPT, 2 μM; VCN-01, 50 MOI; or Medium) and sequences (in which the second treatment is administered at day 4) are detailed below the columns. Bars are mean and SD of 8 replicates. The MTS signal of control untreated cells was set as 100%.

1.2. Infection of retinoblastoma cells exposed to VCN-01 and chemotherapy

We studied the changes promoted by topotecan, carboplatin, and melphalan on VCN-01 infection. First, we analyzed the early viral protein E1A, which is the first protein expressed upon VCN-01 infection. Surprisingly, E1A was highly overexpressed in infected cells treated with topotecan 24 h after VCN-01, but not in cells treated with carboplatin and melphalan (**Fig. 4.3A, B**). Next, we switched the sequence of treatments and exposed the cells first to topotecan and, after 24 h, to VCN-01. Topotecan pretreatment did not modify E1A protein expression, compared to VCN-01 (24 h) (**Fig. 4.3B**), but significantly increased E1A mRNA expression (**Fig. 4.3C**). We found an increase in the levels of E2F-1 (VCN-01 promoter) in those cells treated with topotecan (**Fig. 4.3B**). Cells pretreated with topotecan had higher levels of cPARP and p53 expression (**Fig. 4.3B**). In contrast, topotecan addition after the virus boosted up to two orders of magnitude the expression of E1A (**Fig. 4.3B, C**) and E1B (**Fig. 4.3D**). Another camptothecin, SN-38, increased the expression of E2F-1 and E1A similarly to topotecan in cells pre-exposed to VCN-01, in contrast to the alkylating drugs, the antimetabolite drug hydroxyurea and the topoisomerase II inhibitor etoposide, which did not modify the levels of these proteins (**Fig. 4.3E**). The molecular target of camptothecins, topoisomerase 1, increased upon VCN-01 infection in one primary culture and remained unchanged in another (**Fig. 4.3F**). Overall, the results indicate that adenoviral infection impedes the apoptotic action of topotecan, while this drug favors the expression of early viral proteins in cells pre-exposed to VCN-01, likely by increasing the expression of the viral promoter E2F-1 in cells.

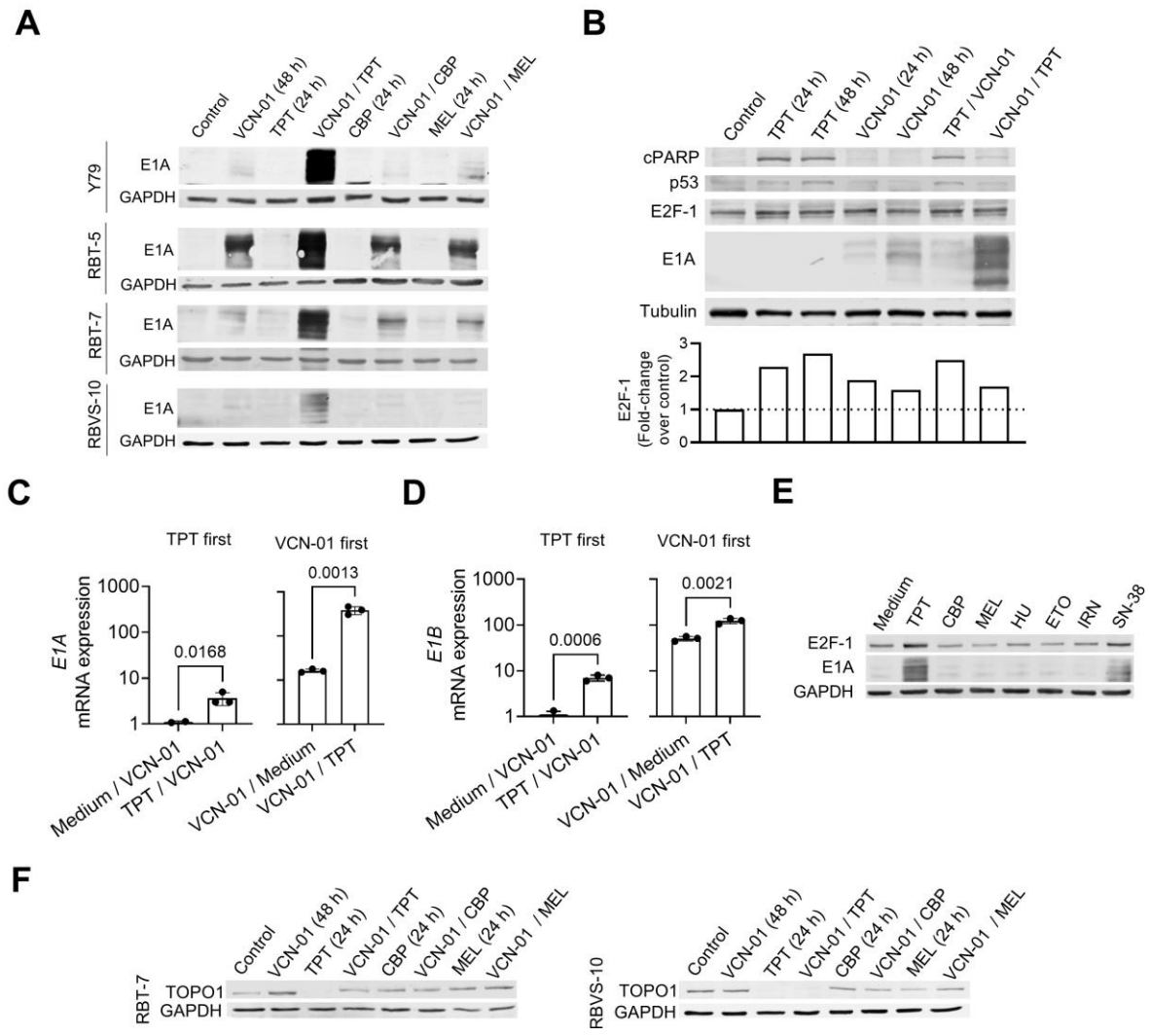

Figure 4.3. Infection of retinoblastoma cells treated with VCN-01 and chemotherapeutics in vitro. A, Immunoblotting of E1A following treatment of Y79 cells with VCN-01 (48 h; 50 MOI), TPT (24 h; 2 µM), VCN-01 and TPT combination (VCN-01 / TPT; 48 h; TPT added at 24 h), CBP (24 h; 12.5 µM), VCN-01 and CBP combination (VCN-01 / CBP; 48 h; CBP added at 24 h), MEL (24 h; 10 µM), and VCN-01 and MEL combination (VCN-01 / MEL; 48 h; MEL added at 24 h). Control cells were not treated. GAPDH was the loading control. B, Immunoblotting of cPARP, p53, E2F-1 and E1A following treatment of Y79 cells with VCN-01 (24 h or 48 h; 50 MOI), TPT (24 h or 48 h; 2 µM) or the combinations at the sequences "TPT first" (TPT / VCN-01; 48 h; VCN-01 added at 24 h) or "VCN-01 first" (VCN-01 / TPT; 48 h; TPT added at 24 h). β-tubulin was the loading control. C, Quantification of *E1A* mRNA in Y79 cells treated with the sequences "TPT first" or "VCN-01 first". Dots are experimental replicates and bars are mean and SD. D, Quantification of *E1B* mRNA in Y79 cells treated with the sequences "TPT first" or "VCN-01 first". E, Immunoblotting of E2F-1 and E1A following treatment of Y79 cells exposed to VCN-01 for 48 h (50 MOI). At 24 h, we added TPT (2

µM), CBP (12.5 µM), MEL (10 µM), hydroxyurea (HU; 100 µM), etoposide (ETO; 2 µM), irinotecan (IRN; 10 µM) or SN-38 (1 µM). GAPDH was the loading control. F, Immunoblotting of topoisomerase I (TOPO 1) following treatment of primary retinoblastoma cells (RBT-7 and RBVS-10) with VCN-01 (48 h; 50 MOI), topotecan (TPT; 24 h; 2 µM), VCN-01 and TPT combination (VCN-01 / TPT; 48 h; TPT added at 24 h), carboplatin (CBP; 24 h; 12.5 µM), VCN-01 and CBP combination (VCN-01 / CBP; 48 h; CBP added at 24 h), melphalan (MEL; 24 h; 10 µM), and VCN-01 and MEL combination (VCN-01 / MEL; 48 h; MEL added at 24 h). Control cells were not treated. GAPDH was the loading control.

1.3. The role of cell cycle and E2F-1 in VCN-01 infection

We explored the cell cycle as a possible underlying factor contributing to the upregulation of early viral proteins induced by topotecan. Because cells in S-phase are more susceptible to adenovirus infection and several chemotherapeutics alter the cell cycle, we addressed the cell cycle profile of retinoblastoma cells exposed to topotecan and carboplatin. We expected that drugs increasing the proportion of cells in S-phase would lead to an increase in viral protein expression. We used hydroxyurea as a positive control of S-phase cell cycle arrest (*237*). After 24 h exposure, we found that topotecan increased the percentage of cells in S-phase, similar to hydroxyurea (**Fig. 4.4A**). Carboplatin increased the percentage of cells in G1-phase (**Fig. 4.4A**). The effect of topotecan was noticeable after 4 h of drug exposition and lasted for at least 48 h (**Fig. 4.4B, C**).

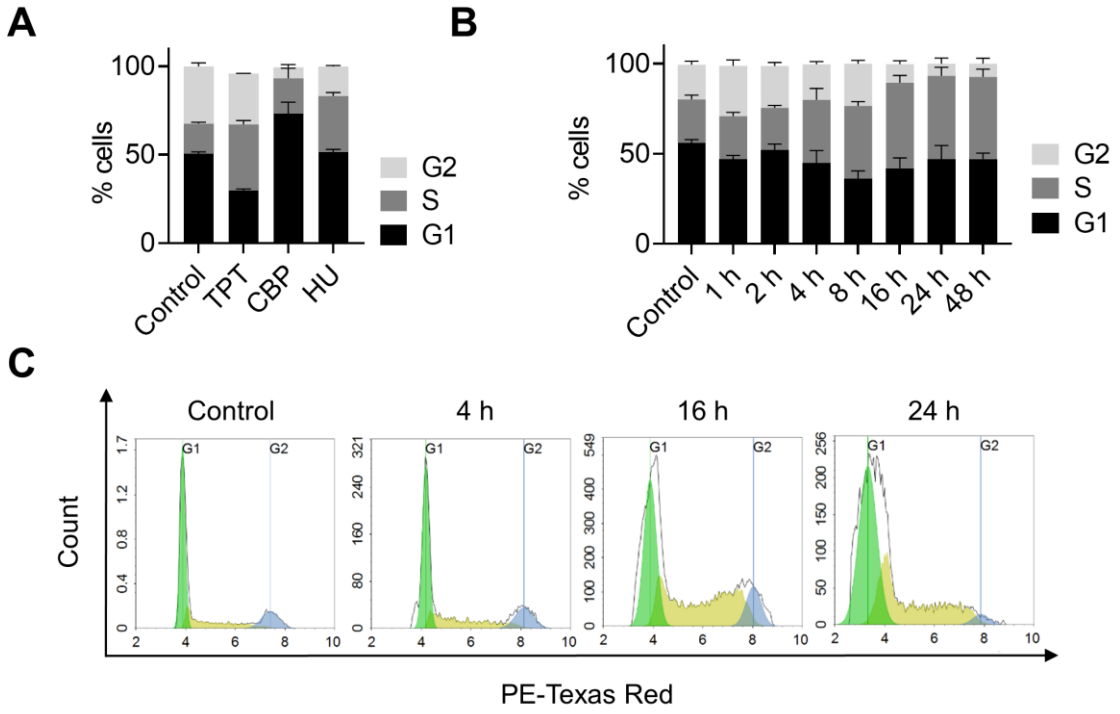

Figure 4.4. Cell cycle profile in retinoblastoma cells exposed to chemotherapeutics. A, Percentage of Y79 cells in G1, S and G2 cell cycle phases following 24 h treatment with culture medium (Control), topotecan (TPT; 2 µM), carboplatin (CBP; 12.5 µM) or hydroxyurea (HU; 100 µM). Bars are means and SD of three replicates. B, Percentage of Y79 cells in G1, S and G2 cell cycle phases following treatment with TPT (2 µM) for up to 48 h. Bars are means and SD of three replicates. C, Representative images of the cell cycle evaluation of Y79 cells treated with TPT (2 µM) for 4, 16 or 24 h. In the plots, G1-phase cells are colored in green (left peak). S-phase cells in yellow (middle) and G2-phase cells in blue (right).

To complement these results, we analyzed proteins involved in the cell cycle. Topotecan, but not carboplatin, melphalan, or hydroxyurea promoted cellular events consistent with G1/S-phase cell cycle progression, such as increased protein expression of E2F-1, p21 and cyclin E1, which were detectable 1 h after exposure, for at least 48 h (**Fig. 4.5A**). SN-38 produced similar effects, although they appeared later than with topotecan (**Fig. 4.5A**). We also performed immunostaining of E2F-1 in mice bearing intraocular Y79 retinoblastoma xenografts. The expression of E2F-1 in cancer cells was higher in the animals treated with topotecan, compared to that found in untreated animals (**Fig. 4.5B**).

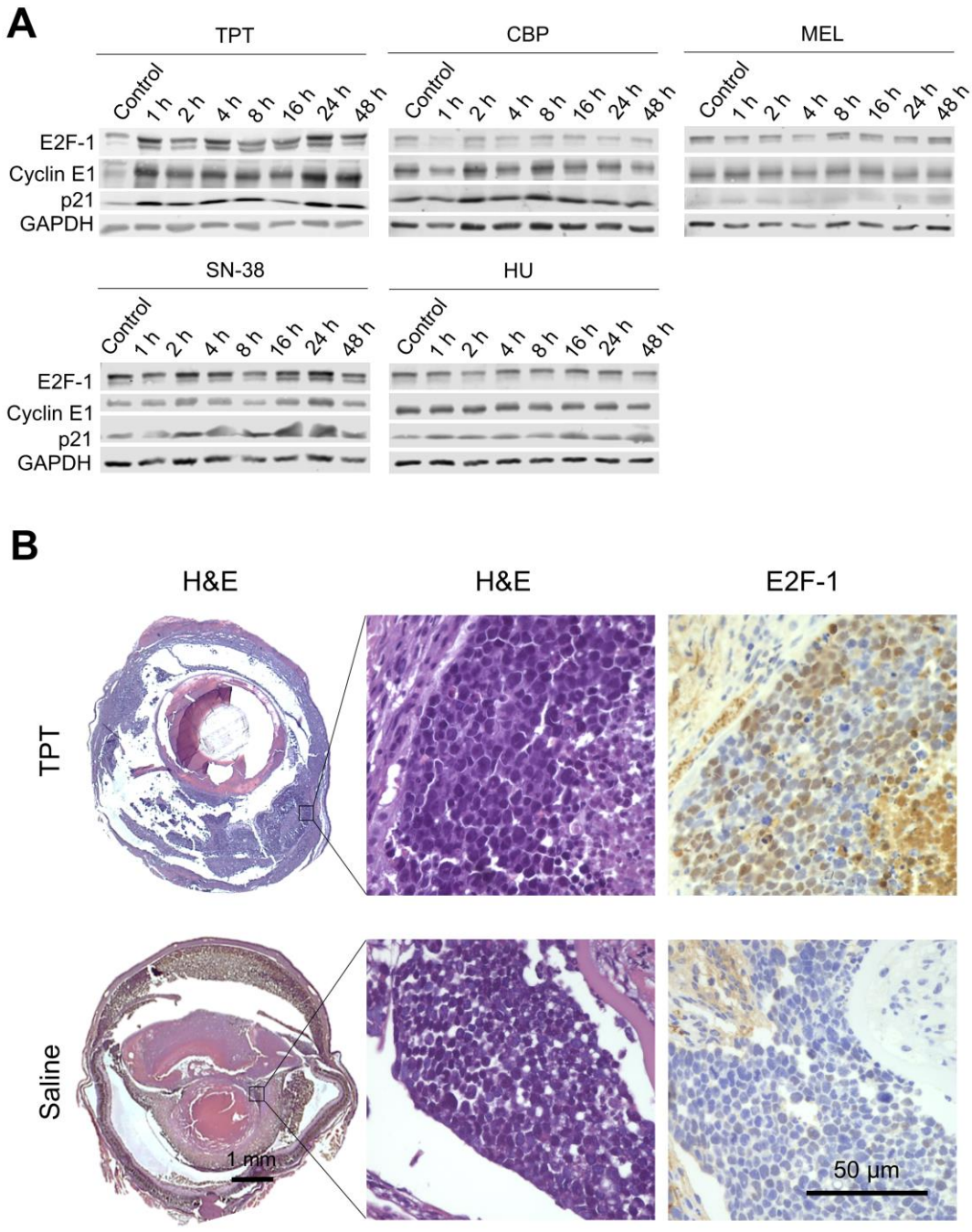

Figure 4.5. Cell cycle related-proteins in retinoblastoma cells and xenografts treated with chemotherapeutics. A, Immunoblotting of E2F-1, Cyclin E1 and p21 following up to 48 h treatment of Y79 cells with TPT (2 µM), CBP (12.5 µM), MEL (10 µM), HU (100 µM) or SN-38 (1 µM). GAPDH was the loading control. B, Immunostaining of E2F-1 (nuclear staining in brown) in Y79 intraocular xenografts treated with TPT (0.6 mg/kg, daily for five consecutively days), or with saline.

Using confocal microscopy, we evaluated the intranuclear distribution of E2F-1 upon cell exposure to topotecan (2 µM), carboplatin (12 µM) and SN-38 (1 µM) for 24 h. Untreated cells (control) showed a heterogeneous pattern of E2F-1 staining, with some cells showing positivity in the nucleus, others in the cytoplasm, and some showing no positivity **(Fig. 4.6A)**. Following topotecan exposure, E2F-1 was recruited to the nucleus, forming foci of high positivity **(Fig. 4.6A)**. In carboplatin-treated cells, we observed a diffuse pattern of E2F-1, both inside and outside the nucleus **(Fig. 4.6A).** SN-38-treated cells showed a pattern of E2F-1 distribution similar to that observed in topotecan-treated cells, with significant nuclear concentration **(Fig. 4.6A)**.

Next, to quantify E2F-1 binding to the VCN-01 promoter sequence, we designed specific oligonucleotides containing the VCN-01 promoter sequence. We used a DNA-protein binding assay kit to measure the interaction between E2F-1 protein and DNA oligonucleotides. In Y79 cells, we observed that treatment with topotecan (2 µM) and SN-38 (1 µM) significantly enhanced E2F-1 activity, as evidenced by the increased binding to the VCN-01 promoter oligonucleotide **(Fig. 4.6B)**. These findings align with our previous observations indicating that increased expression of E2F-1 protein correlates with enhanced activity.

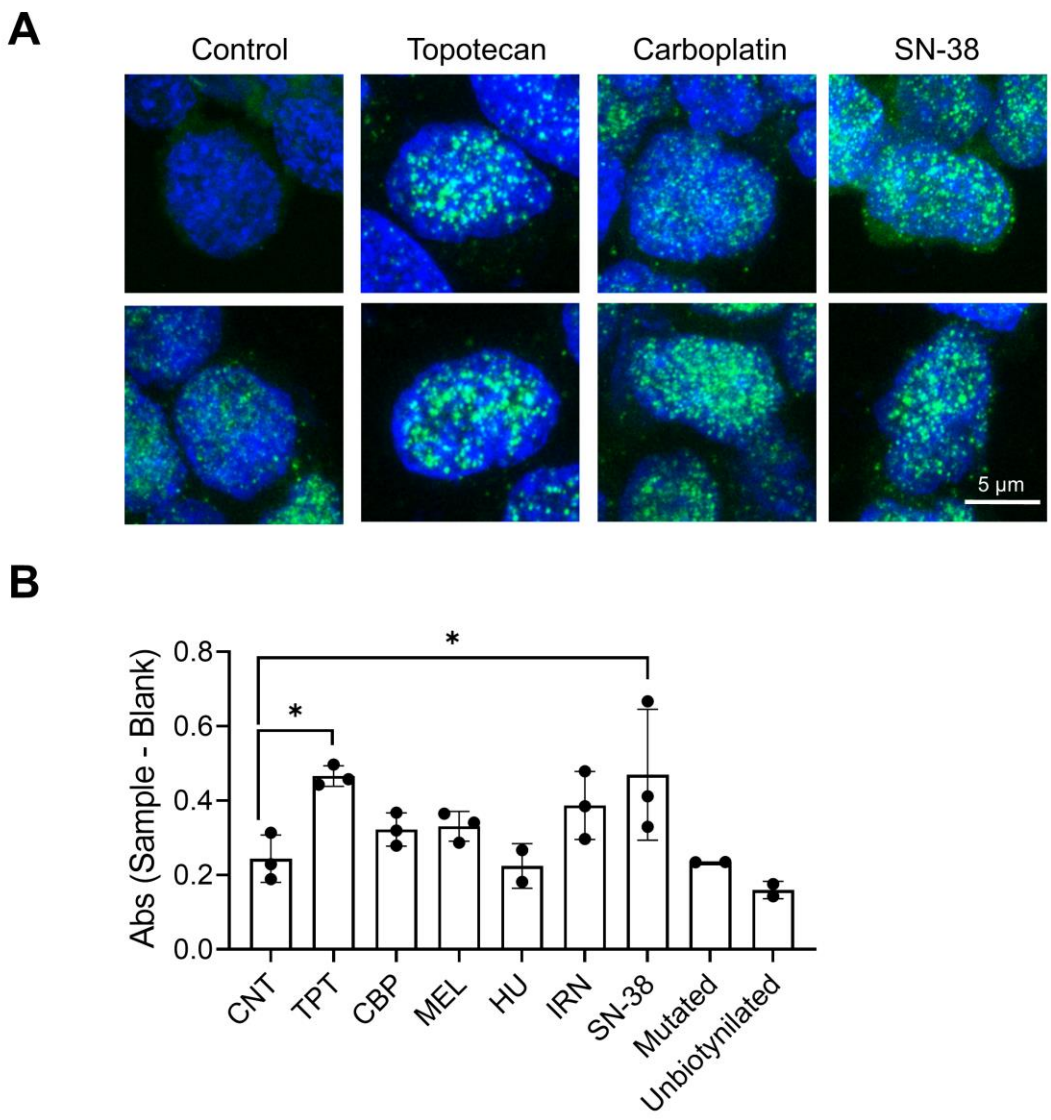

Figure 4.6. E2F-1 distribution and activity upon chemotherapy treatment. A, Immuno fluorescence of E2F-1 after 24 h treatment of Y79 cells with topotecan (2 µM), carboplatin (12.5 µM) and SN-38 (1 µM). B, DNA-protein binding assay using a colorimetric assay kit (ab117139). Biotin-labeled oligonucleotides containing the E2F-1 promoter sequence were used as probes. Nuclear protein extracts were obtained from Y79 cells treated with topotecan (2 µM), carboplatin (12.5 µM), melphalan (10 µM), hydroxyurea (100 µM), irinotecan (10 µM) and SN-38 (1 µM) for 24 h. Mutated oligonucleotides and unbiotinylated oligonucleotides were used as negative controls. Columns represent mean absorbance readings of three independent experiments, performed in different days, normalized by subtracting the absorbance of the blank control. Each dot represents the result of one experiment.

We next assessed cell cycle-related genes in cells pre-infected with VCN-01 and treated with topotecan or carboplatin. In cells pre-infected (48 h) with VCN-01, a real time quantitative polymerase chain reaction (RT-qPCR) gene expression array revealed that topotecan upregulated genes that promote S-phase arrest during the cell cycle, with a 10-fold increase in the expression of the gene *CDKN1A* (cyclin-dependent kinase inhibitor 1A) (**Fig. 4.7A**). Conversely, it downregulated genes that promote G1/S transition, with a 15-fold decrease in the expression of *CDK6* (cyclin dependent kinase 6) (**Fig. 4.7A**). We confirmed the array findings using individual RT-qPCR assays for *CDKN1A* and *CDK6* (**Fig. 4.7B**). Among the E2F-1-target genes, *PCNA* (proliferating cell nuclear antigen) was significantly overexpressed in VCN-01-infected cells exposed to topotecan (**Fig. 4.7C**). These results suggest that topotecan treatment induces cell cycle-related proteins and genes in VCN-01-infected cells.

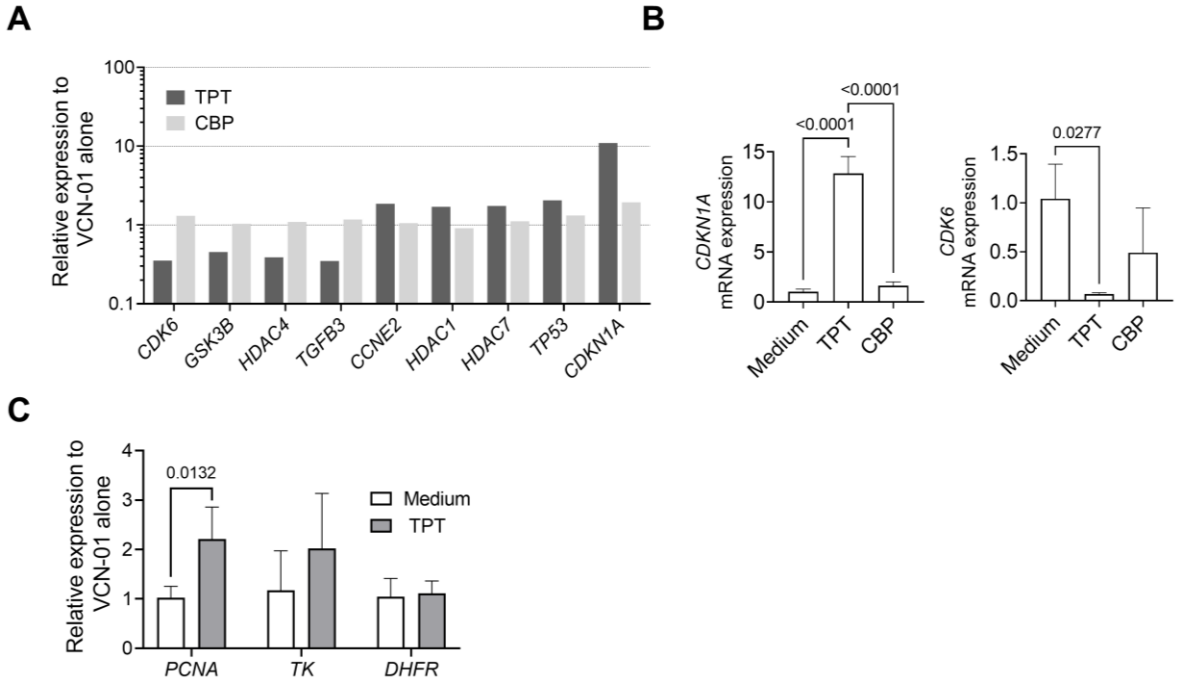

Figure 4.7. Array of human cyclins and cell cycle regulation genes in retinoblastoma cells exposed to VCN-01 and chemotherapeutics. A, Expression of cyclins and cell cycle regulation genes induced by TPT (2 µM; 24 h) and CBP (12.5 µM; 24 h) in RBT-7 cells pre-infected with VCN-01 (50 MOI; 48 h). Values are fold-changes relative to expression in control infected cells exposed to

culture medium. B, Expression of *CDKN1A* and *CDK6* following 48 h treatment of VCN-01-infected RBT-7 cells with TPT (2 µM) or CBP (12.5 µM). Values are fold-changes relative to expression in control infected cells exposed to culture medium. C, Expression of *PCNA, TK* and *DHFR* following 48 h treatment of VCN-01-infected RBT-7 cells with TPT (2 µM). Values are fold-changes relative to expression in control infected cells exposed to culture medium.

1.4. Transgene expression of AdTLRGDK in retinoblastoma cells exposed to chemotherapy

To address whether S-phase cell cycle arrest favored the expression of viral transgenes, we used the non-replicative adenovirus AdTLRGDK, which codifies for a green fluorescent protein (GFP) and shares the same capsid of VCN-01. We synchronized most Y79 cells in the S-phase using hydroxyurea at high concentration (**Fig. 4.8A**). After washing steps, we treated cells with AdTLRGDK. We observed that those cells previously synchronized exhibited a significant increase in their GFP levels (**Fig. 4.8B-D**). After 72 h, 44% of the asynchronized cells were infected, in contrast to 90% of synchronized cells (**Fig. 4.8D**). These results suggest that cells synchronized in S-phase are more suitable for adenoviral transgene expression.

As observed for S-phase-synchronized cells, those cells preinfected with the adenovirus AdTLRGDK and exposed to topotecan and hydroxyurea (both induce S-phase cell cycle arrest), had significantly higher levels of GFP, compared to cells treated with carboplatin or melphalan (**Fig. 4.8E**). The reverse sequence of treatments (i.e., drug exposure before viral infection) did not enhance viral transduction (**Fig. 4.8E**). Following S-phase cell cycle synchronization using hydroxyurea (**Fig. 4.8F**), we found that cells arrested in S-phase were more susceptible to the oncolytic activity of VCN-01, compared to asynchronized cells, resulting in an 8-fold reduction in the IC_{50} of VCN-01 at day 8 post-infection and an 82-fold reduction at day 10 (**Fig. 4.8G**). These results suggest that S-phase cell cycle enrichment increases AdTLRGDK viral infectivity and VCN-01 oncolytic activity. Along with the previous findings, our findings underscore the dual function of topotecan in increasing VCN-01 infectivity, enhancing E2F-1 activity and inducing cell cycle arrest.

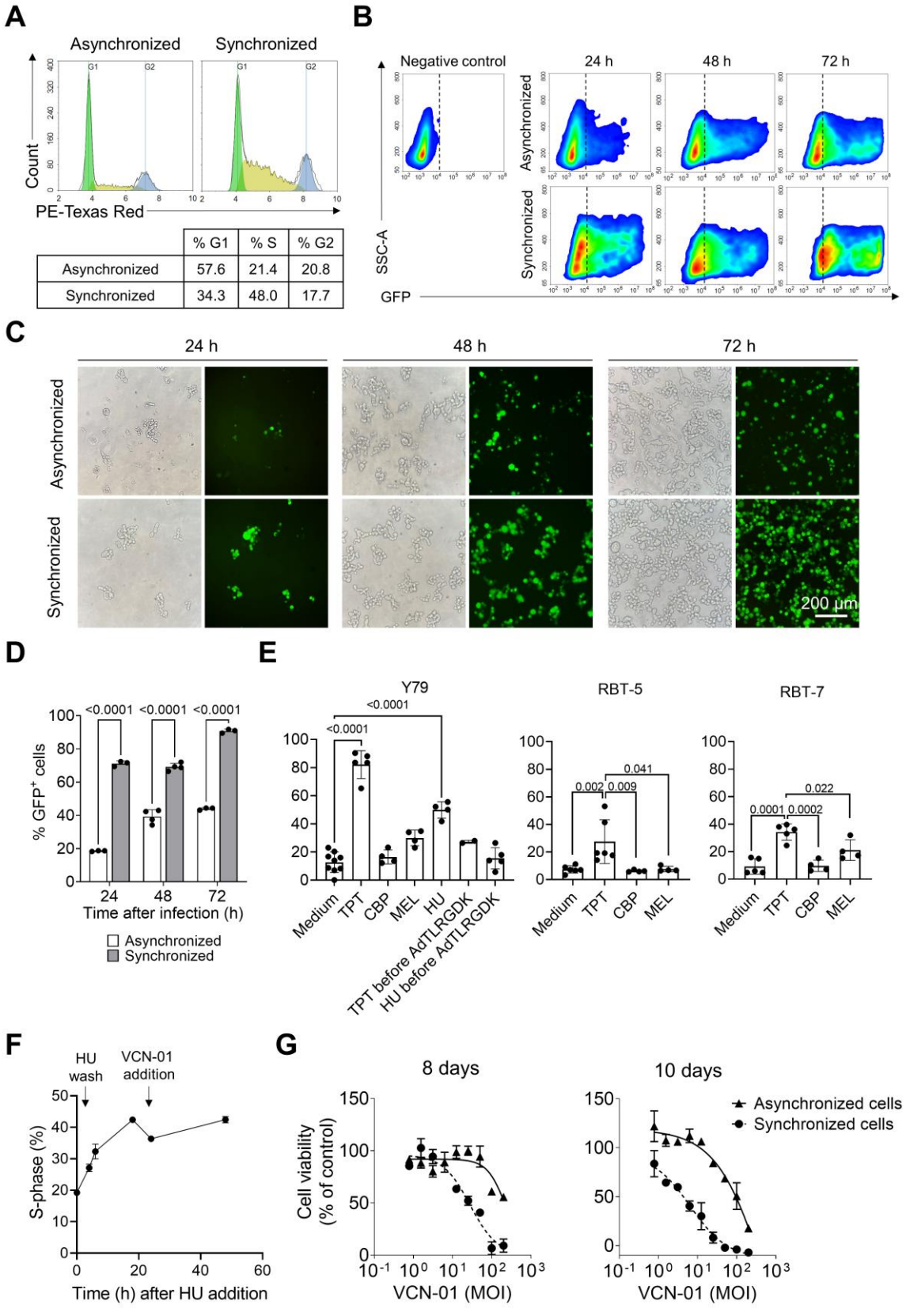

	% G1	% S	% G2
Asynchronized	57.6	21.4	20.8
Synchronized	34.3	48.0	17.7

Figure 4.8. Effect of chemotherapeutics on adenoviral transduction and oncolytic activity in retinoblastoma cells. A, Representative plots of the percentage of Y79 cells in G1, S and G2 cell cycle phases following treatment with hydroxyurea (HU; 4 mM) (synchronized) or culture medium (asynchronized). The table contains the quantification of the plots. B, Representative pseudo-color-flow-plots of Y79 cells pre-exposed to 4 mM HU (synchronized) and treated with AdTLRGDK (50 MOI) for 24, 48 or 72 h. We used uninfected cells as negative control. C, Representative bright light and fluorescence images of the experiment of panel B. We used culture medium as control (asynchronized). D, Proportion (%) of GFP+ cells of the experiment of panel B. Dots are experimental replicates (n = 3-4) and bars are mean and SD. E, Proportion (%) of GFP+ Y79 cells pretreated for 24 h with AdTLRGDK (50 MOI) and exposed for additional 24 h to culture medium (Medium), topotecan (TPT; 2 µM), carboplatin (CBP; 12.5 µM), melphalan (MEL; 12 µM) or HU (100 µM), or exposed to the reverse sequence in which cells were treated with TPT or HU 6 h before AdTLRGDK infection. Dots are experimental replicates and bars are mean and SD. F, Percentage of RBT-7 cells in S-phase following hydroxyurea (HU) treatment (4 mM; washing step at 4 h). Dots are mean of experimental replicates (n = 2) and bars are SD. G, Antiproliferative activity of VCN-01 in RBT-7 cells following S-phase synchronization using hydroxyurea. Cell viability was measured on days 8 and 10 following virus addition. Values are means and SD of three replicates. Lines are the best fitting curves built using the least square regression method of GraphPad. Cell viability is expressed as the relative percentage of the assay signal of treated cells, compared to control untreated cells, which was set as 100%.

1.5. Viral replication and transgene expression of VCN-01 in retinoblastoma cells exposed to chemotherapy

In a preliminary experiment, we established the multiplicity of infection (MOI; i.e., transducing units of virus per cell) of VCN-01 that resulted in 100% infection of Y79 cells in vitro. Such concentration was 500 MOI and was subsequently used for experiments assessing viral replication. Using specific VCN-01 oligonucleotides and the RT-qPCR technique, we determined that topotecan did not increase viral production in Y79 cells pre-infected at 500 MOI (**Fig. 4.9A**), i.e., at 100% infection, topotecan did not help cells produce more virus.

Next, we used s.c. retinoblastoma tumors established from RBT-7 and Y79 cells to analyze the viral counts and *SPAM1* transgene expression after one single intratumoral injection of VCN-01. We found that those mice receiving VCN-01

followed by 5 consecutively doses (one by day) of intraperitoneal topotecan had higher counts of viral genomes after treatment (day 5) compared to mice treated with a single intratumoral injection of VCN-01, mice treated with the combination of VCN-01 and carboplatin, or mice treated with the combination of VCN-01 and hydroxyurea (**Fig. 4.9B**). We did not find different counts of viral genomes after 15 days of virus injection (**Fig. 4.9C**). A similar trend was evident for the quantification of the *SPAM1* transgene encoded by VCN-01, when comparing topotecan-treated cells with untreated cells or carboplatin-treated cells (**Fig. 4.9D**).

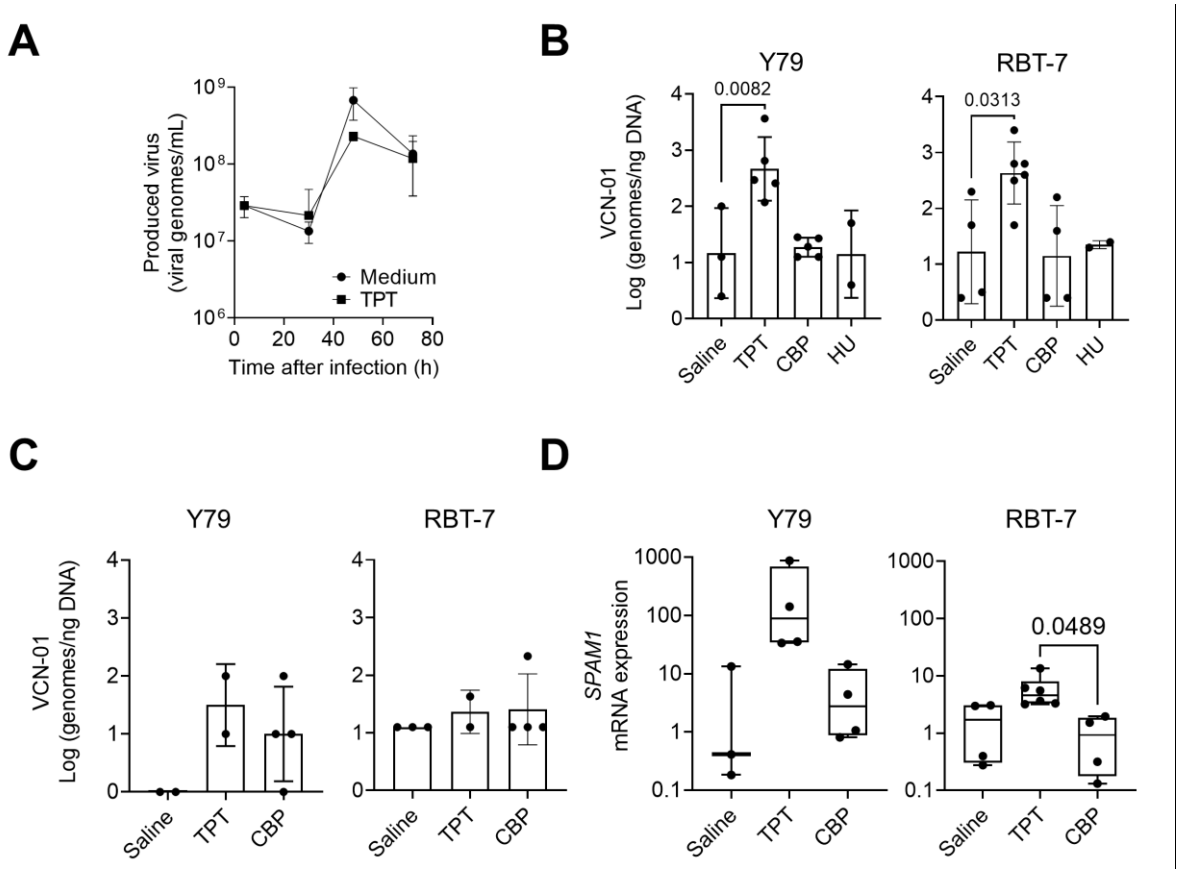

Figure 4.9. Effect of chemotherapeutics on viral production and transgene expression in retinoblastoma cells. A, Effect of TPT (2 μM) on the viral production of VCN-01 in Y79 cells, measured as the number of viral genomes per mL of cell pellet extract. B, Quantification of VCN-01 genomes in s.c. retinoblastomas (Y79 and RBT-7) 5 days after local injection of VCN-01 and subsequent treatment with saline, TPT (0.6 mg/kg, daily for five consecutively days), CBP (40 mg/kg, one single dose at day 1) or HU (200 mg/kg, daily for five consecutively days). Dots are values from individual tumors and error bars represent the SD. C, Quantification of VCN-01 genomes in s.c.

retinoblastomas (Y79 and RBT-7) 15 days after local injection of VCN-01 and subsequent treatment with saline, TPT (0.6 mg/kg, daily for five consecutively days) or CBP (40 mg/kg, one single dose at day 1). Dots are values from individual tumors and error bars represent the SD. D, mRNA expression of recombinant hyaluronidase PH20 (*SPAM1* gene) in s.c. retinoblastomas (Y79 and RBT-7) 5 days after local injection of VCN-01 and subsequent treatment with saline, TPT or CBP.

In the same s.c. retinoblastoma xenografts, tumors treated with VCN-01 and five doses of topotecan had the highest number of E1A-positive cells (**Fig. 4.10A**) and the highest level of E1A protein expression (**Fig. 4.10B**), compared to tumors treated with saline, carboplatin or hydroxyurea. Overall, our results suggest that the mechanism by which topotecan increases viral counts and transgene expression in xenografts is not related to enhanced replication, but rather to topotecan promoting efficient infection of cancer cells in a dynamic in vivo environment, in which both VCN-01 and topotecan are rapidly cleared.

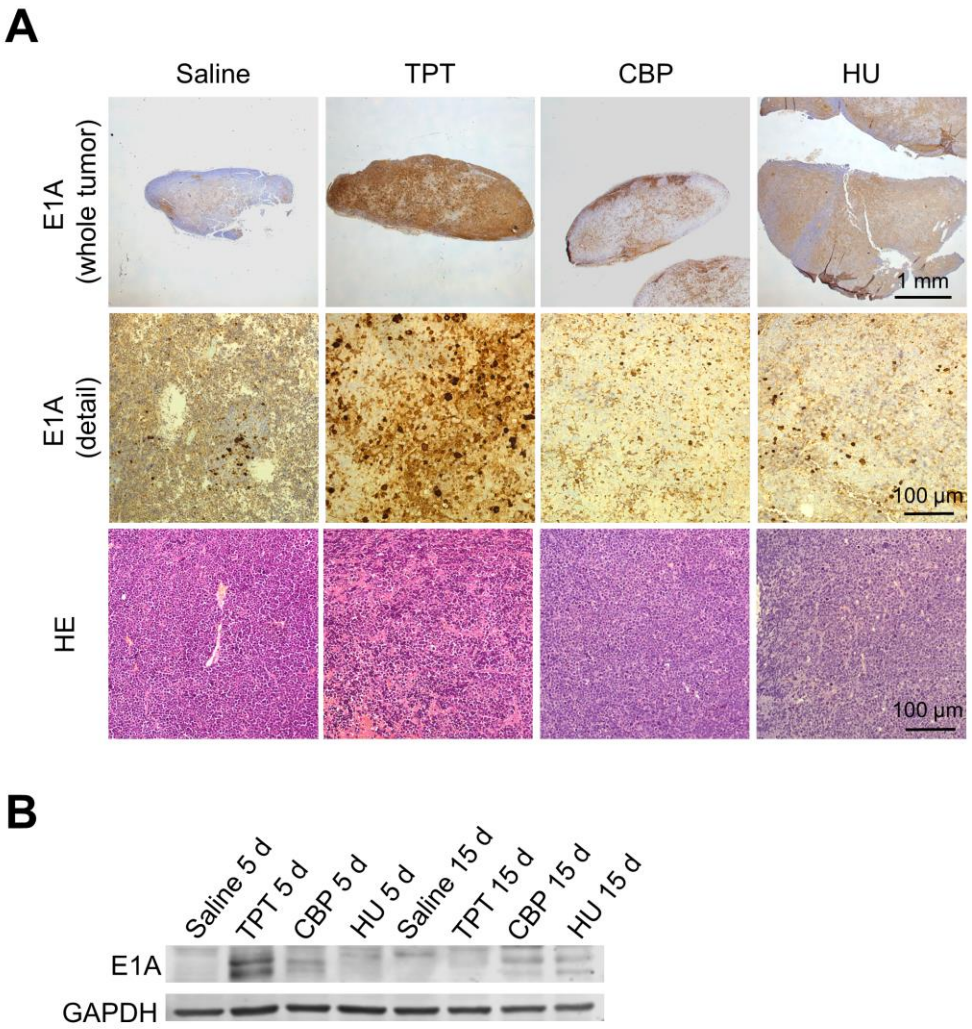

Figure 4.10. Effect of chemotherapeutics on VCN-01 infection in retinoblastoma s.c. xenografts. A, Immunostaining of E1A in s.c. Y79 xenografts 5 days after local injection of VCN-01 and subsequent treatment with TPT, CBP or HU. B, Immunoblotting of E1A in s.c. Y79 xenografts 5 or 15 days after local injection of VCN-01 and subsequent treatment with TPT, CBP or HU. Each sample corresponds to one individual tumor.

2. Activity of VCN-01 and topotecan in retinoblastoma xenografts

So far, I have shown that VCN-01 and topotecan interact leading to high expression of early viral proteins in vitro and more efficient and homogeneous distribution of the viral infection in s.c. xenografts, but whether the anticancer activity of both treatments is better-than-additive remains unclear after these experiments. We attribute such uncertainty to three key factors: i) VCN-01 prevents apoptosis of infected cells, which interferes with the anticancer effects of most chemotherapies; ii) the antiproliferative activity following exposure of cancer cells to chemotherapy needs to be assessed earlier than the effects of VCN-01 infection (at 3 and 10-14 days, respectively), which impedes assessing combinations in vitro; and iii) in vitro studies are unable to simulate the clearance drug dynamics occurring in the tumors in vivo. To tackle this, we performed in vivo experiments to address the therapeutic effect of the treatment. At hospital SJD, we previously established and characterized a series of preclinical models from patients with treatment-naïve and chemoresistant retinoblastoma (*142*). In this thesis, we have evaluated the efficacy of the combination of VCN-01 and chemotherapy in mice bearing orthotopic, s.c. and intracerebral retinoblastoma xenografts. For in vivo experiments, we used three different retinoblastoma cells including two patient-derived retinoblastoma cell models (RBT-7 and RBT-2) and one cell line (Y79).

2.1. Activity of VCN-01 and topotecan in orthotopic retinoblastoma xenografts

We first evaluated the combination of VCN-01 and chemotherapy in orthotopic retinoblastoma xenografts in immunodeficient mice, in which we inoculated 2×10^5 retinoblastoma cells into each eye. After 15 days, mice were randomly distributed into control or treated groups. In a first in vivo study, we aimed to observe the effect of administering a single dose of VCN-01 between two cycles of topotecan, compared to two cycles of topotecan, or VCN-01 alone. We included one group receiving standard-of-care chemotherapy treatment, for comparison. We found that one intraocular dose of VCN-01 administered between two cycles of topotecan

prolonged the median ocular survival of Y79 xenografts longer than 80 days, which was a significant therapeutic benefit compared to untreated control eyes (37 days; *P* = 0.0005) (**Fig. 4.11A**). Treatments with topotecan or with the standard of care (carboplatin and etoposide) resulted in modest improvements in median survival (58 and 55 days, respectively), although not significant compared to controls (*P* = 0.062 and *P* = 0.674, respectively) (**Fig. 4.11A**). As a single agent, the selected dose of VCN-01 was sub-therapeutic (40 days, *P* = 1) (**Fig. 4.11A**).

Our previous in vitro data showed that the sequence of administration of topotecan and VCN-01 affected the results. In vivo, we observed that the sequence of administration producing a better-than-additive efficacy was the one in which VCN-01 was administered first, followed by topotecan (**Fig. 4.11B**). This therapeutic sequence achieved a median ocular survival of 62 days, significantly longer than controls (46 days, *P* = 0.0436). The reverse sequence, topotecan followed by VCN-01, did not result in therapeutic benefit (52 days, *P* = 1) (**Fig. 4.11B**). We confirmed the synergism of VCN-01 and topotecan in one primary retinoblastoma xenograft that achieved a median survival of 67 days, longer than controls (35 days, P < 0.0001), while VCN-01 and topotecan were not effective as single agents (33 days and 39 days, respectively) (**Fig. 4.11C-E**). In tumors treated with the combination we detected areas of active VCN-01 infection at endpoint (i.e., at the time of enucleation due to tumor progression), even at day 65 after one single VCN-01 injection (**Fig. 4.11F**).

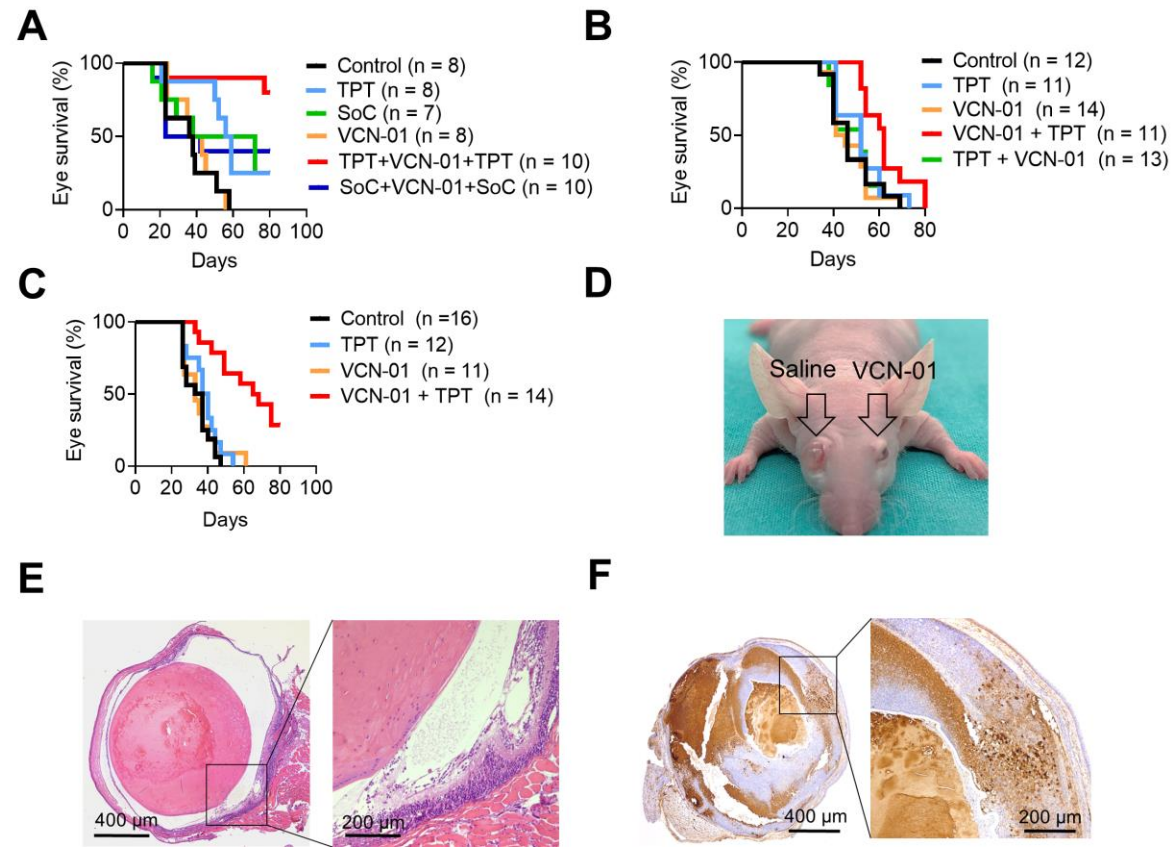

Figure 4.11. **Activity of local VCN-01 and systemic topotecan in orthotopic retinoblastoma xenografts**. A, Ocular survival of eyes with Y79 xenografts treated with intravitreal VCN-01, standard-of-care chemotherapy (SoC), topotecan (TPT) or the combinations. B, Ocular survival of eyes with Y79 xenografts treated with topotecan, VCN-01 or the combination in the sequences topotecan first (TPT + VCN-01) or virus first (VCN-01 + TPT). C, Ocular survival of eyes with RBT-7 xenografts treated with topotecan, VCN-01 or the combination. D, Representative image of a mouse with bilateral RBT-7 intraocular xenografts treated with systemic topotecan and one dose of VCN-01 into the left eye, and saline in the right eye. The image was obtained 30 days after treatment start. E, Representative H&E staining in a survivor eye (day 80) with an RBT-7 xenograft treated with VCN-01 and topotecan. F, E1A immunostaining in an RBT-7 intraocular xenografts injected with one dose of VCN-01 followed by five doses of systemic topotecan. The eye was enucleated after 65 days of VCN-01 inoculation.

Next, we maximized the number of cycles of topotecan (two) and VCN-01 injections (two) in order to achieve a longer antitumor response in orthotopic xenografts. We found that mice receiving the combination of VCN-01 and topotecan obtained a significant extension of the median ocular survival compared to the control group ($P < 0.0001$) (**Fig. 4.12A**). Two doses of VCN-01 did not result in survival benefit at the dose level of 3×10^7 vp/eye (**Fig. 4.12A**). To address whether VCN-01 modified the intraocular distribution of topotecan, we obtained tumor samples from VCN-01-infected eyes, 6 hours after mice received a s.c. infusion of topotecan. We found that the biodistribution of topotecan in intraocular tumors did not change upon concomitant treatment with VCN-01 (**Fig. 4.12B**). Together, these results suggest that the administration of systemic topotecan after the intraocular injection of VCN-01 results in a synergistic antitumor effect that significantly prolongs the overall survival of orthotopic retinoblastoma xenografts.

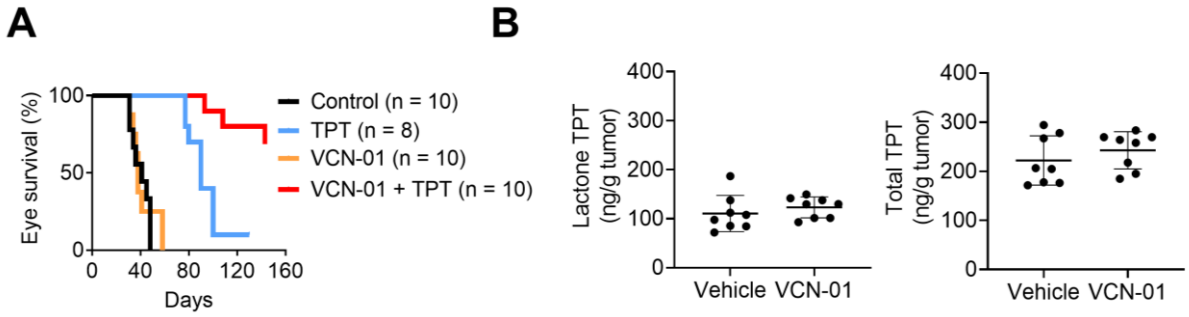

Figure 4.12. Intraocular accumulation of topotecan in intraocular retinoblastoma xenografts infected with VCN-01. A, Ocular survival of eyes with HSJD-RBT-2 (RBT-2) xenografts treated with maximized dosing schedules including VCN-01 (two injections), topotecan (6 cycles) and the combination. B, Intratumoral accumulation of topotecan (TPT), lactone and total, at the steady state (i.e., at constant concentration in plasma), in orthotopic retinoblastoma xenografts (RBT-2) pre-treated with a local intraocular injection of adenovirus (VCN-01) or vehicle solution (vehicle). Dots are values obtained from individual tumors and lines are means and SD.

2.2. Activity of VCN-01 and topotecan in s.c. retinoblastoma xenografts

We used s.c. retinoblastoma xenografts to evaluate the efficacy of the combination in bulky tumors. As previously reported for orthotopic tumors, the combination of intratumoral VCN-01 and systemic topotecan achieved median survivals of 67 and more than 80 days for Y79 and RBT-7 xenografts, respectively. These values were significantly longer than those obtained for the control groups (35 days, *P* = 0.0009, and 35 days, *P* = 0.0021, respectively) (**Fig. 4.13A, B**).

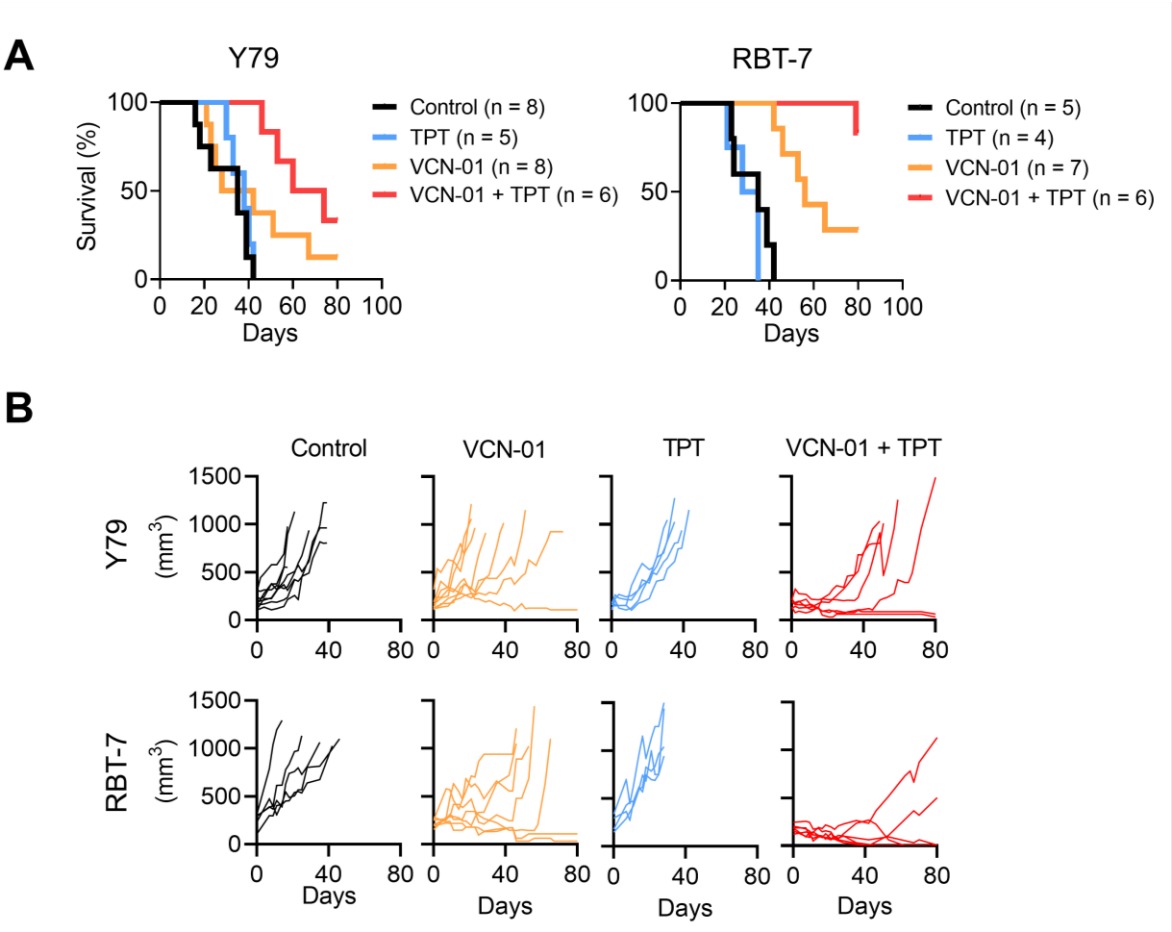

Figure 4.13. Activity of local VCN-01 and systemic topotecan in s.c retinoblastoma xenografts. A, Survival of mice bearing Y79 or RBT-7 s.c. xenografts treated with one intratumoral injection of VCN-01, systemic topotecan, or the combination. B, Antitumor activity of one intratumoral injection of VCN-01, systemic topotecan, or the combination in s.c. retinoblastomas Y79 and RBT-7. Graphs show individual tumor growth.

2.3. Activity of VCN-01 and topotecan in intracerebral retinoblastoma xenografts

We aimed to evaluate our treatment in the most aggressive form of retinoblastoma, which involves its extension to the CNS. Patients with CNS disseminated retinoblastoma usually present tumors in leptomeningeal location and have very poor prognosis. To evaluate therapies for them, we first addressed the need to establish an orthotopic xenograft. In this thesis, I present a novel leptomeningeal model of retinoblastoma reproducing the clinical setting of CNS metastases. We processed the primary culture RBT-7, derived from a patient diagnosed at 6 months old with unilateral retinoblastoma. This patient had not received treatment before enucleation. We cultured and expanded the cells in serum-free neural stem cell medium. Then, we inoculated one million cells targeting the 4^{th} ventricle of the mouse brain (**Fig. 4.14A**). Starting 2 weeks from the surgery, mice presented clear symptoms of tumor progression including progressive motor dysfunction and weight loss. Median survival for mice was 22 days. Histologically, retinoblastoma occupied and enlarged the whole leptomeningeal space, including the meninges surrounding the spinal cord (**Fig. 4.14B, C**). In a preliminary experiment, treatment with standard of care (systemic carboplatin and etoposide) and topotecan significantly prolonged mice survival compared to control group (26 days, $P = 0.01$, and 28 days, $P < 0.0001$, respectively) (**Fig. 4.14D**).

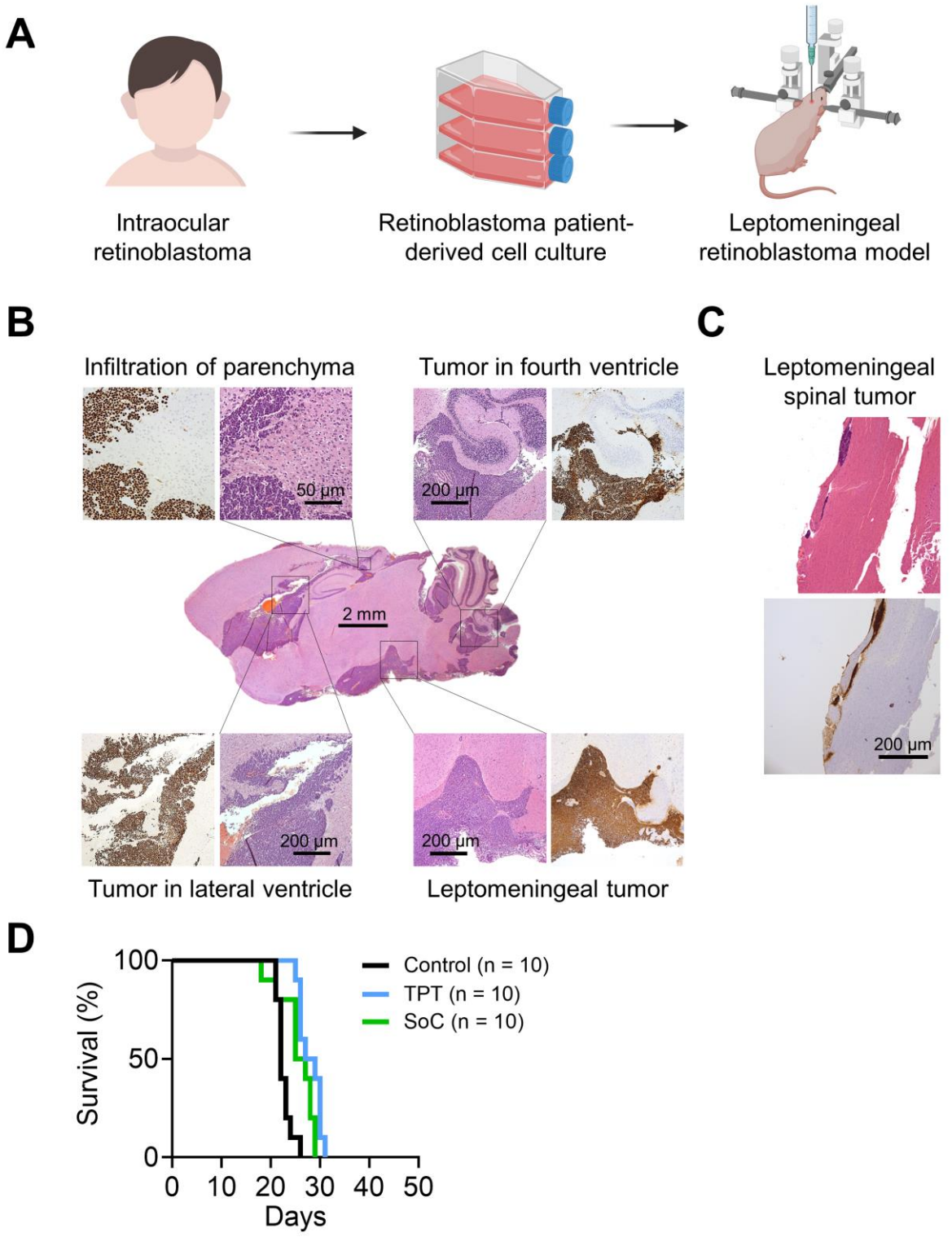

Figure 4.14. **Establishment of a leptomeningeal retinoblastoma model in immunodeficient mice.** A, Experimental diagram of leptomeningeal retinoblastoma model establishment. B, Engraftment of RBT-7 cells in the mouse brain at endpoint. The whole brain is stained with

hematoxylin and eosin (H&E). Cancer cells in the high magnification images are stained with the anti-human nuclei antibody, in brown. C, Engraftment of RBT-7 cells in the mouse meninges surrounding the spinal cord, at endpoint (H&E and anti-human nuclei). D, Survival of mice bearing RBT-7 intracerebral tumors treated with standard of care chemotherapy (SoC) or topotecan (TPT).

We evaluated the efficacy of the combination of VCN-01 and topotecan in the CNS metastatic model. Mice treated with the combination of intraventricular VCN-01 (high dose; 3 x 10^9 vp) and systemic topotecan achieved a median survival of 41 days, significantly longer compared to control (25.5 days, $P = 0.003$), topotecan (31 days, $P < 0.0001$) and VCN-01 (32 days, $P = 0.009$) (**Fig. 4.15A**). Topotecan-treated mice experienced moderate weight loss during treatment and recovered after the end of treatment (**Fig. 4.15B**). We next performed efficacy studies reducing the dose of VCN-01. We used two different dosage levels of VCN-01 (3 x 10^7, 3 x 10^8 vp) in combination with topotecan. Combined treatment with low and medium dose achieved a median survival of 35 and 40 days, respectively, significantly longer compared to VCN-01 alone (26 days, $P = 0.04$, and 24 days, $P = 0.004$, respectively) (**Fig. 4.15C**). In a parallel experiment, we compared tumor load of mice treated with saline, topotecan, standard of care, VCN-01 (3 x 10^9 vp) and the combination. Among the animals sacrificed on day 26, the one treated with VCN-01 and topotecan presented the lowest tumor load (**Fig. 4.15D**).

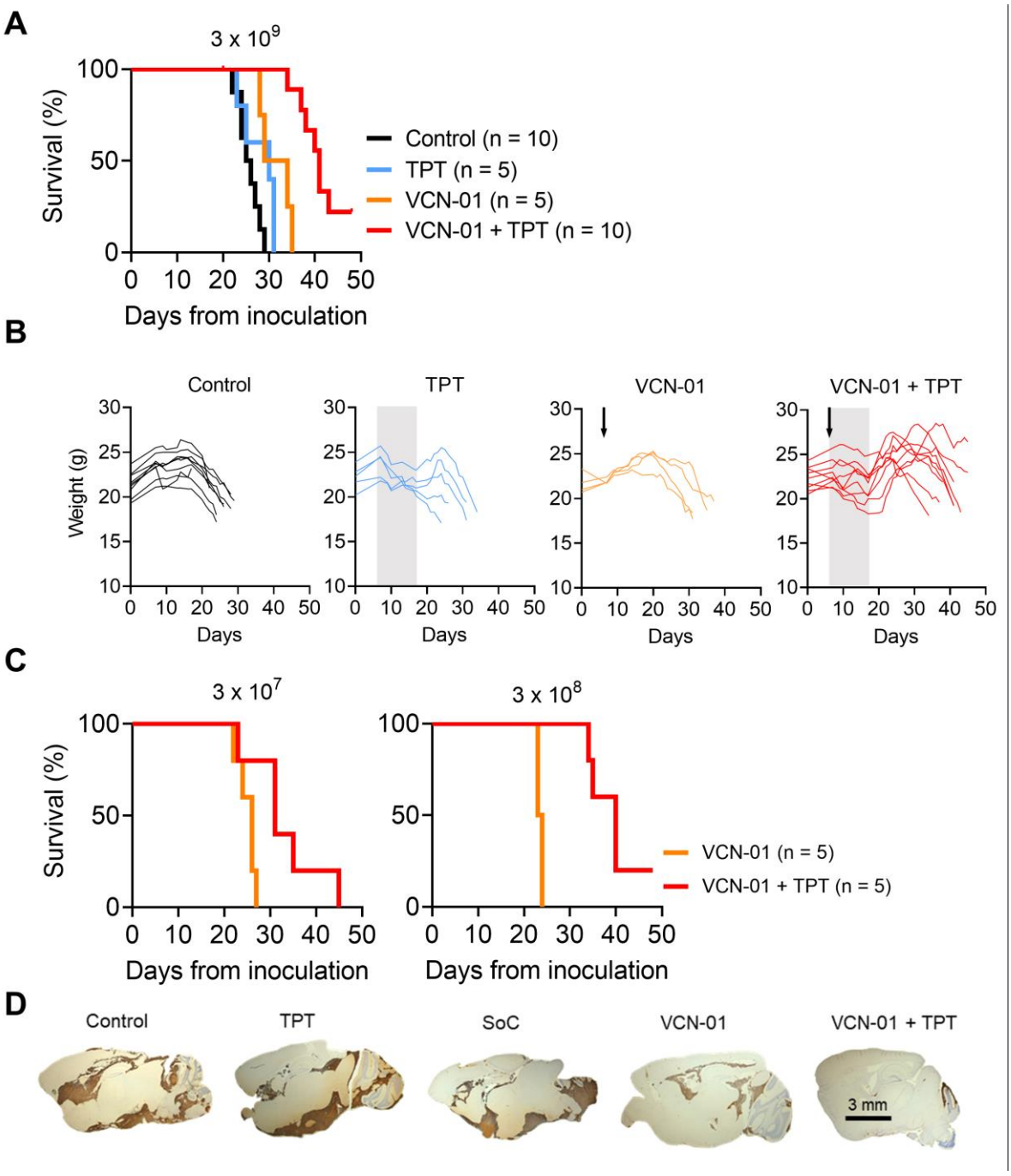

Figure 4.15. Activity of local VCN-01 and systemic topotecan in CNS-disseminated retinoblastoma. A, Survival of mice bearing RBT-7 intracerebral tumors treated with topotecan (TPT), intraventricular VCN-01 (3 x 10^9 vp) or the combination of VCN-01 and TPT. B, Individual weights of mice bearing RBT-7 intracerebral tumors treated with one intraventricular injection of VCN-01 (3 x 10^9 vp), systemic topotecan or the combination of VCN-01 and TPT. Arrows and shadowing indicate VCN-01 (black) and intravitreal TPT (grey) treatments, respectively. C, Survival of mice bearing RBT-7 intracerebral tumors treated with intraventricular VCN-01 (3 x 10^7 or 3 x 10^8 vp) or the

combination with TPT. Control mice were treated with one intraventricular injection of vehicle. Topotecan-treated mice received two cycles of topotecan. E, Immunostaining of human cells (anti-human nuclei, in brown) in mice sacrificed at day 26 after tumor inoculation. Topotecan-treated mice received one cycle of topotecan.

At end of treatment, we sacrificed three mice of each group. We processed the brains of these mice and conducted genomic and proteomic analyses on the brain tissue. We found that all had a similar intracerebral load of retinoblastoma cells (**Fig. 4.16A**). Brain homogenates from mice treated with systemic topotecan, administered alone or after intraventricular VCN-01, had the highest expression of *CDKN1A* (**Fig. 4.16B**). Levels of *E2F1* expression did not vary among groups (**Fig. 4.16B**). The number of E1A-positive cells was higher in mice treated with the combination, compared to mice treated with intraventricular VCN-01 alone (**Fig. 4.16C**). The analysis performed in brain homogenates suggested that the group treated with the combination of VCN-01 and topotecan presented higher counts of VCN-01 genomes (**Fig. 4.16D**), higher expression of human hyaluronidase (**Fig. 4.16E**) and higher positivity for viral hexon (**Fig. 4.16F**) in comparison to VCN-01-treated mice.

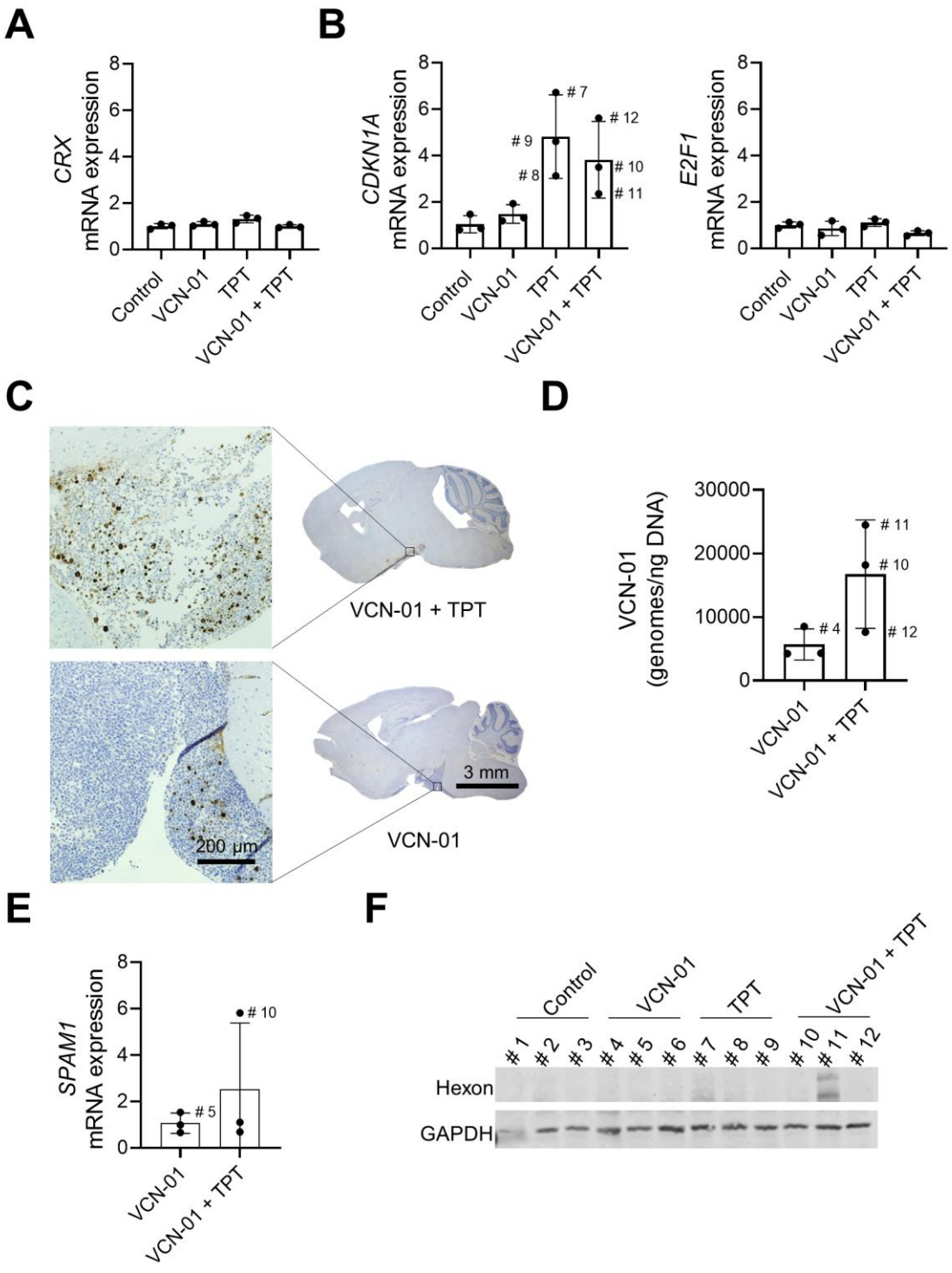

Figure 4.16. End of treatment analysis of local VCN-01 and systemic topotecan in CNS-disseminated retinoblastoma. A, Tumor burden (expression of the gene *CRX*) in brain homogenates at end of treatment (5 days after the intraventricular injection of VCN-01; i.e., at day 12 after tumor inoculation). Dots are data from individual brains and bars are mean and SD. B, mRNA

expression of *CDKN1A* and *E2F1* in brain homogenates at end of treatment. Dots are individual brains, among which the highest values are identified with the mouse number. C, Immunostaining of E1A in the brain of mice bearing RBT-7 xenografts, treated with one intraventricular dose of VCN-01, alone (VCN-01) or in combination with TPT (VCN-01 + TPT). We sacrificed the mice and obtained the samples at the end of treatments. High magnification images correspond to areas with tumor. D, Quantification of VCN-01 genomes at end of treatment in brain homogenates. E, Quantification of mRNA of the human hyaluronidase gene (*PH20*) at end of treatment in brain homogenates. F, Immunoblotting of the adenoviral hexon in brain homogenates obtained at end of treatment. GAPDH was the loading control. Samples are numbered with the identification of the mice.

3. Activity of VCN-01 and topotecan in Ewing sarcoma and neuroblastoma

Because most cancer cells undergoing division express high levels of free E2F-1, we next explored the use of VCN-01 in combination with topotecan for other difficult-to-treat pediatric tumors, such as high-risk neuroblastoma and Ewing sarcoma. First, we used the gene expression public databases GSE16237 (*238*) and GSE34620 (*239*) to verify that Ewing sarcoma and neuroblastoma express *E2F1* and the adenoviral receptors *CXADR* and *ITGA5* (**Fig. 4.17A**). Then, we engrafted two patient-derived xenografts s.c. in immunodeficient mice, one derived from a patient diagnosed at the age of 2 years with neuroblastoma (PDX model: NB-005) and another patient diagnosed at the age of 9 years with Ewing sarcoma (patient model: ES-033). For additional clinical information, see Table 3.2. E2F-1 protein was highly expressed in the patient biopsies and persisted at a lower level in the corresponding PDX of both patients (**Fig. 4.17B**).

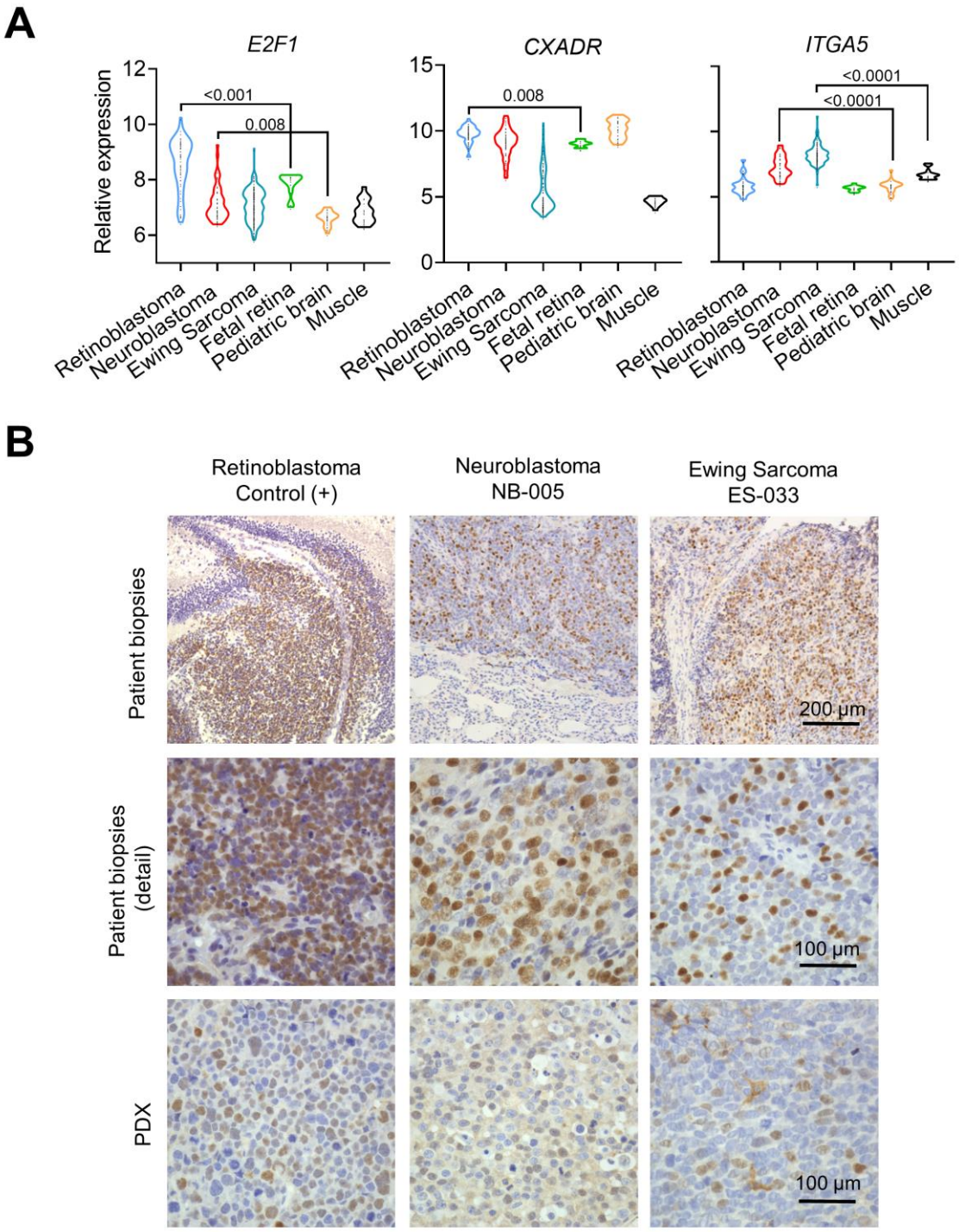

Figure 4.17. *E2F1*, *CDXADR* and *ITGA5* characterization in Ewing sarcoma and neuroblastoma biopsies and PDX. A, Gene expression of *E2F1*, *CXADR* and *ITGA5* in retinoblastoma, neuroblastoma, Ewing sarcoma and their control tissues fetal retina, pediatric brain and muscle, respectively. We compared each tumor to its control (Mann-Whitney test). B, Immunostaining of E2F-1 in patient biopsies of retinoblastoma (positive control), Ewing sarcoma and neuroblastoma

corresponding to Hospital Sant Joan de Deu (HSJD) patients from which we established the PDX HSJD-ES-033 (ES-033) and HSJD-NB-005 (NB-005).

In vitro, VCN-01 inhibited the proliferation of PDX-derived primary cells (**Fig. 4.18A**). We found overexpression of E2F-1 and cyclin E1 after topotecan exposure (**Fig. 4.18B**). Because treatment for relapsed neuroblastoma include high doses of irinotecan, in the efficacy study we included two new groups that received systemic irinotecan or the combination of intratumoral administration of VCN-01 and systemic irinotecan. We also included groups with intravenous (i.v) VCN-01 and its combination with systemic topotecan.

The neuroblastoma PDX was highly resistant to intratumoral VCN-01, topotecan and irinotecan treatments (**Fig. 4.18C, D**). Intratumoral VCN-01 combined with topotecan or irinotecan provided significant survival benefit (P = 0.005 and P = 0.0002, respectively) and inhibition of tumor growth, compared to controls (**Fig. 4.18C, D**). Combined treatment of i.v. VCN-01 and topotecan significantly reduced tumor growth compared to i.v. VCN-01 alone (P = 0.04) (**Fig. 4.18E, F**).

In the Ewing sarcoma PDX, the combination of VCN-01 and topotecan achieved a better-than-additive therapeutic activity in animal survival (P = 0.03, compared to controls), and inhibited tumor growth very significantly (**Fig. 4.18G, H**).

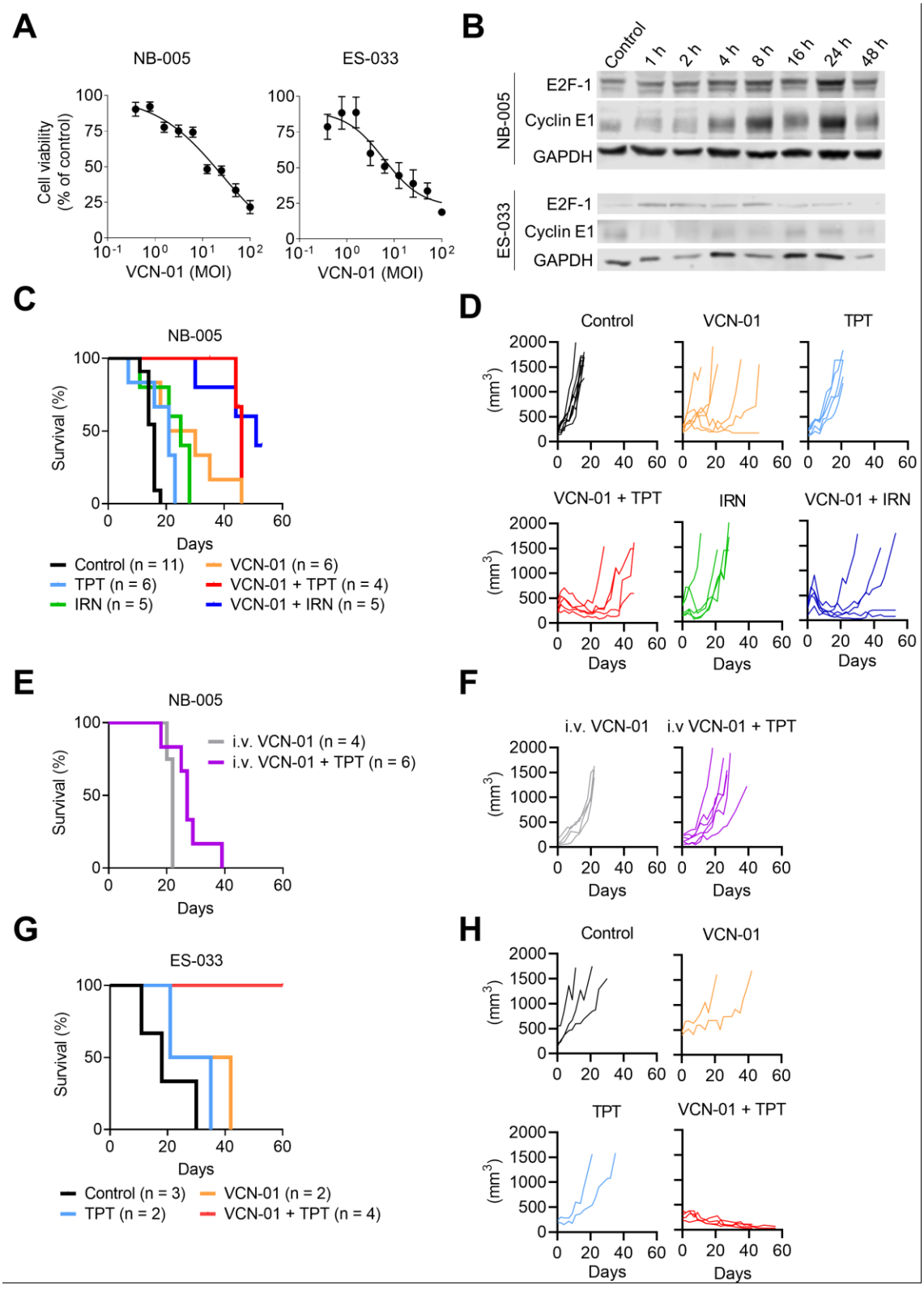
A
NB-005
ES-033
Cell viability (% of control)
VCN-01 (MOI)
B
Control
1 h
2 h
4 h
8 h
16 h
24 h
48 h
NB-005
ES-033
E2F-1
Cyclin E1
GAPDH
C
NB-005
Survival (%)
Days
Control (n = 11)
TPT (n = 6)
IRN (n = 5)
VCN-01 (n = 6)
VCN-01 + TPT (n = 4)
VCN-01 + IRN (n = 5)
D
Control
VCN-01
TPT
VCN-01 + TPT
IRN
VCN-01 + IRN
(mm3)
Days
E
NB-005
Survival (%)
Days
i.v. VCN-01 (n = 4)
i.v. VCN-01 + TPT (n = 6)
F
i.v. VCN-01
i.v VCN-01 + TPT
(mm3)
Days
G
ES-033
Survival (%)
Days
Control (n = 3)
TPT (n = 2)
VCN-01 (n = 2)
VCN-01 + TPT (n = 4)
H
Control
VCN-01
TPT
VCN-01 + TPT
(mm3)
Days

Figure 4.18. Activity of VCN-01 and systemic topotecan or irinotecan in Ewing sarcoma and neuroblastoma PDX. A, Antiproliferative activity of VCN-01 (6 days treatment) against PDX-derived primary cells in culture. Values are means and SD of six replicates. Lines are the best fitting curves built using the least square regression method of GraphPad. Cell viability is the relative percentage of the assay signal of treated cells, compared to control untreated cells, which was set as 100%. B, Immunoblotting of E2F-1 and cyclin E1 in NB-005 and ES-003 cells treated for up to 48 h with topotecan. GAPDH was the loading control. C, Survival of mice bearing neuroblastoma treated with intratumoral VCN-01, topotecan (TPT), irinotecan (IRN) or the combinations. D, Tumor volumes (individual values) of neuroblastoma PDX treated with intratumoral VCN-01, TPT, IRN or the combinations. E, Survival of mice bearing neuroblastoma treated with intravenous (i.v.) VCN-01 or its combination with systemic TPT. F, Tumor volumes (individual values) of neuroblastoma PDX treated with i.v. VCN-01, or its combination with TPT. G, Survival of the PDX ES-033 treated with local VCN-01, TPT or their combination. H, Tumor volumes (individual values) of the Ewing sarcoma PDX treated with local VCN-01, TPT or the combination.

4. First-in-human combination of VCN-01 and topotecan

We actively monitored patients included in the Phase 1 clinical trial NCT03284268 (*101*) for the treatment of chemorefractory intraocular retinoblastoma conducted at Hospital SJD. One of such patients was a heavily pretreated 40-month-old male patient with bilateral retinoblastoma (left eye enucleated previously), with germinal *RB1* mutation (c.608-1G>A) and a chemorefractory intraocular tumor in the right eye. He received three intravitreal VCN-01 doses (2×10^{10} vp) at days 1, 14 and 64. At days 44 and 71 he received two cycles of carboplatin, topotecan and melphalan throughout the ophthalmic artery (IAC). After the last intravitreal administration of VCN-01, he received 5 doses of intravitreal topotecan at days 91, 105, 119, 126 and 138. The treatment was further consolidated with brachytherapy and another 5 doses of intravitreal topotecan at days 163, 189, 203, 217 and 230. Treatments and sampling times are included in **Fig. 4.19A.**

At the time of enrollment in the trial, the patient presented with an active retinal tumor and abundant vitreous seeding (**Fig. 4.19B**). Following the second dose of VCN-01 we observed an objective response of the vitreous seeds and a progression of the retinal tumor by day 28 (**Fig. 4.19B**). To treat the progression of the retinal tumor, the patient received two treatments of intra-arterial chemotherapy (50 mg carboplatin, 5 mg melphalan and 1 mg topotecan), performed as previously published (*150*), at days 44 and 71. To treat the seeding, we administered a third dose of intravitreal VCN-01 at day 64, under compassionate use, followed by a cycle of five biweekly doses of intravitreal topotecan (30 µg) between days 91 and 138. The patient achieved a partial response of the vitreous seeding during the intravitreal topotecan treatment (**Fig. 4.19B**), which was consolidated with brachytherapy (day 155) and a second cycle of intravitreal topotecan between days 163 and 260, until achieving complete resolution of the vitreous seeds and inactivation of the retinal tumor (**Fig. 4.19B**). The patient did not present systemic complications. VCN-01 caused moderate vitreal inflammation, which was controlled with prednisone (3 mg/kg) and topical tobramycin and dexamethasone. We found moderate levels of anti-adenovirus 5 antibodies in the vitreous and blood (**Fig. 4.19C**). Viral genomes in the aqueous humor after the second VCN-01 dose achieved 2070 genomes/mL

on day 64, and decreased progressively, even after the third dose of VCN-01, until they became undetectable on days 105 and 119 (**Fig. 4.19D**). After 47 days from the initiation of the intravitreal topotecan cycle, viral genomes in the aqueous humor increased by one log, measuring 5590 vp/mL by day 138 (**Fig. 4.19D**). We did not detect virus in the blood at any time point (**Fig. 4.19D**). The patient remains free of disease 5 years after the first dose of VCN-01.

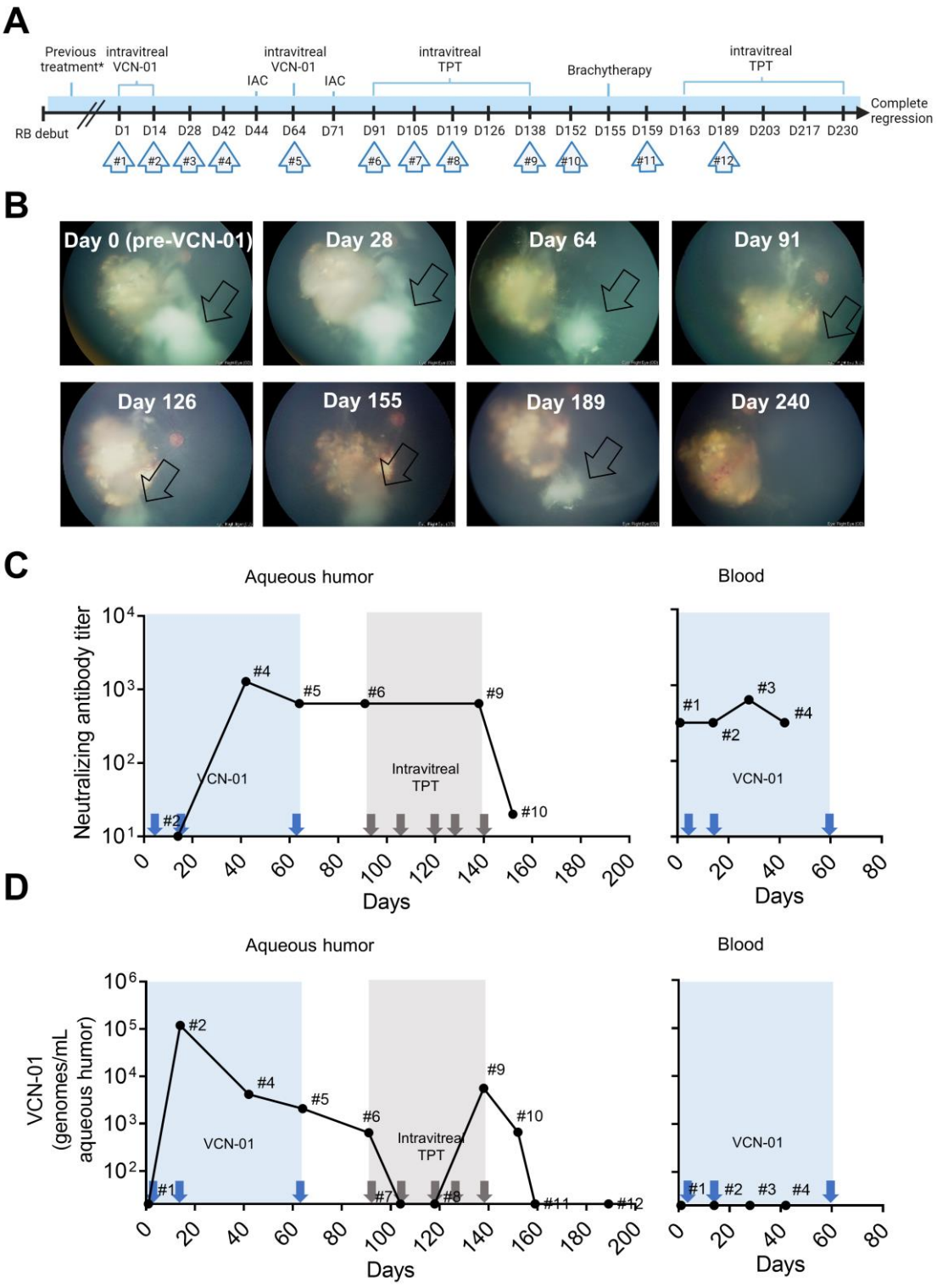

Figure 4.19. **First-in-human experience of topotecan in combination with intravitreal VCN-01**. A, Diagram of the treatments received after the debut of the disease (RB debut), including intravitreal VCN-01 from day 1 (D1), intra-arterial chemotherapy (IAC) administrations of 50 mg carboplatin, 5 mg melphalan and 1 mg topotecan, and intravitreal topotecan (TPT, 30 µg). The sample (aqueous

humor and/or blood) collection scheme is labeled with arrows identified with the sample number. *Previous treatment included six cycles of systemic chemotherapy (carboplatin, etoposide and vincristine), three administrations of IAC and two intravitreal doses of melphalan. B, Representative fundoscopy images of the patient. Arrows label the area of vitreous seeding. C, Neutralizing antibody titer in aqueous humor and blood during treatment. Sample numbers labeling the dots are those of panel A. Arrows and shadowing indicate VCN-01 (grey) and intravitreal TPT (blue) treatments. D, Concentration of viral genomes in the aqueous humor and blood. Sample numbers labeling the dots are those of panel A. Arrows and shadowing indicate VCN-01 (grey) and intravitreal TPT (blue) treatments.

Chapter V: Discussion

The main scientific contribution of this thesis is the preclinical development of a new anticancer therapy involving the combination of intratumoral VCN-01 and systemic topotecan for the treatment of intraocular retinoblastoma, CNS-disseminated retinoblastoma and other difficult-to-treat pediatric tumors. The combination of VCN-01 and topotecan showed synergy and safety in preclinical models and in one patient with chemorefractory retinoblastoma treated with intravitreal topotecan after three administrations of VCN-01. These results provide a basis for further clinical investigations. This research has produced one patent application, already licensed to a pharmaceutical company. It is anticipated that the phase 2 clinical trial will encompass the use of intravitreal VCN-01 in combination with systemic topotecan in patients with intraocular retinoblastoma.

Our first step in this project was to evaluate the synergy between VCN-01 and chemotherapy using in vitro assays. The cell cultures established from patients enabled us to assess the activity of VCN-01 in combination with chemotherapeutics in cell models with diverse phenotypes and sensitivity to the therapies. Virus-chemotherapy combinations have been widely assessed by previous work (*98, 104, 240*). In our work, the potent antiproliferative and pro-apoptotic activity of topotecan in retinoblastoma, which we and others reported before (*201, 241*), limited the design of the in vitro assays. Topotecan impeded the incubation of the cells for times long enough to observe the full oncolytic activity of VCN-01, which we described to occur at 10-14 days in previous work (*101*). Thus, we performed most in vitro studies at early times after infection. Our finding that cells exposed to VCN-01 were resistant to apoptosis induced by cytotoxic drugs would be explained by the expression of anti-apoptotic genes of the virus, such as *E1B*, preventing the host cells from apoptosis and ensuring its progeny (*242, 243*). Conversely, cells exposed to chemotherapy before VCN-01 infection showed less sensitivity to VCN-01, presumably because the initial apoptotic events prevented cell infection. Only when we used sub-cytotoxic concentrations of topotecan, we observed a synergistic effect with VCN-01 at extended exposure times, suggesting that drug pharmacokinetics processes related to dose, clearance, and timing of the treatments is crucial for finding the synergy between VCN-01 and chemotherapeutics.

In vitro studies with the tracer virus AdTLRGDK and in vivo assays with VCN-01 helped us define that the sequential treatment in which the virus is administered first, followed by systemic topotecan, maximized cell infection and anticancer efficacy.

In our study, topotecan increased the infection and oncolysis of VCN-01, likely through the overexpression of the viral promoter E2F-1 and the arrest of tumor cells in S-phase. Previous works proposed explanations contrasting to ours for the synergy of camptothecins and adenoviruses. A first study observed enhanced transgene expression of non-replicative adenoviral vectors following topotecan treatment and suggested that such interaction was due to the overexpression of topoisomerase I, the target of camptothecins, in the infected host cells (*244*). Another study found increased topoisomerase 1 expression following the infection of human gliomas with the oncolytic adenovirus Delta-24 and suggested that irinotecan was more active against Delta-24-infected gliomas due to the increased expression of its target (*106*). In contrast, we did not find significantly overexpressed topoisomerase I in VCN-01-infected retinoblastomas, which in turn became resistant to topotecan-induced apoptosis.

An alternative mechanism to explain the increased anticancer efficacy of the drug-virus combinations in vivo is the improvement of the intratumoral drug delivery upon disruption of the tumor stroma by the hyaluronidases expressed by VCN-01-infected cells (*104*). Our results do not endorse this hypothesis. Regarding drug delivery, we did not expect that stroma disruption by hyaluronidase would play a significant role in pediatric solid tumors, because most of them are stroma-poor, in contrast to the highly desmoplastic tumors in which the enhancement of drug delivery was reported following VCN-01 infection (*105*).

Instead, we propose an alternative mechanism of synergy in which topotecan takes advantage of the genetic background of VCN-01, which contains E2F-binding sites (*95*). In cycling cells, E2F-1 expression peaks at the end of the G1 phase and activates genes required for the G1-S transition and the initiation of DNA synthesis (*9*). Galbiati *et al.* demonstrated that after DNA damage induction by camptothecin, free E2F-1 accumulates in cancer cells, partly as acetylated protein (*33*). Acetylation of free E2F-1 results in higher resistance to protein degradation by ubiquitination and

increased ability to bind DNA and activate transcription (*245*). I did not address the acetylation status of E2F-1 in this study, but we demonstrated that cells exposed to topotecan and other campthotecins had greater activity levels of E2F-1 and increased nuclear foci formation, likely corresponding to high transcriptional activity points (*246, 247*).

We speculate that the increase in the endogenous activity of E2F-1 directly correlates with a higher ability of VCN-01 to infect the host cell. Thus, it is crucial to administer the virus before topotecan increases E2F-1 levels, allowing sufficient time for the virus to internalize and be present in the nucleus once E2F-1 levels peaks. Otherwise, the rapid uptake of topotecan (approximately 10 minutes after exposure (*248*)) will start the apoptotic process which may prevent VCN-01 infection.

We also observed an increased expression of p21 and cyclin E1 in topotecan-treated cells, suggesting that free E2F-1 might have activated these genes, as previously reported (*17, 249*). The cyclin-dependent kinase inhibitor p21 induces cell cycle arrest in the S-phase and inhibits DNA replication and cell proliferation (*250*). The decrease in *CDK6* expression observed in cells treated with topotecan is consistent with p21 inhibiting CDK6 (*250*). We expected the observed increase in cyclin E1, because it interacts with E2F-1 in a feedback loop in which they are mutually amplified (*17*).

S-phase cell cycle arrest plays an important role in enhancing the efficacy of VCN-01, as demonstrated by our antiproliferative assays conducted in S-phase synchronized cells using hydroxyurea. Ferreira *et al.* (*251*) demonstrated that S-phase is the optimal cell cycle phase for adenovirus infection and they found an exponential relationship between the adenovirus production and the amount of cells synchronized in S-phase. Other study demonstrated that cell synchronization using hydroxyurea increased viral transgene expression in colon and hepatocellular carcinoma cells (*109*). Heinemann *et al.* (*110*) observed that S-phase synchronization using hydroxyurea or thymidine increased cell susceptibility to an oncolytic reovirus. They also noted that combination of hydroxyurea following one intratumoral administration of reovirus resulted in decreased tumor growth and increased survival compared to reovirus as a single agent. We did not evaluate

efficacy of repeated administrations of hydroxyurea in VCN-01 treated animals but we did not observe increased biodistribution of the virus into the tumor after five consecutively doses of hydroxyurea. Future experiments may address this in our in vivo retinoblastoma models. We expect that the low therapeutic index of hydroxyurea will likely fail to induce a synergistic effect (*252*). These studies support and align with our research, underscoring the dual function of topotecan in S-phase cell synchronization and enhanced E2F-1 activity.

We infer that the increase in the basal levels of E2F-1 by topotecan facilitates the infection of cancer cells by VCN-01. The lack of functional pRB could play a significant role to enhance the action of topoisomerase I inhibitors in retinoblastoma (*253*). However, in the *RB1*-wild-type Ewing sarcoma and neuroblastoma models we found a similar increase of E2F-1 after topotecan, and the therapeutic activity of the drug-virus combination was equally remarkable. In a study in bladder cancer and Ewing sarcoma xenografts, CDK4/6 inhibitors downregulated the expression of RB1 and totally abolished E2F-1, but their co-operation with the adenovirus XVir-N-31 resulted in increased E2F-1 and enhanced viral gene expression, replication and particle formation (*111*). In contrast, in our study camptothecins increased E2F-1 alone, i.e., without the need of viral co-operation.

Our next step was to evaluate VCN-01 and topotecan combination in animal models. Using tumor specimens from patients, our group established a large preclinical platform of retinoblastoma xenografts, which reproduce the main properties of retinoblastoma (*142*). Pascual-Pastó *et al.* (*101*) demonstrated the feasibility of these models as valuable tools for assessing the therapeutic efficacy of VCN-01 for retinoblastoma treatment. Previous works have used orthotopic or subcutaneous retinoblastoma models for drug evaluation (*204, 254-256*). In our work, we used both: subcutaneous and orthotopic models. Subcutaneous models are larger and more homogeneous than orthotopic, making them suitable for studying virus distribution and extracting multiple samples from the same tumor for subsequent analysis. In subcutaneous tumors treated with one intratumoral administration of VCN-01, we observed increased tumor infection in those mice treated with topotecan. This is clinically relevant because one of the main limitations of oncolytic

virus therapies is the limited penetration and distribution into the tumor (*103*). To enhance viral concentration at the tumor site, certain strategies involve the administration of repeated doses of oncolytic viruses (*257, 258*). The use of systemic topotecan to potentiate viral infection and penetration may allow for a reduction in the number of virus administrations, thereby minimizing associated risks. Even though topotecan crosses the blood-brain barrier at not sufficient levels to achieve efficacy against tumors with intact blood-brain barrier (*259*), it has the property of accumulating in the CSF at much higher concentration than in the brain parenchyma (*260*). This property can be especially crucial in scenarios involving brain tumors growing into the leptomeningeal system.

In retinoblastoma orthotopic models, we obtained a significant improvement in the preclinical oncolytic activity of VCN-01 after only one 5-day cycle of topotecan. Individually, each agent lacked therapeutic effect. Pascual-Pastó *et al.* (*101*) reported moderate antitumor activity following one single dose of 3×10^9 vp of VCN-01 in mice bearing orthotopic retinoblastoma tumors. We reduced the dose to 3×10^8 vp, to mimic better a scenario in which two treatments that are not sufficiently active as single agents become synergistic. In our RBT-2 orthotopic model, we maximized the number of topotecan cycles (from 1 cycle to 6 cycles) achieving a better antitumor response in the combined treatment, even though reducing the dose of VCN-01 (6×10^7 vp divided in two administrations). This finding is consistent with previous observations in subcutaneous tumors and implies the potential for dose reduction or fewer administrations of VCN-01, while still achieving a robust tumor response.

In this work, we have successfully generated a new model of disseminated retinoblastoma into the central nervous system with 100% engraftment rate. These models are highly relevant due to the low prevalence and the poor prognosis of the disease. Recently, Zugbi *et al.* (*228*), in collaboration with our group, reported on a new preclinical platform of metastatic retinoblastoma models including a leptomeningeal model of Y79 cell line. They found similar infiltration patterns as observed in our RBT-7 model (i.e. occupation of the leptomeningeal space and

spinal cord infiltration). Thus, these models accurately recapitulate the clinical course observed in patients who rapidly die of leptomeningeal disease.

We assessed the efficacy of combining intrathecal VCN-01 with systemic topotecan in our leptomeningeal model of retinoblastoma. The combination of intracerebral VCN-01 ($3x10^9$ vp) and systemic topotecan resulted in a 30% and 37% increase in mice survival compared to those treated with VCN-01 or topotecan alone, respectively. Combined treatment with lower doses, $3x10^7$ and $3x10^8$ vp, also elicited potent therapeutic effect compared to VCN-01 alone (19 and 70% increase in mice survival, respectively). This therapeutic approach might hold an important clinical potential given the poor prognosis of patients with this pattern of disease (*134*). Current treatment for CNS retinoblastoma dissemination includes the use of intrathecal (*155*). Moreover, several clinical trials investigated the use of intracerebral administration of oncolytic viruses to treat brain tumors, with promising results in terms of efficacy and safety (*69, 76, 257*). Previous preclinical works used doses of 10^7 and 10^8 vp administered intracerebrally to evaluate VCN-01 efficacy in glioblastoma multiforme and neuroectodermal tumors (*261, 262*). VCN-01 significantly improved mouse survival in both models and demonstrated a good safety profile, with no adverse effects observed following virus administration (*261, 262*). In our efficacy study, we did not observed toxicity related to the administration of VCN-01 at any of the three selected doses ($3x10^7$, $3x10^8$ and $3x10^9$ vp). Nevertheless, we used immunodeficient animals which may prevent immune response against the virus. Future experiments employing immune-competent animals may provide a more comprehensive understanding of these dynamics, aiding in the development of strategies to mitigate potential immunotoxicity associated with VCN-01 administration. Only the mice treated with the combination of intrathecal VCN-01 and systemic topotecan reached their maximum weight after discontinuation of topotecan. We did not administer another cycle of topotecan because mice treated with systemic topotecan had already reached their endpoint. Topotecan dose selection was based on previous published works (*101, 201*). Other work reported poor toxicity and good response in long-term topotecan treatments with a reduced dose (*263*). Therefore, future experiments may explore the

administration of a third cycle of topotecan or a reduction in dose with prolonged topotecan exposure. Repeated topotecan administration may enhance VCN-01 oncolytic activity over time; thus, protocols involving long-term topotecan exposure may increase VCN-01 antitumor activity. Based on our results, it might be feasible to explore an intrathecal injection of VCN-01 concomitant with systemic or intrathecal cycles of topotecan in the clinics.

Overexpression of E2F-1 found in our analysis was consistent with published data in Ewing sarcoma (*264*) and neuroblastoma (*265*). The PDX we selected for these two diseases were obtained from patients with chemorefractory and disseminated tumors (*222*). For neuroblastoma patients, topotecan is administered in protracted schedules, as 5-day intravenous cycles repeated every 21 days for almost one year (*171*). Protracted regimens used in patients might further enhance the activity of each dose of VCN-01, prolonging its effect throughout the course of the therapy. In the in vivo study with neuroblastoma subcutaneous tumors, we included two groups administered with systemic VCN-01. In our experience, systemic administration of VCN-01 delayed tumor growth; however, the activity was lower than the obtained after intratumoral administration, probably due to adenovirus clearance in the blood (*266*).

In extra cranial disseminated diseases, we anticipate the design of clinical trials in which both VCN-01 and topotecan or irinotecan will be administered systemically. Both topotecan and irinotecan are used for the treatment of neuroblastoma and Ewing sarcoma (*171, 180, 267, 268*), which further substantiates the translational potential of our findings.

Our first patient experience supports the feasibility and efficacy of the combination approach. In our clinical experiment, the time between VCN-01 and topotecan was longer than in the preclinical assays, the administration route of topotecan was local instead of systemic, and we added several concomitant interventions to maximize the curative options. We acknowledge that these factors impede the clear interpretation of the observed anticancer activity. However, we suggest that the marked rise in viral copies in the aqueous humor after intravitreal topotecan is attributable to an improved infection of the vitreous tumor seeding, amplified locally

by the replication cycle of the virus. This preliminary observation should be addressed in prospective clinical trials.

In summary, we have identified the synergistic antitumor activity of VCN-01 and camptothecins in highly aggressive and chemorefractory pediatric solid tumors expressing E2F-1. Our molecular data support that S-phase cell arrest and E2F-1 accumulation and stabilization upon DNA damage produced by topotecan leads to an increase in the selectivity and infectivity of VCN-01. Our work may be applicable to improve the oncolytic activity of viruses containing E2F-1 promoters and supports the development of clinical trials.

Chapter VI: Conclusions

In this thesis I explored the use of VCN-01 in combination with topotecan for the treatment of different pediatric tumors including intraocular retinoblastoma, central nervous system disseminated retinoblastoma, neuroblastoma and Ewing sarcoma. The main conclusions related to my work are:

1. In vitro, in cancer cells, VCN-01 prevented apoptosis induced by topotecan, likely by the expression of E1B in the infected cells.

2. In vitro, in cancer cells, topotecan increased the expression of the early viral protein E1A when administered after VCN-01 infection. Conversely, topotecan treatment before VCN-01 resulted in reduced expression of E1A.

3. In vitro, in cancer cells, carboplatin, melphalan, hydroxyurea, etoposide or irinotecan had no effect on E1A expression when administered after VCN-01 infection. SN-38, similar to topotecan, enhanced viral protein expression in pre-infected cells.

4. Topotecan increased the percentage of cancer cells in S-phase and promoted cellular events consistent with G1/S-phase cell cycle progression, such as increased expression of the proteins E2F-1, p21, and cyclin E1.

5. S-phase-synchronized cancer cells were more susceptible to infection and transduction by the non-replicative adenovirus AdTLRGDK.

6. Retinoblastoma xenografts established in mice receiving one intratumoral VCN-01 injection followed by systemic topotecan exhibited higher viral genome counts, higher number of E1A-positive cells and higher expression of *SPAM1*, compared to mice receiving only VCN-01.

7. In efficacy studies using intraocular and subcutaneous retinoblastoma models, the sequence of administration of VCN-01 first, followed by topotecan, showed better-than-additive efficacy, significantly prolonging median ocular survival, compared to controls.

8. Using a patient-derived retinoblastoma culture, we established a novel leptomeningeal model of retinoblastoma that effectively recapitulated patient disease, with cancer cells filling the mouse ventricles and surrounding the spinal cord.

9. Combined treatment consisting in intraventricular VCN-01 and systemic topotecan demonstrated efficacy in the CNS retinoblastoma model, significantly extending median survival, compared to control and monotherapies.

10. Analysis of gene expression databases confirmed the overexpression of *E2F1* and the presence of adenoviral receptors in Ewing sarcoma and neuroblastoma tumors.

11. In neuroblastoma and Ewing sarcoma subcutaneous xenografts, the combination of VCN-01 and topotecan resulted in significant therapeutic benefit, compared to VCN-01 or topotecan- treated tumors. In neuroblastoma PDX, intratumoral VCN-01 and systemic irinotecan combination also showed antitumor effect.

12. In one patient included in the clinical trial of intraocular VCN-01, five doses of intravitreal topotecan increased the count of viral genomes in the aqueous humor of the affected eye, suggesting enhanced viral replication following the combination of VCN-01 and topotecan.

Bibliography

1. N. J. Dyson, RB1: a prototype tumor suppressor and an enigma. *Genes development* **30**, 1492-1502 (2016).
2. B. O'Leary, R. S. Finn, N. C. Turner, Treating cancer with selective CDK4/6 inhibitors. *Nature Reviews Clinical Oncology* **13**, 417-430 (2016).
3. S. Lapenna, A. Giordano, Cell cycle kinases as therapeutic targets for cancer. *Nature Reviews Drug Discovery* **8**, 547-566 (2009).
4. J. Y. Hsu, N. D. Seligson, J. L. Hays, W. O. Miles, J. L. Chen, Clinical Utility of CDK4/6 Inhibitors in Sarcoma: Successes and Future Challenges. *JCO Precision Oncology*, e2100211 (2022).
5. S. Goel, J. S. Bergholz, J. J. Zhao, Targeting CDK4 and CDK6 in cancer. *Nature Reviews Cancer* **22**, 356-372 (2022).
6. A. C. Mandigo *et al.*, RB/E2F1 as a Master Regulator of Cancer Cell Metabolism in Advanced Disease. *Cancer Discovery* **11**, 2334-2353 (2021).
7. D. Cobrinik, Pocket proteins and cell cycle control. *Oncogene* **24**, 2796-2809 (2005).
8. E. Zacksenhaus, Z. Jiang, R. A. Phillips, B. L. Gallie, Dual mechanisms of repression of E2F1 activity by the retinoblastoma gene product. *Embo j* **15**, 5917-5927 (1996).
9. L. N. Kent, G. Leone, The broken cycle: E2F dysfunction in cancer. *Nature Reviews Cancer* **19**, 326-338 (2019).
10. H. Z. Chen, S. Y. Tsai, G. Leone, Emerging roles of E2Fs in cancer: an exit from cell cycle control. *Nature Reviews Cancer* **9**, 785-797 (2009).
11. S. Y. Tsai *et al.*, Mouse development with a single E2F activator. *Nature* **454**, 1137-1141 (2008).
12. J. L. Chong *et al.*, E2f3a and E2f3b contribute to the control of cell proliferation and mouse development. *Molecular Cell Biology* **29**, 414-424 (2009).
13. L. Yamasaki *et al.*, Loss of E2F-1 reduces tumorigenesis and extends the lifespan of Rb1(+/−) mice. *Nature Genetics* **18**, 360-364 (1998).

14. D. L. Burkhart, J. Sage, Cellular mechanisms of tumour suppression by the retinoblastoma gene. *Nature Reviews Cancer* **8**, 671-682 (2008).
15. B. R. Topacio *et al.*, Cyclin D-Cdk4,6 Drives Cell-Cycle Progression via the Retinoblastoma Protein's C-Terminal Helix. *Molecular Cell* **74**, 758-770 e754 (2019).
16. S. Mittnacht, Control of pRB phosphorylation. *Current Opinion Genetics Development* **8**, 21-27 (1998).
17. S. M. Rubin, J. Sage, J. M. Skotheim, Integrating Old and New Paradigms of G1/S Control. *Molecular Cell* **80**, 183-192 (2020).
18. K. Ohtani, J. DeGregori, J. R. Nevins, Regulation of the cyclin E gene by transcription factor E2F1. *Proceedings of the National Academy of Sciences* **92**, 12146-12150 (1995).
19. L. Wu *et al.*, The E2F1–3 transcription factors are essential for cellular proliferation. *Nature* **414**, 457-462 (2001).
20. H. K. Matthews, C. Bertoli, R. A. M. de Bruin, Cell cycle control in cancer. *Nature Reviews Molecular Cell Biology* **23**, 74-88 (2022).
21. E. S. Knudsen, K. E. Knudsen, Tailoring to RB: tumour suppressor status and therapeutic response. *Nature Reviews Cancer* **8**, 714-724 (2008).
22. S. Polager, D. Ginsberg, E2F - at the crossroads of life and death. *Trends Cell Biology* **18**, 528-535 (2008).
23. D. G. Johnson, K. Ohtani, J. R. Nevins, Autoregulatory control of E2F1 expression in response to positive and negative regulators of cell cycle progression. *Genes development* **8**, 1514-1525 (1994).
24. V. Glorian *et al.*, DNA damage and S phase-dependent E2F1 stabilization requires the cIAP1 E3-ubiquitin ligase and is associated with K63-poly-ubiquitination on lysine 161/164 residues. *Cell Death Disease* **8**, e2816-e2816 (2017).
25. M. Xu, K. A. Sheppard, C. Y. Peng, A. S. Yee, H. Piwnica-Worms, Cyclin A/CDK2 binds directly to E2F-1 and inhibits the DNA-binding activity of E2F-1/DP-1 by phosphorylation. *Molecular Cellular Biology* **14**, 8420-8431 (1994).

26. R. D. Meng, P. Phillips, W. S. El-Deiry, p53-independent increase in E2F-1 expression enhances the cytotoxic effects of etoposide and of adriamycin. *International journal of oncology* **14**, 5-14 (1999).
27. M. Höfferer, C. Wirbelauer, B. Humar, W. Krek, Increased levels of E2F-1-dependent DNA binding activity after UV- or gamma-irradiation. *Nucleic acids research* **27**, 491-495 (1999).
28. Y. Huang *et al.*, Role for E2F in DNA damage-induced entry of cells into S phase. *Cancer Research* **57**, 3640-3643 (1997).
29. C. Blattner, A. Sparks, D. Lane, Transcription factor E2F-1 is upregulated in response to DNA damage in a manner analogous to that of p53. *Molecular Cellular Biology* **19**, 3704-3713 (1999).
30. W. C. Lin, F. T. Lin, J. R. Nevins, Selective induction of E2F1 in response to DNA damage, mediated by ATM-dependent phosphorylation. *Genes development* **15**, 1833-1844 (2001).
31. N. Pediconi *et al.*, Differential regulation of E2F1 apoptotic target genes in response to DNA damage. *Nature Cell Biology* **5**, 552-558 (2003).
32. M. A. Martínez-Balbás, U. M. Bauer, S. J. Nielsen, A. Brehm, T. Kouzarides, Regulation of E2F1 activity by acetylation. *Embo j* **19**, 662-671 (2000).
33. L. Galbiati, R. Mendoza-Maldonado, M. I. Gutierrez, M. Giacca, Regulation of E2F-1 after DNA damage by p300-mediated acetylation and ubiquitination. *Cell Cycle* **4**, 930-939 (2005).
34. A. C. Mandigo, S. A. Tomlins, W. K. Kelly, K. E. Knudsen, Relevance of pRB Loss in Human Malignancies. *Clincal Cancer Research* **28**, 255-264 (2022).
35. B. S. Paugh *et al.*, Integrated molecular genetic profiling of pediatric high-grade gliomas reveals key differences with the adult disease. *Journal of Clinical Oncol*ogy **28**, 3061-3068 (2010).
36. A. Mackay *et al.*, Integrated Molecular Meta-Analysis of 1,000 Pediatric High-Grade and Diffuse Intrinsic Pontine Glioma. *Cancer cell* **32**, 520-537 e525 (2017).
37. D. R. Lohmann, RB1 gene mutations in retinoblastoma. *Human mutation* **14**, 283-288 (1999).

38. C. Stirzaker *et al.*, Extensive DNA methylation spanning the Rb promoter in retinoblastoma tumors. *Cancer Research* **57**, 2229-2237 (1997).
39. J. Liu *et al.*, A high-risk retinoblastoma subtype with stemness features, dedifferentiated cone states and neuronal/ganglion cell gene expression. *Nature Communications* **12**, 5578 (2021).
40. B. Wadayama *et al.*, Mutation spectrum of the retinoblastoma gene in osteosarcomas. *Cancer Research* **54**, 3042-3048 (1994).
41. J. J. Molenaar *et al.*, Cyclin D1 is a direct transcriptional target of GATA3 in neuroblastoma tumor cells. *Oncogene* **29**, 2739-2745 (2010).
42. B. D. Crompton *et al.*, The genomic landscape of pediatric Ewing sarcoma. *Cancer Discovery* **4**, 1326-1341 (2014).
43. A. L. Reed *et al.*, High frequency of p16 (CDKN2/MTS-1/INK4A) inactivation in head and neck squamous cell carcinoma. *Cancer Research* **56**, 3630-3633 (1996).
44. C. Gillett *et al.*, Amplification and overexpression of cyclin D1 in breast cancer detected by immunohistochemical staining. *Cancer Research* **54**, 1812-1817 (1994).
45. R. Michalides *et al.*, A clinicopathological study on overexpression of cyclin D1 and of p53 in a series of 248 patients with operable breast cancer. *British Journal of Cancer* **73**, 728-734 (1996).
46. S. Oesterreich, S. A. Fuqua, Tumor suppressor genes in breast cancer. *Endocrine-related cancer* **6**, 405-419 (1999).
47. J. I. Herschkowitz, X. He, C. Fan, C. M. Perou, The functional loss of the retinoblastoma tumour suppressor is a common event in basal-like and luminal B breast carcinomas. *Breast Cancer Research* **10**, R75 (2008).
48. Y. Ichikawa *et al.*, Inactivation of p16/CDKN2 and p15/MTS2 genes in different histological types and clinical stages of primary ovarian tumors. *International Journal of Cancer* **69**, 466-470 (1996).
49. C. Caldas *et al.*, Frequent somatic mutations and homozygous deletions of the p16 (MTS1) gene in pancreatic adenocarcinoma. *Nature Genetics* **8**, 27-32 (1994).

50. B. Gerdes *et al.*, p16INK4a is a prognostic marker in resected ductal pancreatic cancer: an analysis of p16INK4a, p53, MDM2, an Rb. *Annals of surgery* **235**, 51-59 (2002).
51. L. Huang *et al.*, Deletion and mutation analyses of the P16/MTS-1 tumor suppressor gene in human ductal pancreatic cancer reveals a higher frequency of abnormalities in tumor-derived cell lines than in primary ductal adenocarcinomas. *Cancer Research* **56**, 1137-1141 (1996).
52. S. Gansauge *et al.*, Overexpression of cyclin D1 in human pancreatic carcinoma is associated with poor prognosis. *Cancer Research* **57**, 1634-1637 (1997).
53. C. McNair *et al.*, Differential impact of RB status on E2F1 reprogramming in human cancer. *Journal of Clinical Investigaton* **128**, 341-358 (2018).
54. D. F. Jarrard *et al.*, Alterations in the p16/pRb cell cycle checkpoint occur commonly in primary and metastatic human prostate cancer. *Cancer Letters* **185**, 191-199 (2002).
55. R. Di Fiore, A. D'Anneo, G. Tesoriere, R. Vento, RB1 in cancer: different mechanisms of RB1 inactivation and alterations of pRb pathway in tumorigenesis. *Journal Cellular Physiology* **228**, 1676-1687 (2013).
56. A. A. Mäkitie *et al.*, Loss of p16 expression has prognostic significance in human nasopharyngeal carcinoma. *Clinical Cancer Research* **9**, 2177-2184 (2003).
57. J. DeGregori, T. Kowalik, J. R. Nevins, Cellular targets for activation by the E2F1 transcription factor include DNA synthesis- and G1/S-regulatory genes. *Molecular Cellular Biology* **15**, 4215-4224 (1995).
58. G. E. Konecny *et al.*, Expression of p16 and retinoblastoma determines response to CDK4/6 inhibition in ovarian cancer. *Clinical Cancer Research* **17**, 1591-1602 (2011).
59. C. A. Kurtyka, L. Chen, W. D. Cress, E2F inhibition synergizes with paclitaxel in lung cancer cell lines. *PLoS One* **9**, e96357 (2014).

60. M. Sangwan *et al.*, Established and new mouse models reveal E2f1 and Cdk2 dependency of retinoblastoma, and expose effective strategies to block tumor initiation. *Oncogene* **31**, 5019-5028 (2012).
61. L. A. Bell, J. O'Prey, K. M. Ryan, DNA-binding independent cell death from a minimal proapoptotic region of E2F-1. *Oncogene* **25**, 5656-5663 (2006).
62. J. G. Gomez-Gutierrez *et al.*, Adenovirus-mediated expression of truncated E2F-1 suppresses tumor growth in vitro and in vivo. *Cancer* **116**, 4420-4432 (2010).
63. D. Lin, Y. Shen, T. Liang, Oncolytic virotherapy: basic principles, recent advances and future directions. *Signal Transduction and Targeted Therapy* **8**, 156 (2023).
64. H. L. Kaufman, F. J. Kohlhapp, A. Zloza, Oncolytic viruses: a new class of immunotherapy drugs. *Nature Reviews Drug Discovery* **14**, 642-662 (2015).
65. N. Bayo-Puxan *et al.*, Replacement of adenovirus type 5 fiber shaft heparan sulfate proteoglycan-binding domain with RGD for improved tumor infectivity and targeting. *Human gene therapy* **20**, 1214-1221 (2009).
66. R. Alemany, Oncolytic Adenoviruses in Cancer Treatment. *Biomedicines* **2**, 36-49 (2014).
67. R. Alemany, Designing adenoviral vectors for tumor-specific targeting. *Methods in molecular biology (Clifton, N.J.)* **542**, 57-74 (2009).
68. F. F. Lang *et al.*, Phase I Study of DNX-2401 (Delta-24-RGD) Oncolytic Adenovirus: Replication and Immunotherapeutic Effects in Recurrent Malignant Glioma. *Journal of Clinical Oncology* **36**, 1419-1427 (2018).
69. J. Gallego Perez-Larraya *et al.*, Oncolytic DNX-2401 Virus for Pediatric Diffuse Intrinsic Pontine Glioma. *New England Journal of Medicine* **386**, 2471-2481 (2022).
70. S. Ebrahimi *et al.*, Interferon-Mediated Tumor Resistance to Oncolytic Virotherapy. *Journal Cellular Biochemistry* **118**, 1994-1999 (2017).
71. J. M. Ricca *et al.*, Pre-existing Immunity to Oncolytic Virus Potentiates Its Immunotherapeutic Efficacy. *Molecular Therapy* **26**, 1008-1019 (2018).

72. M. S. Ferguson, N. R. Lemoine, Y. Wang, Systemic delivery of oncolytic viruses: hopes and hurdles. *Advances in virology* **2012**, 805629 (2012).
73. M. Bazan-Peregrino, R. C. Carlisle, L. Purdie, L. W. Seymour, Factors influencing retention of adenovirus within tumours following direct intratumoural injection. *Gene Therapy* **15**, 688-694 (2008).
74. N. Bayo-Puxan *et al.*, Role of the putative heparan sulfate glycosaminoglycan-binding site of the adenovirus type 5 fiber shaft on liver detargeting and knob-mediated retargeting. *Journal General Virology* **87**, 2487-2495 (2006).
75. S. Guedan *et al.*, Hyaluronidase expression by an oncolytic adenovirus enhances its intratumoral spread and suppresses tumor growth. *Molecular Therapy* **18**, 1275-1283 (2010).
76. F. Nassiri *et al.*, Oncolytic DNX-2401 virotherapy plus pembrolizumab in recurrent glioblastoma: a phase 1/2 trial. *Nature Medicine* **29**, 1370-1378 (2023).
77. H. Sauthoff *et al.*, Intratumoral Spread of Wild-Type Adenovirus Is Limited After Local Injection of Human Xenograft Tumors: Virus Persists and Spreads Systemically at Late Time Points. *Human Gene Therapy* **14**, 425-433 (2003).
78. R. Garcia-Carbonero *et al.*, Phase 1 study of intravenous administration of the chimeric adenovirus enadenotucirev in patients undergoing primary tumor resection. *Journal Immunotherapy Cancer* **5**, 71 (2017).
79. M. Garcia *et al.*, A Phase 1 Trial of Oncolytic Adenovirus ICOVIR-5 Administered Intravenously to Cutaneous and Uveal Melanoma Patients. *Human Gene Therapy* **30**, 352-364 (2019).
80. J. Gallardo, M. Perez-Illana, N. Martin-Gonzalez, C. San Martin, Adenovirus Structure: What Is New? *International Journal of Molecular Sciences* **22**, (2021).
81. R. W. Walters *et al.*, Adenovirus fiber disrupts CAR-mediated intercellular adhesion allowing virus escape. *Cell* **110**, 789-799 (2002).
82. A. J. Davison, M. Benko, B. Harrach, Genetic content and evolution of adenoviruses. *Journal General Virology* **84**, 2895-2908 (2003).

83. G. Akusjärvi, Proteins with transcription regulatory properties encoded by human adenoviruses. *Trends in Microbiology* **1**, 163-170 (1993).
84. Y. S. Ahi, S. K. Mittal, Components of Adenovirus Genome Packaging. *Frontiers Microbiology* **7**, 1503 (2016).
85. V. S. Reddy, G. R. Nemerow, Structures and organization of adenovirus cement proteins provide insights into the role of capsid maturation in virus entry and infection. *Proceedings of the National Academy of Sciences* **111**, 11715-11720 (2014).
86. S. M. Frisch, J. S. Mymryk, Adenovirus-5 E1A: paradox and paradigm. *Nature Reviews Molecular Cell Biology* **3**, 441-452 (2002).
87. E. White, Regulation of the cell cycle and apoptosis by the oncogenes of adenovirus. *Oncogene* **20**, 7836-7846 (2001).
88. P. Whyte *et al.*, Association between an oncogene and an anti-oncogene: the adenovirus E1A proteins bind to the retinoblastoma gene product. *Nature* **334**, 124-129 (1988).
89. S. Mittnacht *et al.*, Distinct sub-populations of the retinoblastoma protein show a distinct pattern of phosphorylation. *Embo j* **13**, 118-127 (1994).
90. M. A. Ikeda, J. R. Nevins, Identification of distinct roles for separate E1A domains in disruption of E2F complexes. *Molecular Cellular Biology* **13**, 7029-7035 (1993).
91. S. W. Lowe, H. E. Ruley, Stabilization of the p53 tumor suppressor is induced by adenovirus 5 E1A and accompanies apoptosis. *Genes development* **7**, 535-545 (1993).
92. E. Querido *et al.*, Degradation of p53 by adenovirus E4orf6 and E1B55K proteins occurs via a novel mechanism involving a Cullin-containing complex. *Genes development* **15**, 3104-3117 (2001).
93. M. Debbas, E. White, Wild-type p53 mediates apoptosis by E1A, which is inhibited by E1B. *Genes development* **7**, 546-554 (1993).
94. M. Cascallo *et al.*, Systemic toxicity-efficacy profile of ICOVIR-5, a potent and selective oncolytic adenovirus based on the pRB pathway. *Molecular Therapy* **15**, 1607-1615 (2007).

95. A. Rodríguez-García *et al.*, Safety and Efficacy of VCN-01, an Oncolytic Adenovirus Combining Fiber HSG-Binding Domain Replacement with RGD and Hyaluronidase Expression. *Clinical Cancer Research* **21**, 1406-1418 (2015).
96. J. L. Jakubczak *et al.*, An oncolytic adenovirus selective for retinoblastoma tumor suppressor protein pathway-defective tumors: dependence on E1A, the E2F-1 promoter, and viral replication for selectivity and efficacy. *Cancer Research* **63**, 1490-1499 (2003).
97. M. Majem *et al.*, Control of E1A under an E2F-1 promoter insulated with the myotonic dystrophy locus insulator reduces the toxicity of oncolytic adenovirus Ad-Δ24RGD. *Cancer Gene Therapy* **13**, 696-705 (2006).
98. M. M. Alonso *et al.*, Combination of the oncolytic adenovirus ICOVIR-5 with chemotherapy provides enhanced anti-glioma effect in vivo. *Cancer Gene Therapy* **14**, 756-761 (2007).
99. J. J. Rojas *et al.*, A modified E2F-1 promoter improves the efficacy to toxicity ratio of oncolytic adenoviruses. *Gene Therapy* **16**, 1441-1451 (2009).
100. P. Nokisalmi *et al.*, Oncolytic adenovirus ICOVIR-7 in patients with advanced and refractory solid tumors. *Clinical Cancer Research* **16**, 3035-3043 (2010).
101. G. Pascual-Pasto *et al.*, Therapeutic targeting of the RB1 pathway in retinoblastoma with the oncolytic adenovirus VCN-01. *Science Translational Medicine* **11**, eaat9321 (2019).
102. S. Barui, S. Saha, G. Mondal, S. Haseena, A. Chaudhuri, Simultaneous delivery of doxorubicin and curcumin encapsulated in liposomes of pegylated RGDK-lipopeptide to tumor vasculature. *Biomaterials* **35**, 1643-1656 (2014).
103. L. Wang, L. S. Chard Dunmall, Z. Cheng, Y. Wang, Remodeling the tumor microenvironment by oncolytic viruses: beyond oncolysis of tumor cells for cancer treatment. *Journal Immunotherapy Cancer* **10**, e004167 (2022).
104. M. Bazan-Peregrino *et al.*, VCN-01 disrupts pancreatic cancer stroma and exerts antitumor effects. *Journal Immunotherapy Cancer* **9**, e003254 (2021).
105. R. Garcia-Carbonero *et al.*, Phase I, multicenter, open-label study of intravenous VCN-01 oncolytic adenovirus with or without nab-paclitaxel plus

gemcitabine in patients with advanced solid tumors. *Journal Immunotherapy Cancer* **10**, e003255 (2022).

106. C. Gomez-Manzano *et al.*, Delta-24 increases the expression and activity of topoisomerase I and enhances the antiglioma effect of irinotecan. *Clinical Cancer Research* **12**, 556-562 (2006).
107. A. R. Nelson, J. Davydova, D. T. Curiel, M. Yamamoto, Combination of conditionally replicative adenovirus and standard chemotherapies shows synergistic antitumor effect in pancreatic cancer. *Cancer Science* **100**, 2181-2187 (2009).
108. A. Gros *et al.*, Verapamil enhances the antitumoral efficacy of oncolytic adenoviruses. *Molecular Therapy* **18**, 903-911 (2010).
109. X. W. Huang, Z. Y. Tang, T. S. Lawrence, M. Zhang, 5-fluorouracil and hydroxyurea enhance adenovirus-mediated transgene expression in colon and hepatocellular carcinoma cells. *Journal Cancer Research Clinical Oncology* **131**, 184-190 (2005).
110. L. Heinemann *et al.*, The effect of cell cycle synchronization on tumor sensitivity to reovirus oncolysis. *Molecular Therapy* **18**, 2085-2093 (2010).
111. J. Koch *et al.*, Targeting the Retinoblastoma/E2F repressive complex by CDK4/6 inhibitors amplifies oncolytic potency of an oncolytic adenovirus. *Nature Communications* **13**, 4689 (2022).
112. H. Soliman *et al.*, A Phase I Trial of Talimogene Laherparepvec in Combination with Neoadjuvant Chemotherapy for the Treatment of Nonmetastatic Triple-Negative Breast Cancer. *Clinical Cancer Research* **27**, 1012-1018 (2021).
113. H. Soliman *et al.*, Oncolytic T-VEC virotherapy plus neoadjuvant chemotherapy in nonmetastatic triple-negative breast cancer: a phase 2 trial. *Nature Medicine* **29**, 450-457 (2023).
114. M. Toulmonde *et al.*, Randomized phase 2 trial of intravenous oncolytic virus JX-594 combined with low-dose cyclophosphamide in patients with advanced soft-tissue sarcoma. *Journal Hematology Oncology* **15**, 149 (2022).

115. J. R. Hecht *et al.*, A phase I/II trial of intratumoral endoscopic ultrasound injection of ONYX-015 with intravenous gemcitabine in unresectable pancreatic carcinoma. *Clinical Cancer Research* **9**, 555-561 (2003).
116. V. Moreno *et al.*, Safety and efficacy of the tumor-selective adenovirus enadenotucirev with or without paclitaxel in platinum-resistant ovarian cancer: a phase 1 clinical trial. *Journal Immunotherapy Cancer* **9**, e003645 (2021).
117. O. World Health, *CureAll framework: WHO global initiative for childhood cancer: increasing access, advancing quality, saving lives*. (World Health Organization, Geneva, 2021).
118. E. Steliarova-Foucher *et al.*, International incidence of childhood cancer, 2001–10: a population-based registry study. *The Lancet Oncology* **18**, 719-731 (2017).
119. S. M. Pfister *et al.*, A Summary of the Inaugural WHO Classification of Pediatric Tumors: Transitioning from the Optical into the Molecular Era. *Cancer Discovery* **12**, 331-355 (2022).
120. E. A. Sweet-Cordero, J. A. Biegel, The genomic landscape of pediatric cancers: Implications for diagnosis and treatment. *Science* **363**, 1170-1175 (2019).
121. E. Butler *et al.*, Recent progress in the treatment of cancer in children. *CA: A Cancer Journal for Clinicians* **71**, 315-332 (2021).
122. K. C. Oeffinger *et al.*, Chronic Health Conditions in Adult Survivors of Childhood Cancer. *New England Journal of Medicine* **355**, 1572-1582 (2006).
123. M. Sanchez-Guixe *et al.*, Origins of Second Malignancies in Children and Mutational Footprint of Chemotherapy in Normal Tissues. *Cancer Discovery* **14**, 953-964 (2024).
124. S. Newman *et al.*, Genomes for Kids: The Scope of Pathogenic Mutations in Pediatric Cancer Revealed by Comprehensive DNA and RNA Sequencing. *Cancer Discovery* **11**, 3008-3027 (2021).
125. M. S. Lawrence *et al.*, Mutational heterogeneity in cancer and the search for new cancer-associated genes. *Nature* **499**, 214-218 (2013).

126. B. Vogelstein *et al.*, Cancer Genome Landscapes. *Science* **339**, 1546-1558 (2013).
127. V. Thatikonda *et al.*, Comprehensive analysis of mutational signatures reveals distinct patterns and molecular processes across 27 pediatric cancers. *Nature Cancer* **4**, 276-289 (2023).
128. C. Kandoth *et al.*, Mutational landscape and significance across 12 major cancer types. *Nature* **502**, 333-339 (2013).
129. S. N. Grobner *et al.*, The landscape of genomic alterations across childhood cancers. *Nature* **555**, 321-327 (2018).
130. J. Zhang *et al.*, Germline Mutations in Predisposition Genes in Pediatric Cancer. *New England Journal of Medicine* **373**, 2336-2346 (2015).
131. A. M. Acanda De La Rocha *et al.*, Feasibility of functional precision medicine for guiding treatment of relapsed or refractory pediatric cancers. *Nature Medicine* **30**, 990-1000 (2024).
132. D. Thompson *et al.*, Identification of patient subgroups with markedly disparate rates of MYCN amplification in neuroblastoma: A report from the International Neuroblastoma Risk Group project. *Cancer* **122**, 935-945 (2016).
133. R. E. Phillips, A. A. Soshnev, C. D. Allis, Epigenomic Reprogramming as a Driver of Malignant Glioma. *Cancer cell* **38**, 647-660 (2020).
134. F. L. Munier *et al.*, Conservative management of retinoblastoma: Challenging orthodoxy without compromising the state of metastatic grace. "Alive, with good vision and no comorbidity". *Progress in Retinal and Eye Research* **73**, 100764 (2019).
135. H. Dimaras *et al.*, Retinoblastoma. *Nature Reviews Disease Primers* **1**, (2015).
136. D. Cobrinik, Retinoblastoma Origins and Destinations. *New England Journal of Medicine* **390**, 1408-1419 (2024).
137. S. H. Friend *et al.*, A human DNA segment with properties of the gene that predisposes to retinoblastoma and osteosarcoma. *Nature* **323**, 643-646 (1986).

138. H. El Zomor *et al.*, Unilateral retinoblastoma; natural history and an age-based protocol in 248 patients. *Eye* **35**, 2564-2572 (2021).
139. S. Canturk *et al.*, Survival of retinoblastoma in less-developed countries impact of socioeconomic and health-related indicators. *British Journal Ophthalmology* **94**, 1432-1436 (2010).
140. K. Gunduz, O. Muftuoglu, I. Gunalp, E. Unal, N. Tacyildiz, Metastatic retinoblastoma clinical features, treatment, and prognosis. *Ophthalmology* **113**, 1558-1566 (2006).
141. V. E. Laurent *et al.*, Minimal Disseminated Disease in Nonmetastatic Retinoblastoma With High-Risk Pathologic Features and Association With Disease-Free Survival. *JAMA Ophthalmology* **134**, 1374-1379 (2016).
142. G. Pascual-Pasto *et al.*, Preclinical platform of retinoblastoma xenografts recapitulating human disease and molecular markers of dissemination. *Cancer Letters* **380**, 10-19 (2016).
143. J. E. Lu *et al.*, Metastases and death rates after primary enucleation of unilateral retinoblastoma in the USA 2007-2017. *British Journal Ophthalmology* **103**, 1272-1277 (2019).
144. I. Magramm, D. H. Abramson, R. M. Ellsworth, Optic nerve involvement in retinoblastoma. *Ophthalmology* **96**, 217-222 (1989).
145. H. Dimaras, T. W. Corson, Retinoblastoma, the visible CNS tumor: A review. *Journal Neuroscience Research* **97**, 29-44 (2019).
146. D. H. Abramson, I. J. Dunkel, S. E. Brodie, B. Marr, Y. P. Gobin, Superselective ophthalmic artery chemotherapy as primary treatment for retinoblastoma (chemosurgery). *Ophthalmology* **117**, 1623-1629 (2010).
147. D. H. Abramson *et al.*, Intravitreal chemotherapy in retinoblastoma: expanded use beyond intravitreal seeds. *British Journal Ophthalmology* **103**, 488-493 (2019).
148. F. L. Munier *et al.*, Intravitreal chemotherapy for vitreous disease in retinoblastoma revisited: from prohibition to conditional indications. *British Journal Ophthalmology* **96**, 1078-1083 (2012).

149. J. H. Francis *et al.*, Efficacy and Toxicity of Intravitreous Chemotherapy for Retinoblastoma: Four-Year Experience. *Ophthalmology* **124**, 488-495 (2017).
150. A. Parareda *et al.*, Intra-arterial chemotherapy for retinoblastoma. Challenges of a prospective study. *Acta Ophthalmologica* **92**, 209-215 (2014).
151. E. Pavlidou *et al.*, Anterior Segment Seeding in Eyes With Retinoblastoma Failing to Respond to Intraophthalmic Artery Chemotherapy. *JAMA Ophthalmology* **133**, 1455-1458 (2015).
152. G. L. Chantada *et al.*, Results of a prospective study for the treatment of unilateral retinoblastoma. *Pediatric Blood Cancer* **55**, 60-66 (2010).
153. A. MacCarthy *et al.*, Second and subsequent tumours among 1927 retinoblastoma patients diagnosed in Britain 1951-2004. *British Journal of Cancer* **108**, 2455-2463 (2013).
154. K. I. Woo, J. W. Harbour, Review of 676 Second Primary Tumors in Patients With Retinoblastoma: Association Between Age at Onset and Tumor Type. *Archives of Ophthalmology* **128**, 865-870 (2010).
155. A. Rodriguez *et al.*, Combined high-dose intra-arterial and intrathecal chemotherapy for the treatment of a case of extraocular retinoblastoma. *Pediatric Blood Cancer* **65**, e27385 (2018).
156. K. K. Matthay *et al.*, Neuroblastoma. *Nature Reviews Disease Primers* **2**, 16078 (2016).
157. G. M. Marshall *et al.*, The prenatal origins of cancer. *Nature Reviews Cancer* **14**, 277-289 (2014).
158. V. Llombart, M. R. Mansour, Therapeutic targeting of "undruggable" MYC. *EBioMedicine* **75**, 103756 (2022).
159. R. Dhanasekaran *et al.*, The MYC oncogene - the grand orchestrator of cancer growth and immune evasion. *Nature Reviews Clinical Oncology* **19**, 23-36 (2022).
160. G. Bretones, M. D. Delgado, J. León, Myc and cell cycle control. *Biochimica et biophysica acta* **1849**, 506-516 (2015).
161. V. Korber *et al.*, Neuroblastoma arises in early fetal development and its evolutionary duration predicts outcome. *Nature Genetics* **55**, 619-630 (2023).

162. M. S. Irwin *et al.*, Revised Neuroblastoma Risk Classification System: A Report From the Children's Oncology Group. *Journal of Clinical Oncology* **39**, 3229-3241 (2021).
163. H. Shimada *et al.*, The International Neuroblastoma Pathology Classification (the Shimada system). *Cancer* **86**, 364-372 (1999).
164. B. Qiu, K. K. Matthay, Advancing therapy for neuroblastoma. *Nature Reviews Clinical Oncology* **19**, 515-533 (2022).
165. A. L. Yu *et al.*, Anti-GD2 antibody with GM-CSF, interleukin-2, and isotretinoin for neuroblastoma. *New England Journal of Medicine* **363**, 1324-1334 (2010).
166. R. Mody *et al.*, Irinotecan-temozolomide with temsirolimus or dinutuximab in children with refractory or relapsed neuroblastoma (COG ANBL1221): an open-label, randomised, phase 2 trial. *Lancet Oncology* **18**, 946-957 (2017).
167. N. K. Cheung *et al.*, Murine anti-GD2 monoclonal antibody 3F8 combined with granulocyte-macrophage colony-stimulating factor and 13-cis-retinoic acid in high-risk patients with stage 4 neuroblastoma in first remission. *Journal of Clinical Oncology* **30**, 3264-3270 (2012).
168. A. L. Yu *et al.*, Long-Term Follow-up of a Phase III Study of ch14.18 (Dinutuximab) + Cytokine Immunotherapy in Children with High-Risk Neuroblastoma: COG Study ANBL0032. *Clinical Cancer Research* **27**, 2179-2189 (2021).
169. W. B. London *et al.*, Historical time to disease progression and progression-free survival in patients with recurrent/refractory neuroblastoma treated in the modern era on Children's Oncology Group early-phase trials. *Cancer* **123**, 4914-4923 (2017).
170. L. Moreno *et al.*, Outcome of children with relapsed or refractory neuroblastoma: A meta-analysis of ITCC/SIOPEN European phase II clinical trials. *Pediatric Blood Cancer* **64**, 25-31 (2017).
171. W. B. London *et al.*, Phase II randomized comparison of topotecan plus cyclophosphamide versus topotecan alone in children with recurrent or refractory neuroblastoma: a Children's Oncology Group study. *Journal of Clinical Oncololgy* **28**, 3808-3815 (2010).

172. R. Bagatell *et al.*, Phase II study of irinotecan and temozolomide in children with relapsed or refractory neuroblastoma: a Children's Oncology Group study. *Journal of Clinical Oncology* **29**, 208-213 (2011).
173. A. Di Giannatale *et al.*, Phase II study of temozolomide in combination with topotecan (TOTEM) in relapsed or refractory neuroblastoma: a European Innovative Therapies for Children with Cancer-SIOP-European Neuroblastoma study. *European Journal Cancer* **50**, 170-177 (2014).
174. F. Herd, N. O. Basta, R. J. Q. McNally, D. A. Tweddle, A systematic review of re-induction chemotherapy for children with relapsed high-risk neuroblastoma. *European Journal Cancer* **111**, 50-58 (2019).
175. N. Riggi, M. L. Suva, I. Stamenkovic, Ewing's Sarcoma. *New England Journal of Medicine* **384**, 154-164 (2021).
176. T. G. P. Grunewald *et al.*, Ewing sarcoma. *Nature Reviews Disease Primers* **4**, 5 (2018).
177. N. Gaspar *et al.*, Ewing Sarcoma: Current Management and Future Approaches Through Collaboration. *Journal of Clinical Oncology* **33**, 3036-3046 (2015).
178. C. Juergens *et al.*, Safety assessment of intensive induction with vincristine, ifosfamide, doxorubicin, and etoposide (VIDE) in the treatment of Ewing tumors in the EURO-E.W.I.N.G. 99 clinical trial. *Pediatric Blood Cancer* **47**, 22-29 (2006).
179. A. Raciborska *et al.*, Vincristine, irinotecan, and temozolomide in patients with relapsed and refractory Ewing sarcoma. *Pediatric Blood Cancer* **60**, 1621-1625 (2013).
180. P. J. Leavey *et al.*, Phase III Trial Adding Vincristine-Topotecan-Cyclophosphamide to the Initial Treatment of Patients With Nonmetastatic Ewing Sarcoma: A Children's Oncology Group Report. *Journal of Clinical Oncology* **39**, 4029-4038 (2021).
181. J. Mora *et al.*, GEIS-21: a multicentric phase II study of intensive chemotherapy including gemcitabine and docetaxel for the treatment of

Ewing sarcoma of children and adults: a report from the Spanish sarcoma group (GEIS). *British Journal of Cancer* **117**, 767-774 (2017).

182. M. Paulussen *et al.*, Ewing's tumors with primary lung metastases: survival analysis of 114 (European Intergroup) Cooperative Ewing's Sarcoma Studies patients. *Journal of Clinical Oncology* **16**, 3044-3052 (1998).
183. O. Oberlin *et al.*, Impact of high-dose busulfan plus melphalan as consolidation in metastatic Ewing tumors: a study by the Societe Francaise des Cancers de l'Enfant. *Journal of Clinical Oncology* **24**, 3997-4002 (2006).
184. N. M. Marina *et al.*, Longitudinal follow-up of adult survivors of Ewing sarcoma: A report from the Childhood Cancer Survivor Study. *Cancer* **123**, 2551-2560 (2017).
185. M. Stahl *et al.*, Risk of recurrence and survival after relapse in patients with Ewing sarcoma. *Pediatric Blood Cancer* **57**, 549-553 (2011).
186. H. Castillo-Ecija *et al.*, Treatment-driven selection of chemoresistant Ewing sarcoma tumors with limited drug distribution. *Journal Controlled Release* **324**, 440-449 (2020).
187. R. Bagatell *et al.*, Phase 1 trial of temsirolimus in combination with irinotecan and temozolomide in children, adolescents and young adults with relapsed or refractory solid tumors: a Children's Oncology Group Study. *Pediatric Blood Cancer* **61**, 833-839 (2014).
188. U. Anand *et al.*, Cancer chemotherapy and beyond: Current status, drug candidates, associated risks and progress in targeted therapeutics. *Genes Diseases* **10**, 1367-1401 (2023).
189. R. W. Johnstone, A. A. Ruefli, S. W. Lowe, Apoptosis: a link between cancer genetics and chemotherapy. *Cell* **108**, 153-164 (2002).
190. D. Fu, J. A. Calvo, L. D. Samson, Balancing repair and tolerance of DNA damage caused by alkylating agents. *Nature Reviews Cancer* **12**, 104-120 (2012).
191. M. A. Jordan, L. Wilson, Microtubules as a target for anticancer drugs. *Nature Reviews Cancer* **4**, 253-265 (2004).

192. L. Bo *et al.*, The Battlefield of Chemotherapy in Pediatric Cancers. *Cancers (Basel)* **15**, (2023).
193. A. B. Daniels *et al.*, Efficacy, Toxicity, and Pharmacokinetics of Intra-Arterial Chemotherapy Versus Intravenous Chemotherapy for Retinoblastoma in Animal Models and Patients. *Translational vision science technology* **10**, 10 (2021).
194. J. H. Francis, A. M. Levin, E. C. Zabor, Y. P. Gobin, D. H. Abramson, Ten-year experience with ophthalmic artery chemosurgery: Ocular and recurrence-free survival. *PLoS One* **13**, e0197081 (2018).
195. P. Schaiquevich, A. W. Fabius, J. H. Francis, G. L. Chantada, D. H. Abramson, OCULAR PHARMACOLOGY OF CHEMOTHERAPY FOR RETINOBLASTOMA. *Retina (Philadelphia, Pa.)* **37**, 1-10 (2017).
196. M. E. Wall *et al.*, Plant Antitumor Agents. I. The Isolation and Structure of Camptothecin, a Novel Alkaloidal Leukemia and Tumor Inhibitor from Camptotheca acuminata1,2. *Journal of the American Chemical Society* **88**, 3888-3890 (1966).
197. Y. Pommier, A. Nussenzweig, S. Takeda, C. Austin, Human topoisomerases and their roles in genome stability and organization. *Nature Reviews Molecular Cell Biology* **23**, 407-427 (2022).
198. S. B. Horwitz, M. S. Horwitz, Effects of Camptothecin on the Breakage and Repair of DNA during the Cell Cycle1. *Cancer Research* **33**, 2834-2836 (1973).
199. F. Goldwasser, I. Bae, M. Valenti, K. Torres, Y. Pommier, Topoisomerase I-related Parameters and Camptothecin Activity in the Colon Carcinoma Cell Lines from the National Cancer Institute Anticancer Screen1. *Cancer Research* **55**, 2116-2121 (1995).
200. R. G. Shao *et al.*, Abrogation of an S-phase checkpoint and potentiation of camptothecin cytotoxicity by 7-hydroxystaurosporine (UCN-01) in human cancer cell lines, possibly influenced by p53 function. *Cancer Research* **57**, 4029-4035 (1997).

201. G. Pascual-Pasto *et al.*, Increased delivery of chemotherapy to the vitreous by inhibition of the blood-retinal barrier. *Journal Controlled Release* **264**, 34-44 (2017).
202. Y. P. Gobin, I. J. Dunkel, B. P. Marr, S. E. Brodie, D. H. Abramson, Intra-arterial Chemotherapy for the Management of Retinoblastoma: Four-Year Experience. *Archives of Ophthalmology* **129**, 732-737 (2011).
203. M. Sen, R. Rao, K. Mulay, V. A. P. Reddy, S. G. Honavar, Intravitreal Topotecan for Vitreous Seeds in Retinoblastoma: A Long-term Review of 91 Eyes. *Ophthalmology*, (2024).
204. N. A. Laurie *et al.*, Topotecan combination chemotherapy in two new rodent models of retinoblastoma. *Clinical Cancer Research* **11**, 7569-7578 (2005).
205. C. B. Pratt *et al.*, Phase I study of topotecan for pediatric patients with malignant solid tumors. *Journal of Clinical Oncology* **12**, 539-543 (1994).
206. U. Winter *et al.*, Schedule-Dependent Antiangiogenic and Cytotoxic Effects of Chemotherapy on Vascular Endothelial and Retinoblastoma Cells. *PLoS One* **11**, e0160094 (2016).
207. P. Schaiquevich *et al.*, Intra-arterial chemotherapy is more effective than sequential periocular and intravenous chemotherapy as salvage treatment for relapsed retinoblastoma. *Pediatric Blood Cancer* **60**, 766-770 (2013).
208. H. Dimaras *et al.*, Retinoblastoma CSF metastasis cured by multimodality chemotherapy without radiation. *Ophthalmic genetics* **30**, 121-126 (2009).
209. M. R. Middleton, G. P. Margison, Improvement of chemotherapy efficacy by inactivation of a DNA-repair pathway. *Lancet Oncology* **4**, 37-44 (2003).
210. A. J. Wagstaff, A. Ward, P. Benfield, R. C. Heel, Carboplatin. *Drugs* **37**, 162-190 (1989).
211. B. L. Samuels, J. D. Bitran, High-dose intravenous melphalan: a review. *Journal of Clinical Oncology* **13**, 1786-1799 (1995).
212. H. Xu, M. Lv, X. Tian, A review on hemisynthesis, biosynthesis, biological activities, mode of action, and structure-activity relationship of podophyllotoxins: 2003-2007. *Current medicinal chemistry* **16**, 327-349 (2009).

213. Y. Pommier, E. Leo, H. Zhang, C. Marchand, DNA topoisomerases and their poisoning by anticancer and antibacterial drugs. *Chemistry Biology* **17**, 421-433 (2010).
214. B. G. Mohney *et al.*, Preclinical Acute Ocular Safety Study of Combined Intravitreal Carboplatin and Etoposide Phosphate for Retinoblastoma. *Ophthalmic surgery, lasers imaging retina* **48**, 151-159 (2017).
215. P. Schaiquevich *et al.*, Treatment of Retinoblastoma: What Is the Latest and What Is the Future. *Frontiers Oncology* **12**, 822330 (2022).
216. M. A. Westhoff *et al.*, Cell death-based treatment of childhood cancer. *Cell Death Disease* **9**, 116 (2018).
217. E. Stewart *et al.*, Orthotopic patient-derived xenografts of paediatric solid tumours. *Nature* **549**, 96-100 (2017).
218. D. M. Langenau, A. Sweet-Cordero, R. Wechsler-Reya, M. A. Dyer, Preclinical Models Provide Scientific Justification and Translational Relevance for Moving Novel Therapeutics into Clinical Trials for Pediatric Cancer. *Cancer Research* **75**, 5176-5186 (2015).
219. C. Chaves *et al.*, Characterization of the Blood-Brain Barrier Integrity and the Brain Transport of SN-38 in an Orthotopic Xenograft Rat Model of Diffuse Intrinsic Pontine Glioma. *Pharmaceutics* **12**, (2020).
220. N. Maricic *et al.*, Zebrafish as an Orthotopic Tumor Model for Retinoblastoma Mimicking Routes of Human Metastasis. *Cancers (Basel)* **14**, (2022).
221. J. I. Johnson *et al.*, Relationships between drug activity in NCI preclinical in vitro and in vivo models and early clinical trials. *British Journal of Cancer* **84**, 1424-1431 (2001).
222. G. Pascual-Pasto *et al.*, Low Bcl-2 is a robust biomarker of sensitivity to nab-paclitaxel in Ewing sarcoma. *Biochemical Pharmacology* **208**, 115408 (2023).
223. G. Pascual-Pasto *et al.*, SPARC-mediated long-term retention of nab-paclitaxel in pediatric sarcomas. *Journal Controlled Release* **342**, 81-92 (2022).
224. C. Monterrubio *et al.*, Targeted drug distribution in tumor extracellular fluid of GD2-expressing neuroblastoma patient-derived xenografts using SN-38-

loaded nanoparticles conjugated to the monoclonal antibody 3F8. *Journal Controlled Release* **255**, 108-119 (2017).

225. H. Castillo-Ecija *et al.*, Prognostic value of patient-derived xenograft engraftment in pediatric sarcomas. *Journal Pathology Clinical Research* **7**, 338-349 (2021).
226. D. M. Carvalho *et al.*, Repurposing Vandetanib plus Everolimus for the Treatment of ACVR1-Mutant Diffuse Intrinsic Pontine Glioma. *Cancer Discovery* **12**, 416-431 (2022).
227. B. L. Gallie, D. M. Albert, J. J. Wong, N. Buyukmihci, C. A. Pullafito, Heterotransplantation of retinoblastoma into the athymic "nude" mouse. I*nvestigative Ophthalmology Visual Science* **16**, 256-259 (1977).
228. S. Zugbi *et al.*, Establishment and Comprehensive Characterization of a Novel Preclinical Platform of Metastatic Retinoblastoma for Therapeutic Developments. *Investigative Ophthalmology Visual Science* **64**, 27 (2023).
229. Y. Zhuang *et al.*, Topotecan central nervous system penetration is altered by a tyrosine kinase inhibitor. *Cancer Research* **66**, 11305-11313 (2006).
230. M. Cuadrado-Vilanova *et al.*, Identification of immunosuppressive factors in retinoblastoma cell secretomes and aqueous humor from patients. *Journal of Pathology* **257**, 327-339 (2022).
231. R. Aschero *et al.*, Prognostic value of xenograft engraftment in patients with metastatic high-risk neuroblastoma. *Pediatric Blood Cancer*, e30318 (2023).
232. K. J. Livak, T. D. Schmittgen, Analysis of relative gene expression data using real-time quantitative PCR and the 2(-Delta Delta C(T)) Method. *Methods* **25**, 402-408 (2001).
233. S. Polager, Y. Kalma, E. Berkovich, D. Ginsberg, E2Fs up-regulate expression of genes involved in DNA replication, DNA repair and mitosis. *Oncogene* **21**, 437-446 (2002).
234. L. Gautier, L. Cope, B. M. Bolstad, R. A. Irizarry, affy--analysis of Affymetrix GeneChip data at the probe level. *Bioinformatics* **20**, 307-315 (2004).

235. C. Kilkenny, W. J. Browne, I. C. Cuthill, M. Emerson, D. G. Altman, Improving bioscience research reporting: The ARRIVE guidelines for reporting animal research. *Journal Pharmacology Pharmacotherapeutics* **1**, 94-99 (2010).
236. G. Paxinos, K. B. J. Franklin, *The mouse brain in stereotaxic coordinates*. (Academic Press, San Diego, 2001).
237. L. Yiangou *et al.*, Method to Synchronize Cell Cycle of Human Pluripotent Stem Cells without Affecting Their Fundamental Characteristics. *Stem Cell Reports* **12**, 165-179 (2019).
238. M. Ohtaki *et al.*, A robust method for estimating gene expression states using Affymetrix microarray probe level data. *BMC Bioinformatics* **11**, 183 (2010).
239. S. Postel-Vinay *et al.*, Common variants near TARDBP and EGR2 are associated with susceptibility to Ewing sarcoma. *Nature Genetics* **44**, 323-327 (2012).
240. I. Liikanen *et al.*, Oncolytic adenovirus with temozolomide induces autophagy and antitumor immune responses in cancer patients. *Molecular Therapy* **21**, 1212-1223 (2013).
241. R. C. Brennan *et al.*, Ocular Salvage and Vision Preservation Using a Topotecan-Based Regimen for Advanced Intraocular Retinoblastoma. *Journal of Clinical Oncology* **35**, 72-77 (2017).
242. A. J. Berk, Recent lessons in gene expression, cell cycle control, and cell biology from adenovirus. *Oncogene* **24**, 7673-7685 (2005).
243. G. Chinnadurai, Control of Apoptosis by Human Adenovirus Genes. *Seminars in Virology* **8**, 399-408 (1998).
244. G. Zamir *et al.*, Replication-deficient adenovirus induces host topoisomerase I activity: implications for adenovirus-mediated gene expression. *Molecular Therapy* **15**, 772-781 (2007).
245. P. Meng, R. Ghosh, Transcription addiction: can we garner the Yin and Yang functions of E2F1 for cancer therapy? *Cell Death Disease* **5**, e1360 (2014).
246. R. Vélez-Cruz, D. G. Johnson, E2F1 and p53 Transcription Factors as Accessory Factors for Nucleotide Excision Repair. *International Journal of Molecular Sciences* **13**, 13554-13568 (2012).

247. K. Liu, F. T. Lin, J. M. Ruppert, W. C. Lin, Regulation of E2F1 by BRCT domain-containing protein TopBP1. *Molecular Cellular Biology* **23**, 3287-3304 (2003).
248. R. Gilabert-Oriol, L. Chernov, M. Anantha, W. H. Dragowska, M. B. Bally, In vitro assay for measuring real time topotecan release from liposomes: release kinetics and cellular internalization. *Drug Delivery Translational Research* **7**, 544-557 (2017).
249. S. K. Radhakrishnan *et al.*, Constitutive expression of E2F-1 leads to p21-dependent cell cycle arrest in S phase of the cell cycle. *Oncogene* **23**, 4173-4176 (2004).
250. K. Engeland, Cell cycle regulation: p53-p21-RB signaling. *Cell Death Differentiation* **29**, 946-960 (2022).
251. T. B. Ferreira *et al.*, 293 cell cycle synchronisation adenovirus vector production. *Biotechnology Progress* **25**, 235-243 (2009).
252. K. Madaan, D. Kaushik, T. Verma, Hydroxyurea: a key player in cancer chemotherapy. *Expert Review of Anticancer Therapy* **12**, 19-29 (2012).
253. F. Coussy *et al.*, BRCAness, SLFN11, and RB1 loss predict response to topoisomerase I inhibitors in triple-negative breast cancers. *Science Translational Medicine* **12**, (2020).
254. S. Duan *et al.*, Histone deacetylase inhibitor, AR-42, exerts antitumor effects by inducing apoptosis and cell cycle arrest in Y79 cells. *Journal Cellular Physiology* **234**, 22411-22423 (2019).
255. R. C. Brennan *et al.*, Targeting the p53 pathway in retinoblastoma with subconjunctival Nutlin-3a. *Cancer Res*earch **71**, 4205-4213 (2011).
256. D. Y. Kim, J. A. Choi, J. Y. Koh, Y. H. Yoon, Efficacy and safety of aflibercept in in vitro and in vivo models of retinoblastoma. *Journal of Experimental Clinical Cancer Research* **35**, 171 (2016).
257. T. Todo *et al.*, Intratumoral oncolytic herpes virus G47Δ for residual or recurrent glioblastoma: a phase 2 trial. *Nature Medicine* **28**, 1630-1639 (2022).

258. L. Vassilev *et al.*, Repeated intratumoral administration of ONCOS-102 leads to systemic antitumor CD8(+) T-cell response and robust cellular and transcriptional immune activation at tumor site in a patient with ovarian cancer. *Oncoimmunology* **4**, e1017702 (2015).
259. E. T. Wong, A. Berkenblit, The Role of Topotecan in the Treatment of Brain Metastases. *The Oncologist* **9**, 68-79 (2004).
260. C. Sung, S. M. Blaney, D. E. Cole, F. M. Balis, R. L. Dedrick, A pharmacokinetic model of topotecan clearance from plasma and cerebrospinal fluid. *Cancer Research* **54**, 5118-5122 (1994).
261. B. Vera *et al.*, Characterization of the Antiglioma Effect of the Oncolytic Adenovirus VCN-01. *PLoS One* **11**, e0147211 (2016).
262. M. Garcia-Moure *et al.*, The oncolytic adenovirus VCN-01 promotes anti-tumor effect in primitive neuroectodermal tumor models. *Scientific Reports* **9**, 14368 (2019).
263. S. Taschner-Mandl *et al.*, Metronomic topotecan impedes tumor growth of MYCN-amplified neuroblastoma cells in vitro and in vivo by therapy induced senescence. *Oncotarget* **7**, 3571-3586 (2016).
264. X. Jiang *et al.*, E2F1 promotes Warburg effect and cancer progression via upregulating ENO2 expression in Ewing sarcoma. *Molecular Medicine Reports* **26**, (2022).
265. H. Wang, X. Wang, L. Xu, J. Zhang, Prognostic analysis of E2F transcription factors E2F1 and E2F3 in four independent pediatric neuroblastoma cohorts. *BMC Pediatrics* **22**, 376 (2022).
266. R. Alemany, K. Suzuki, D. T. Curiel, Blood clearance rates of adenovirus type 5 in mice. *Journal Gene Virology* **81**, 2605-2609 (2000).
267. R. Mody *et al.*, Irinotecan, Temozolomide, and Dinutuximab With GM-CSF in Children With Refractory or Relapsed Neuroblastoma: A Report From the Children's Oncology Group. *Journal of Clinical Oncology* **38**, 2160-2169 (2020).

268. P. Anderson *et al.*, Pilot Study of Recurrent Ewing's Sarcoma Management with Vigil/Temozolomide/Irinotecan and Assessment of Circulating Tumor (ct) DNA. *Clinical Cancer Research* **29**, 1689-1697 (2023).